Development of higher efficiency photocathodes for gas filleddetectors

Guillaume Potdevin

THÈSE

pour obtenir le titre de

Docteur de l'Université Joseph Fourier

Discipline :

Physique

présentée et soutenue publiquement par

Guillaume POTDEVIN

Sujet de thèse :

Development of higher efficiency photocathodes for gas filled detectors

---

Soutenance le 29 Janvier 2008 devant le jury composé de :

François Montanet	LPSC, CNRS, Grenoble	Représentant de l'université
Imad Laktineh	IPNL, CNRS, Lyon	Rapporteur
Ralf Menk	Elettra, Trieste	Rapporteur
Johann Collot	LPSC, CNRS, Grenoble	Directeur Académique
Menhard Kocsis	ESRF, Grenoble	Superviseur à l'ESRF

Contents

1 Introduction **1**

1.1 Why Detectors ? . . . 1

1.1.1 A small history of X-ray sources . . . 2

1.1.2 A new Science is born: Photon Science . . . 4

1.1.3 A typical experimental setup . . . 6

1.1.4 The place of the detector in the chain . . . 9

1.2 Detectors in the hard X-ray energy range . . . 10

1.2.1 What are the detector main characteristics? . . . 10

1.2.2 The Detective Quantum Efficiency . . . 11

1.2.2.1 The DQE dependence on the Quantum Efficiency. . . . 12

1.2.2.2 The dependence of the DQE on the spatial resolution . . . 13

1.2.3 The mode of operation, speed and behavior of one detector at large intensities 15

1.3 Spectroscopy detectors . . . 18

1.4 Imaging detectors . . . 21

1.4.1 current mature technologies . . . 21

1.4.2 technologies under developments . . . 23

1.4.2.1 Spectroscopy Detectors under development . . . 23

1.4.2.2 Imaging Detectors under development . . . 23

2 The basics of gas-filled detectors **29**

2.1 historical background . . . 29

2.2 Principle of gas-filled detectors . . . 30

2.2.1 The X-ray absorption in the gas . . . 30

2.2.2 The amplification and the modes of operation of gas-filled detectors . . . 31

2.2.3 The benefits of gas-filled detectors . . . 33

2.2.4 The limitations of gas-filled detectors . . . 33

2.3 Recent Evolutions of gas-filled detectors . . . 35

2.4 Gas amplification compared to Microchannel plates . . . 37
2.5 A promising approach to overcome Gas-filled detectors limitations . . . 38

3 Photocathode for gas-filled detectors 41
3.1 Basics of Photocathodes . . . 41
3.2 Improved Models of Photocathodes . . . 45
3.3 Major technologies of photocathodes currently available . . . 45
3.3.1 Metallic Photocathode . . . 46
3.3.2 Semiconducting Photocathode . . . 46
3.3.3 Organic Photocathode . . . 47
3.3.4 CsI . . . 47
3.3.5 Conclusions on available technologies of Photocathodes and the issues related to their use . . . 48

4 The Simulations by Monte Carlo Method 55
4.1 A first approach to Monte Carlo . . . 55
4.1.1 History . . . 55
4.1.2 Description of the Monte Carlo Method . . . 56
4.1.3 The Monte Carlo Method in Particle Transport . . . 57
4.2 The Geant4 toolkit for particle transport into matter . . . 57
4.2.1 The way Geant4 computes particle propagation . . . 58
4.2.1.1 The tracking of the particles . . . 58
4.2.1.2 The physical interactions in Geant4 . . . 61
4.2.1.3 Analysis and Representation tools . . . 62
4.2.2 The simulation tool developed . . . 62
4.2.2.1 Description and Functionalities . . . 62
4.2.2.2 The test of the code, comparison with experimental values . . . 64
4.2.2.3 The limits of the Monte Carlo Method . . . 66
4.3 The simulation performed . . . 67
4.3.1 The simulations performed . . . 67
4.3.2 Use of the simulations for thickness optimization . . . 70
4.3.3 Simulation of the impact of structures on the photocathode . . . 71
4.4 Conclusion on this part of the work . . . 71

5 Experimental Setup and Sample Preparation 77
5.1 Design of the measurement setup . . . 77
5.1.1 A few general considerations . . . 77
5.1.2 The chamber and the ammeter . . . 78
5.1.2.1 The Photocathode holder, the electrical shielding . . . 78
5.1.2.2 The Chamber . . . 80
5.1.2.3 The Keithley 6430 ammeter . . . 81

5.1.3 Results of calibration and test of the chamber . . . 81
5.1.4 Conclusion concerning the setup . . . 83

6 The different concepts to make a photocathode 87
6.1 Indirect conversion . . . 87
6.1.1 Photocathodes in visible and UV . . . 88
6.1.2 Scintillation materials . . . 89
6.1.3 Possible combinations . . . 90
6.1.4 Conclusion . . . 91
6.2 Direct conversion . . . 92
6.2.1 Modify the geometry to increase the yield of one material . . . 92
6.2.1.1 Porous Photocathodes . . . 93
6.2.1.2 Regular Structures . . . 93
6.2.2 Field emission . . . 97
6.2.3 A new material: CsI_3 . . . 98

7 Experimental tests and discussion of the results 101
7.1 Modify the geometry to increase the yield of a material . . . 101
7.1.1 Analysis of the microstructures characteristics . . . 102
7.1.2 Efficiency measurements . . . 103
7.2 Field Emission . . . 103
7.2.1 Analysis of the microstructure characteristics . . . 103
7.2.2 Efficiency Measurements . . . 104
7.3 CsI_3 as a new photocathodes material . . . 104
7.3.0.1 Physical and chemical characteristics . . . 104
7.3.1 The CsI_3 samples . . . 105
7.3.1.1 Preparation of the different samples . . . 106
7.3.1.2 Analysis of the microstructures of the samples and their evolution . . . 107
7.3.2 CsI_3 quantum efficiency and comparison with CsI. . . . 110
7.3.2.1 The quantum efficiency of CsI and its evolution in air . . . 110
7.3.2.2 The quantum efficiency of CsI_3, its evolution in air and comparison with CsI. . . . 112
7.3.3 Analysis of the results obtained with CsI_3 . . . 118
7.3.4 Conclusion on the use of CsI_3 as a photocathode . . . 120

8 Conclusion 123

A Detector characteristics 125
A.1 Position resolution in the case of gas-filled detectors . . . 125
A.2 Energy Resolution . . . 125
A.3 Space Charging in gas-filled detectors . . . 126

Annexes **125**

B Monte Carlo Application Examples **129**

B.1 Simple Examples of statistical sampling methods 129

B.1.1 Calculus of an integral 129

B.1.2 An historical example: Buffon's needles 130

Chapter 1

Introduction

1.1 Why Detectors ?

Probably the first human being already was driven by a strong sense of curiosity, as it is some of the deepest law of human nature. This force has pushed mankind to develop more and more powerful investigation tools to help him understand its environment. Outstanding examples in the past are the telescope used by *Galilée* to make the first observation for Jupiter's satellites, or *Van Leewenhoek*'s microscope, which enabled the discovery of microscopic animals... In this frame, X-rays are nothing but an extension to humans' capabilities to explore the world, and X-ray detectors are their eyes, adapted for such investigations.

This work is intended to contribute to the development of modern tools for matter studies. It is part of a more global program to provide modern light sources with reliable and efficient detectors, able to answer the growing needs of the scientific community in this domain.

1.1.1 A small history of X-ray sources

Figure 1.1 : *Conrad Wilhelm RÖNTGEN (March 27, 1845 - February 10, 1923), German physicist.*

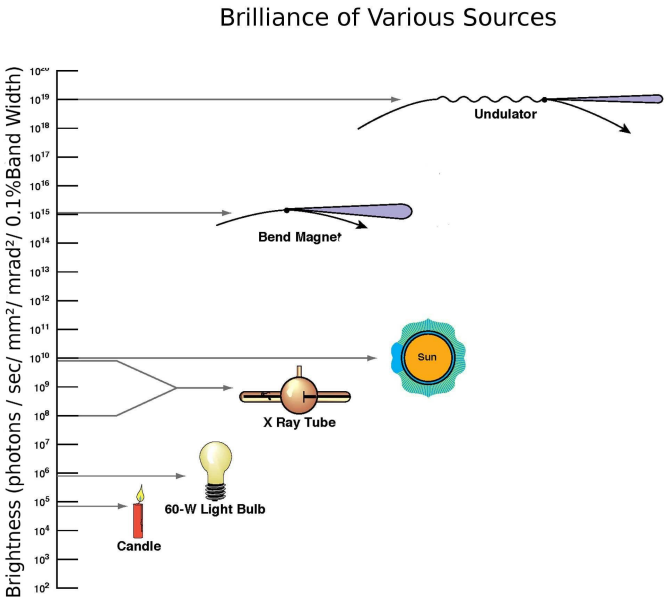

Figure 1.2 : *Brilliance of various light sources. The brilliance enables to measure the* quality *of a light source.*

Since their first identification by Wilhelm Röntgen in the late 18th century (for which he was awarded the first Nobel Prize for Physics in 1901), X-rays have been at the origins of several revolutions in numerous fields of research.
This broadening of the usefulness of X-rays is mainly due to the fantastic development of X-ray sources. The following lines give a short history of those sources.

Discharge tubes or Crookes tube

William Crookes, an English physicist, is the inventor of the first artificial source of X-rays: while he was studying the effects of electric currents in gas at low pressure, he used glass vacuum cylinders, containing electrodes for discharges of a high voltage electric current[1]. He noticed that unexposed photographic plates were shadowed when approached from those tubes, even though he did not identify this to be caused by a particular sort of radiation.
Fernando Sanford later bettered this principle of emissions and published in 1893 in the Journal *Physical Review* an article entitled *Observed tubes with energy rays extending from a negative electrode.* It is interesting to note that even after deeper studies by Heinrich Hertz of those specific radiations, they were not identified as a new sort of radiation. Only the work of Wilhelm Röntgen with Vacuum tubes enabled to actually identify X-rays as *a new kind of ray.*
Those tubes are actually the ancestors of modern X-ray tubes, which are the result of a technological

[1] this sort of tube had already been used by the physicist Johann Hittorf who observed tubes with energy rays extending from a negative electrode.

improvement of the original Crookes tube.

Synchrotron radiation sources

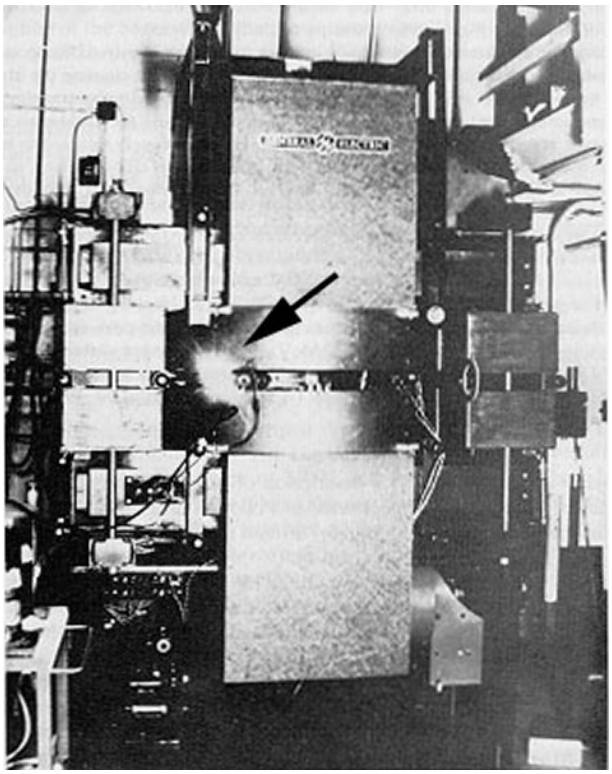

Figure 1.3 : *The* General electric particle accelerator*, at the origin of the discovery of synchrotron radiations. The arrow indicates the trace of the synchrotron radiation beam on the picture. It is the first observation of synchrotron radiations.*

The history of synchrotron radiations is closely related to that of particle physics. First considered as a nuisance sapping the energy of the particles, it was later recognized as a powerful tool to study matter. One usually distinguishes three major steps on the way to modern light sources:

First Generation Sources were mainly synchrotrons built for the study of particle physics (*High Energy Physics* HEP), which were refurbished as light sources, as the frontiers of HEP were pushed forward. This way, it is often said that the use of those synchrotrons as light sources was a sort of `parasitic operation` of the synchrotrons. A big step occurred in the 50's as the first *electron storage rings* were built, providing a much more stable, fixed energy, and continuous beam of particles (and thus photon beam). Those machines have been the models for all synchrotron light sources until now.

Second Generation Sources were the first machines dedicated for light emission. They were the first machines able to operate a large number of beamlines, with optimized emittance parameters (quality of the beam), stable energy and beam position. The development of those machines

was associated to important developments in optics and gave birth to new types of experiments such as EXAFS or large protein crystallography.

Third Generation Sources are storage rings optimized to have numerous long straight sections, in which undulators and wrigglers can take place, so providing a much higher brightness and flux of photon beams. This is the birth of large facilities (800 to 1400m) offering several tens of beamlines, typically welcoming several thousands of users every year.

The future of light sources will probably see a parallel development of *the third generation light sources*, which keep bettering in terms of performance, and the birth of *the fourth generation sources*, also called `Free electron lasers` (FEL). FEL will be able to offer peak of brightness of several order of magnitude higher than third generation sources, as well as pulses as short as 100 fs and highly coherent. FELs will be constituted of very long undulators in high-energy linear accelerators. Those devices will offer a new range of possibility of investigation of matter, but will not directly compete with third generation sources as they will not be able to offer the many beamlines that storage rings have.
Indeed, several projects of third and fourth generation sources have been launched recently or are even in their commissioning phase (the synchrotrons Diamond and Soleil in Oxford and Paris, the European X-FEL in Hamburg...). Yet it is unlikely that all those sources will be able to answer the growing demand for high brightness sources.

1.1.2 A new Science is born: Photon Science

Figure 1.4 : *The ESRF seen from top. The ESRF is one the modern lightsources able to provide high brightness photon beams.©P.Ginter/ESRF.*

Photon Sciences encompass all the techniques using high brilliance photon beams, such as those produced in Synchrotron Radiation Facilities, and Free Electron Lasers. Those sophisticated and permanently evolving machines enable the production of highly intense beams of photons. The brilliance (which measures the quality of the beam) is now more than 10 orders of magnitudes higher than that of conventional sources (see Figure 1.2).

Among those new generation sources, a majority of them are dedicated to the production of X-rays, and to the development of techniques making use of them.
Since their first direct application (photography of Wilhelm Röntgen's wife's hand), X-rays have become the base of applications as various as:

Medical imaging and treatment: radiography techniques, scanners, cancer treatments, computer tomography, are just some of the numerous applications of X-rays in medicine.
Now modern sources have pushed the development of new techniques, like: high-resolution 3D tomography imaging techniques, therapeutic treatments, drugs research,

Physics: Numerous physical characterization techniques are based on X-rays. If historically X-rays first enabled the study of crystals by mean of the crystallography, they are now routinely used to study soft matter (diffuse scattering), the chemical composition of elements (spectroscopy), magnetic structures (magnetic scattering-magnetic dichroism), the surface and interface properties of various materials (small angle scattering) etc...

Biology. Biology always beneficiated from the development of physics techniques for its development (the structure of DNA was discovered thanks to the X-ray diffraction technique). Now a wide range of techniques is specifically devoted to biological applications: macromolecular crystallography has become a science on its own, and more and more techniques benefit from developments specific to biological applications.

Archeology and art. Archeological and artistic pieces are by definition unique and fragile. Since most X-ray based techniques are non destructive, they are of prime interest to learn more on those precious "samples".

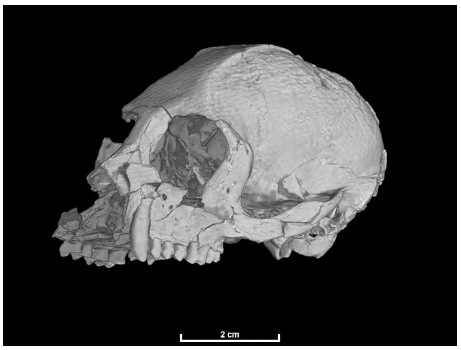

Figure 1.5 : *Toumai's skull, as obtained thanks to a tomographic technique.*

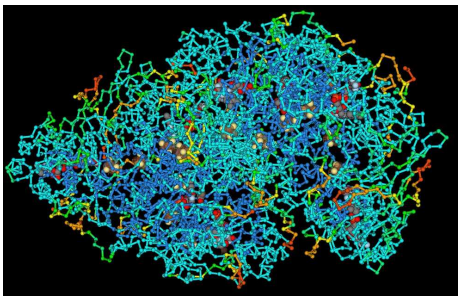

Figure 1.6 : *example of a protein structure resolved by diffraction technique.*

For example it is now possible to know with a precision better than one Angstrom, the position of each atoms in biological macromolecules (typically several thousands of amino acids). One can find in all kind of samples the rarest traces of impurities, and get extremely useful information on the history of the sample, or on its composition. It is possible to reconstruct in 3 dimensions the structure of various samples with a precision of the order of a few microns, to determine the inner structure of micro-objects, and directly study the properties of nanometer size objects...

Another big advantage is the fact that those analysis are mostly non destructive.

→ It is possible to study unique samples, like archeological objects or space objects (brought back by various space missions or even by the fall of asteroids)

→ It is possible to follow in situ complex process like chemical or biological reactions with a time resolution of the picosecond or even less.

→ It enables eventually to repeat the experiment, which is not always easy to do when the sample itself is hard to make.

→ It is possible to combine different techniques on the same sample.

As a result, there are more and more "*photon factories*" in the world to answer the growing need of scientists for those techniques of analysis. Experiments, which were just impossible to do even 20 years ago are now routinely achieved in synchrotrons and have become the standard in a lot of fields. The area of interest for synchrotrons and the future X-FELs also keeps growing as new applications (such as medical applications, nano-analysis) arise and revolutionize the possibilities in their respective fields.
In the future, it is likely that the demand for high quality sources will keep growing, especially with the arrival of more and more hybrid techniques, combining various apparatus like *electron imaging combined with magnetic dichroism imaging* or *atomic force microscopes combined with nano-focused photon beams, LEED analysis and photoemission spectroscopy...*

1.1.3 A typical experimental setup

An experiment using high quality sources involves a lot of elements, each being highly optimized.

A typical beamline (where the photon beams is shaped and positioned, and where experiments are carried out) is almost always composed of four main parts (see fig. 1.7):

- **A source**
- **An optics hutch,**
- **An experimental hutch,**
- **A control hutch.**

The source is composed of the particles circulating in the storage ring. Charged particles like electrons or positrons used in synchrotrons emit light when submitted to acceleration. For those particles have a very high energy (several GeV), the emitted light is tangential to their direction of motion. This results in a very concentrated beam with a low divergence, and high flux.

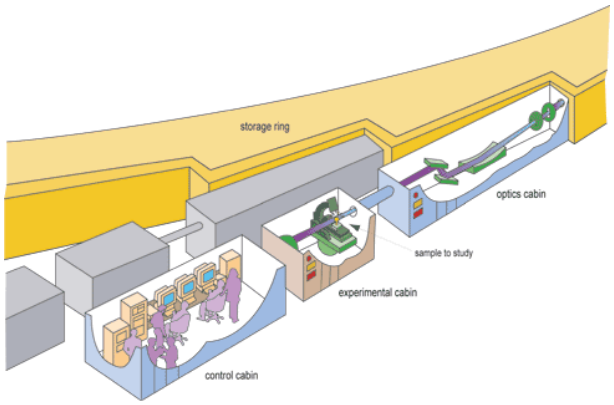

Figure 1.7 : *Schematic of a typical beamline. After the beam was produced in the* storage ring*, it enters the* optic cabin *and then the* experimental cabin *where it hits the sample. All elements are remotely controlled from the* control cabin*.*

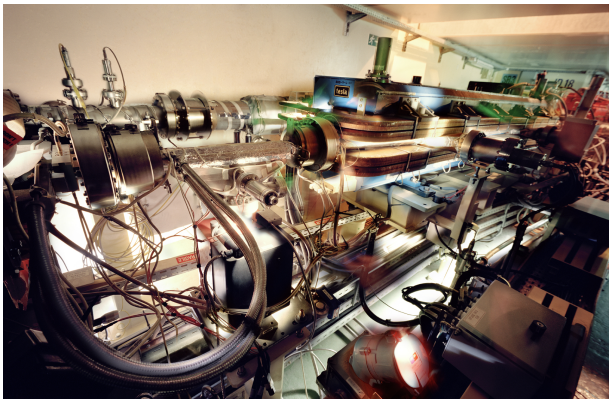

Figure 1.8 : *Picture of a (blue) bending Magnet. The bending magnets are one type of source of photon beam in synchrotron radiation facilities. ©P.Ginter/ESRF*

The storage ring in reality is a large polygon. At each of its angles one can find bending magnets, which produce an intense magnetic field, where the particles trajectory is bent. This is also the place where light is produced. Beamline find their origins in those bending magnets.

In addition, elements called *insertion devices* are specifically made to produce a very large flux (see picture 1.10 for the example of an *undulator*). Those elements consist of straight sections in which an alternative magnetic field is applied on the pathway of particles (with a small period and permanent magnet they are called *undulators*, and with long period electromagnets, they are called *wigglers*). In those elements the particles follow a zigzag trajectory. The quantity of light obtained is largely increased, as each turn adds light to that of the previous one, and because the emitted light is all emitted in the direction of the straight section and not spread all along a large curve, like in bending magnets.

In the case of undulators (small period) the light emitted by the device is coherent enough (spatially and temporally) to create a phenomenon of interference. This results in the concentration of the emitted energies at a fundamental frequency and a few harmonics. The Figure 1.9 gives the respective spectrums of a bending magnet, a wiggler and an undulator. One can clearly see the gain in terms of flux and monochromaticity (in particular when comparing undulators to bending magnets).

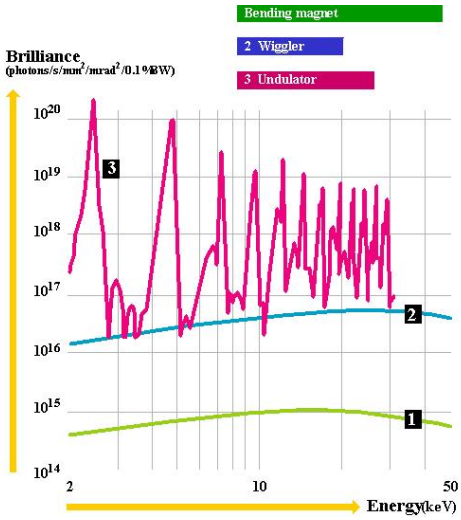

Figure 1.9 : *Emission Spectrum of a bending magnet, a wriggler, and an undulator*

Figure 1.10 : *Photo of an Undulator. Undulators are the brightest sources of photon beams in synchrotron radiation facilities. ©P.Ginter/ESRF*

The optics hutch contains the elements, which shape the beam: it usually contains several elements such as:

→ *a shutter*, which controls the entrance of the beam in the hutch (this is a crucial element for the safety of persons).

→ *slits*. They give its shape to the spot, by removing the non-focused part of the beam (especially in the case of the bending magnets),

→ *monochromator*. It selects very precisely the energy (selects the good wavelengths from the white beam),

→ *focusing mirrors and/or lenses*. They concentrate the beam to a spot, which can be as small as a few microns or even less. Alternatively, they can be used to make a very wide and homogeneous beam (ex. case of medical tomography).

The experimental hutch provides all the *sample environment* and *detection systems* needed to carry out the experiments.

- *The sample Environment* is made of elements, which control the conditions of the experiment: vacuum chambers and high pressure gaskets, sample heaters and cryogenic coolers, gas flows and electrochemistry cells are some examples of systems mandatory to make several sorts of experiments.
- *The detector*. The detector is in charge of collecting the information provided by the interaction of the beam with the sample. It will be further detailed in the next section.

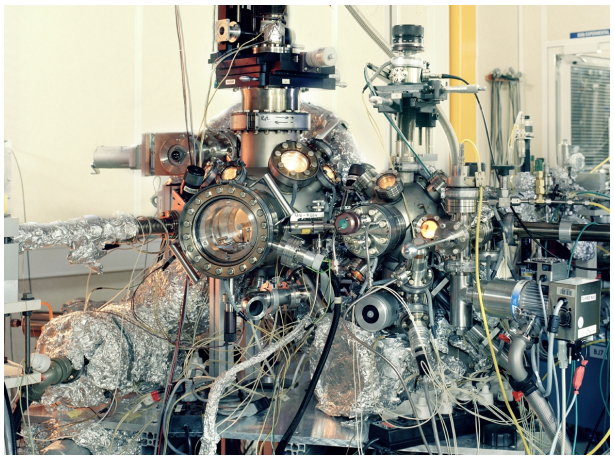

Figure 1.11 : *An example of experimental setup, illustrating the complexity of experimental setup to provide the right sample environment. ©P.Ginter/ESRF*

Figure 1.12 : *A beamline seen from the top. The storage beam is hidden behind the concrete blocks on the left side of the picture. Photons enter the beamline at the top of the photo. ©P.Ginter/ESRF*

1.1.4 The place of the detector in the chain

The detector occupies a central place in the experimental setup, in this that it collects the photons scattered after the beam/sample interaction. So the detector is a main source of information in any photon science experiment.
So far, lots of efforts have been put in the production of high quality beams in terms of stability, monochromaticity... The fantastic progress in this field is highlighted by the exponential rise of the brilliance of the light sources during the last few decades (see Figure 1.2).
After those great achievements in brilliance, now comes the time to harvest this huge amount of scattered photons with detectors. Indeed, **in a lot of experiments, the main limiting factor is the detector itself**. The ESRF long-term strategy, which defines the future developments at ESRF, states that *"detectors are generally recognized as the weak link in the modern use of SR"*[1].
Detectors used in the experiments usually suffer from:

- Low efficiency (only a very small fraction of the monitored particle are actually detected, so the radiation dose received by the sample has to be increased)
- limited speed (fast reactions cannot be recorded. This also increases the dose received by the sample)
- limited size (lowers the speed of the experiments forcing to make several acquisition.)
- limited dynamic range (a problem for techniques giving a high contrast, like small angle diffusion scattering analysis).

Now more emphasis is put on instrumentation in the beamlines. Most large facilities have specific programs for the development of new generation detectors. To answer the high cost associated to these developments, collaborations among several institutes are created.
Already, various development projects have started to provide the beamlines with detectors, which would suit the current requirements of experiments carried out in modern lightsources.

In particular, this thesis is part of a project to develop a new generation of gas-filled detectors with a high dynamic, large area, good efficiency and good robustness.
This thesis explores the possibility to use a photocathode as a first step photons → electrons converter to ensure a good efficiency and spatial resolution of the detector.

1.2 Detectors in the hard X-ray energy range

A short introduction to the most common technologies of detectors used in the synchrotron radiation community can be found in the well-known orange X-ray data booklet [2]. For each technologies an extensive description can be found in K.Knoll's Radiation and Measurement [3].

It should be noted that in what follows only detectors technologies designed for X-rays are described. Yet, most of those detectors can also be used with other sort of particles/radiations.

1.2.1 What are the detector main characteristics?

Basically, a detector provides information about the:

- position
- time
- eventually energy and direction
- intensity

of an incoming particle/photon beam.
The measurement of one physical quantity is never perfect, but suffers from several imprecision and uncertainties. Those uncertainties have several origins:

- The measured signal itself suffers from statistical fluctuations. Those intrinsic fluctuations cannot be avoided, but several measurements of the same quantity enable to determine the distribution function of the physical quantity. Statistical models then enable to determine more accurately the physical quantity, and also to calculate the statistical error of the measurement.
- In addition to the intrinsic fluctuations of the measured physical quantity, the detector suffers from a limited precision in measuring it. The characteristics of one detector give information on the accuracy of one measurement, and on the error of measurement.
- The signal is never recorded alone, but several *fake* events appear with the measurement and tend to blur/hide the physical quantity measured. This contribution is often called background, and finds its origin both in the detector imperfectness, and in the environment of the detector, which can be source of such unwanted contributions to the signal.

The last two contributions (fluctuation and background) are usually referred to as *Noise*. The noise can be analyzed in terms of *power, spectrum*, as well as uniformity. The quality of one measurement is then evaluated thanks to the

$$\textit{Signal to Noise ratio} = \frac{Power_{signal}}{Power_{noise}} = \left(\frac{A_{signal}}{A_{noise}}\right)^2, \tag{1.1}$$

where A is the RMS[2] amplitude of the signal.

The detector characteristics give information about:

- The quality of the measurement performed by the detector. This comprises among other aspects: the resolutions in energy and position, the contrast the detector offers, and the noise it adds to the signal.
- The speed of the detector: the minimum amount of time between successive measurement (dead time) and the maximum intensity it can measure.
- The geometrical information about the detector: mainly its active surface. Also the volume of the detector can be of importance in crowded spaces.

1.2.2 The Detective Quantum Efficiency

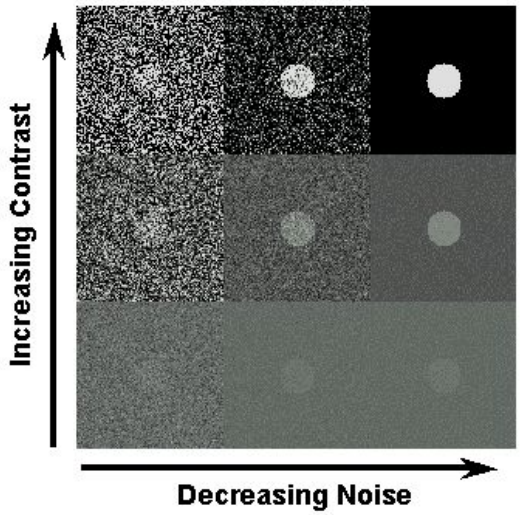

Figure 1.13 : *Illustration of the effect of the noise and contrast on the quality of one image.*

The detective quantum efficiency (DQE) characterizes the measurement uncertainty introduced by a detector.
It is now recognized as the best figure of merit of a detector. It provides extensive information about the capabilities of a 1D or 2D detector to return images with sharp and noiseless images. So it expresses the ability of one detector to sense a signal against a background of radiation, and without deteriorating the intrinsic noise of the incident beam.
The *Detective Quantum Efficiency* (sometimes spelled Detection Quantum Efficiency), is defined as

$$DQE = \frac{SNR_{out}^2}{SNR_{in}^2}, \tag{1.2}$$

with SNR_{out} and SNR_{in} being the signal-to-noise ratios at input and output of the detector.

[2]root of mean square: the quadratic mean of the signal $\sqrt{< x^2 >}$.

It differs from the quantum efficiency QE in the sense that it takes into account, not only the fraction of the photons, which are actually recorded, but also all the system losses due to the limited resolution, noise performance... of one real detector.
SNR_{in} can be seen as the best achievable detector performance, and in this sense, $0 < DQE < 1$.
The DQE is function of several parameters[4, 5, 6]:

- The Quantum Efficiency,
- The spatial frequency,
- The particle energy,
- The signal intensity.

It is often used as a Figure of Merit of the detector, but it strongly varies with the conditions of acquisition of the data, and as the available data are often incomplete, its utility is still limited. A lot of discussions are still ongoing to define standard conditions of measurement of the DQE of one detector.
Yet some methods are now recognized as standard for the evaluation of detectors DQE. Practical methods of evaluation of the DQE and associated parameters, and more globally of the performance of one detector can be found in references [6, 7, 8].
In the following section, some of the most important characteristics of imaging detectors are shown, through their impact on the DQE. Yet, the DQE is rarely fully measured and in most cases, only those characteristics of the detectors, which have been measured.

1.2.2.1 The DQE dependence on the Quantum Efficiency.

The Quantum Efficiency QE, in its most fundamental definition is *the fraction of the incident quanta, which participate in the signal formation.* So it is evident that the QE is a limiting factor to the DQE of one detector.
Indeed, if we go back to the definition of the $DQE = \frac{SNR_{out}^2}{SNR_{in}^2}$ (eq. 1.1), by writing $SNR_x = \frac{S_x}{\sigma_x}$ we obtain $\frac{S_{out}}{\sigma_{out}} = \sqrt{DQE}\frac{S_{in}}{\sigma_{in}}$ and $\frac{S_{out}}{S_{in}} = \sqrt{DQE}\frac{\sigma_{out}}{\sigma_{in}}$. For $\sigma_{out} \geqslant \sigma_{in}$, and $\frac{S_{out}}{S_{in}} = \sqrt{QE}$ the Quantum Efficiency, we have

$$DQE \leqslant QE. \tag{1.3}$$

The quantum efficiency QE acts as an absolute limit to the detective quantum efficiency DQE of the detector. In particular, a perfect detector (with no intrinsic noise: $\sigma_{out} = \sigma_{in}$, infinite resolution...) have a $DQE = QE$. For a real system, the DQE is equal to the QE of a perfect detector, which would give the same image statistics for the same input flux [7].
In conclusion, for an imaging detector, the DQE is best with:

- small detector noise σ_{dno},
- high quantum efficiency QE,
- high input signal $\overline{S_i}$,

as expected.

1.2.2.2 The dependence of the DQE on the spatial resolution

Figure 1.14 : *0.1 mm thick engraved lead line pattern used to test the spatial resolution of detectors*

The properties given in the previous section do not show the influence on the detection efficiency of the spatial resolution of the detector. Indeed, it is well known that detectors have a "limited resolution", meaning they cannot resolve objects smaller than a certain size. This characteristic of the detector is also known as the *Position Resolution*.

Several mechanisms can decrease the spatial resolution of one detector

The Position Resolution of one detector

In a position sensitive detector, there is a shift between the incoming position and the detected one of a particle. This is due to pixel size, as well as by charge spread and parallax errors. The spatial resolution gives information on the accuracy of the position given by the detector.
It is best measured with the *Modulation Transfer Function* (M), which gives the system response to a *sine-wave spatial-frequency amplitude*. In other words, the modulation transfer function gives the spatial frequency response of an imaging system or a component.
the modulation, Mi, of the image divided by the modulation of the stimulus Mo
M at a certain spatial frequency ν is defined as the ratio of the modulation of the image at output and input:

$$M(\nu) = \frac{Modulation_{out}}{Modulation_{in}}$$

with $Modulation = \frac{I_{max}-I_{min}}{I_{max}+I_{min}}$, in analogy with Michelson's definition of visibility of interference fringes.
It enables to evaluate easily the response of a complex system as simple *product of the individual MTF's* of the components of the system. For example for a classical Fluorescent screen + Optic +

CCD camera, the MTF would be given by:

$$\mathbf{M} = M_{Fluo.Screen} \cdot M_{Optic} \cdot M_{CCD}.$$

The MTF allows to calculate the **output signal**, which is basically the **input signal multiplied by the MTF**.

Contrast Transfer Function

In practice yet, it is much easier to measure the *Contrast Transfer Function* (C) defined as the *square wave spatial frequency response*. It is related to M by:

$$\mathbf{M}(N) = \frac{\pi}{4}[C(N) + \frac{C(3N)}{3} - \frac{C(5N)}{5} + \frac{C(7N)}{7} - \ldots] \tag{1.4}$$

where N is the signal spatial modulation frequency in 'line pairs' per unit distance.
In practice, one uses masks with several patterns of lines (see 1.14 of various spaces and thickness to evaluate the detector response. The resolution is given by the smallest pattern distinguishable by the detector.

Line spread function

NB. In the same way one can define the *Point spread function*.
This is the response of the system illuminated by a narrow slit (or small point). It is related to M by the 'simple' Fourier Transform:

$$\mathbf{M}(\nu) = \frac{\left| \sum_{k=-\infty}^{+\infty} LSF(k\Delta x) e^{-i2\pi\nu k\Delta x} \right|)}{\left| \sum_{k=-\infty}^{+\infty} LSF(k\Delta x) \right|} \tag{1.5}$$

So the LSF basically gives the detector response as function of the spatial frequency of the image.
Here again it is easy to measure experimentally for it is enough to measure the response of a detector to a mask.
In most cases, the LSF (or PSF) can be very well described by a Gaussian. It is then fully described by the standard deviation σ_{det} (considering that the gaussian is centered at the point/line entry). σ_{det} is often called (a bit abusively) *position resolution*.
One can also notice that from the PSF one can determine the output intensity:

$$I_{out}(x, y) = PSF(x, y) * I_{in}(x, y) \tag{1.6}$$

where $*$ is a convolution.

The dependence of the DQE on the MTF

The dependency of the output intensity from the spatial frequency (cf. the relation between the MTF **M** and the contrast transfer function) is taken into account in the DQE. This corresponds to a dependency of the DQE on the MTF, which fully describes the response of the detector as function of the spatial frequency.

To take into account the impact of the noise in the frequency domain, one has to consider the power spectrum of this noise, also named Wiener Spectrum[3]. This notion enables to write, in analogy with the definition of the DQE, its dependence on the frequency:
The dependence of the SNR_o from the MTF can be written as [9]:

$$DQE = \frac{\frac{\overline{S_o}^2 MTF^2}{N_o^2}}{SNR_i} \tag{1.7}$$

with N_o^2 being the noise power spectrum, and SNR_i the signal to noise ratio at the input ; SNR_i corresponds to the inherent fluctuation of the signal at the input, and is often considered to follow a poisson statistics (like was done in section 1.2.2.1). MTF as well as N_o are functions of the spatial frequency.
Details on the dependence of the DQE from the MTF and noise are given in [10].

1.2.3 The mode of operation, speed and behavior of one detector at large intensities

Integrating vs. Counting detectors

There are two modes of operation of detectors, which differ on two approaches to evaluate the intensity of the measured signal:

- Counting detectors, which count the deposited quantas of energy one by one ;
- Integrating detectors, which accumulate the deposited energy before it is evaluated.

While counting detectors have been around for a while (for example, the *Geiger Muller Counter*), most of the detectors used nowadays are based on the principle of integration of the signal.

In an integrating detector, the charge deposited by the particle(s) is accumulated (integrated) over a period τ. The measurement of the intensity is obtained from the height of the signal obtained.
The maximum amount of energy the detector can accumulate before the signal is measured corresponds to the maximum intensity the detector can measure (saturation level). This maximum intensity is often limited by physical processes in the detector.
The frequency at which the image is read gives the *frame rate* of the detector. In the case of area detectors, the frame rate is typically of a few 10 of hertz / cm^2.

In a counting detector, each electrical pulse (corresponding to each particle) will be counted if it is above a predefined threshold. The intensity is given by the number of single events, which were counted during the period τ.
The maximum intensity the detector can record is limited by the detector's *maximum count rate*, which is the maximum number of pulses, which can be recorded. Modern electronics allow count rates as high as several megahertz.

[3]The power spectrum is the average power of the spectrum of the signal/noise in a unitary bandwidth centered at the frequency f.

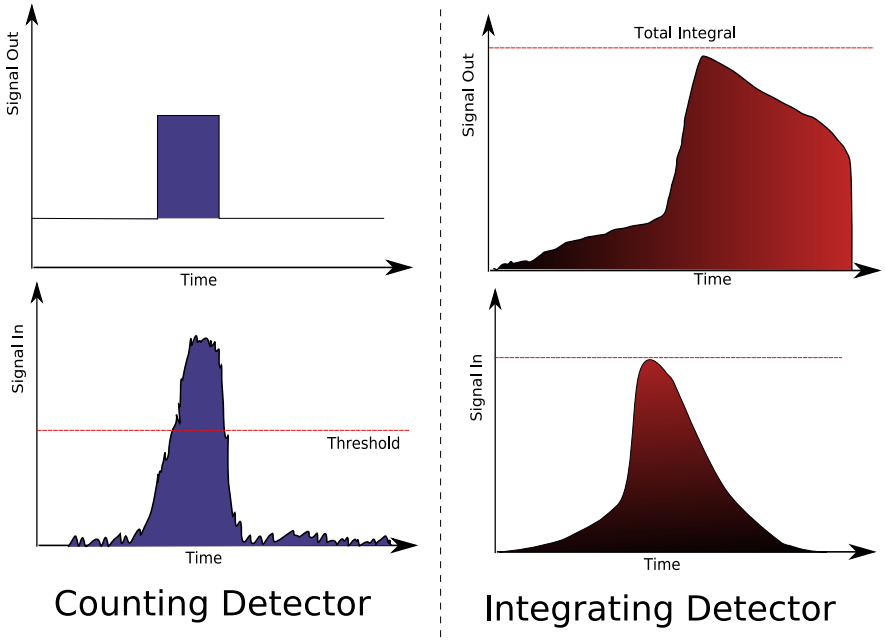

Figure 1.15 :
Signal as analyzed by an *integrating detector* and a *counting detector.*

Counting detectors are considered as superior (especially for flat field detectors) because of their very low noise (the threshold enables to discriminate real events from noise) and ability to count single events. Theoretically those detectors are almost noiseless...
This is their higher cost (both for development and manufacturing) as well as the limitation of the electronics, which have limited their use so far: counting detectors could not answer the needs in terms of speed. Recently, the fantastic developments in terms of integration and speed of electronics has made it possible to develop fast detectors with high dynamics and low noise. Now counting detectors can compete in terms of speed (count rate) with integrating detectors.
In practice yet, counting detectors are not always better. So, as a compromise, some systems try to adapt their modes of operation according to the incident flux, in order to offer the best efficiency (DQE -detective quantum efficiency- see 1.2.2) [11].

Dynamic range

The dynamic range is the range of intensity the detector can measure: *[min Nb Quanta;Max Nb Quanta]*.So it is the *signal to noise ratio*, computed from the greatest signal acceptable by the detector:

$$Dynamic = \frac{Max\ Intensity}{Noise} \tag{1.8}$$

In the case of integrating detectors: the max intensity corresponds to the maximum signal measurable

in each picture, while Noise correspond to the detected intensity in the case of no intensity coming on the detector.

In the case of counting detectors, the dynamic is the maximum count rate over the dark count rate, which is the mean frequency of appearance of fake events (count rate recorded at zero intensity).

Associated to those definitions, there are a few notions of importance to evaluate the performances of one detector:

Differential/Integral Non Linearity

The differential and integral non linearities (DNL and INL) measure the dependence of the detector response as function of the signal intensity. The perfect detector has a constant DNL: $\frac{\partial Response}{\partial Intensity} = Cte$ (and a linear INL: $Response \propto Intensity$).
Deviations are always present but can be corrected (eventually pixel by pixel in the case of position sensitive detectors) afterwards.

The maximum intensity a detector can accept is limited by the so called *dead time* τ of this detector. The dead time enables to measure the minimum time during, which a detector cannot record another event. Theoretically, the maximum frequency of events the detector can accept is $\frac{1}{\tau}$.
But there are two behaviors when successive events occur in a time inferior to τ (see Figure 1.16.

Dead Time Behavior

The dead time of one detector is the gap of time after one event was recorded when the detector is unable to record another event. This minimum time between consecutive events can come from limitations in the electronic of the detector, or from by physical processes in the detector itself.

For the income of photons on the detector is a random process, the probability that real events can be lost is non zero. This limitation can be severe in the case of high flux, as a large number of events are separated by a gap of time inferior to the dead time of the detector. There are two important models for dead time behavior of the detector:

In the case of a non paralyzable behavior, the detector is able to count a new event immediately after the dead time of the first event is finished. In this case at high intensity, the detector records events every τ, and a asymptotic saturation of the recorded signal occurs.

In the case of a paralyzable behavior, if two events occur successively in a time inferior to τ, then the dead time is prolonged of a value τ from the second event. In the case of high intensities, the average time between events becomes shorter than τ, and no event can be recorded until two successive events have a time separation superior to τ. The saturation appears then as a decrease of the recorded signal.

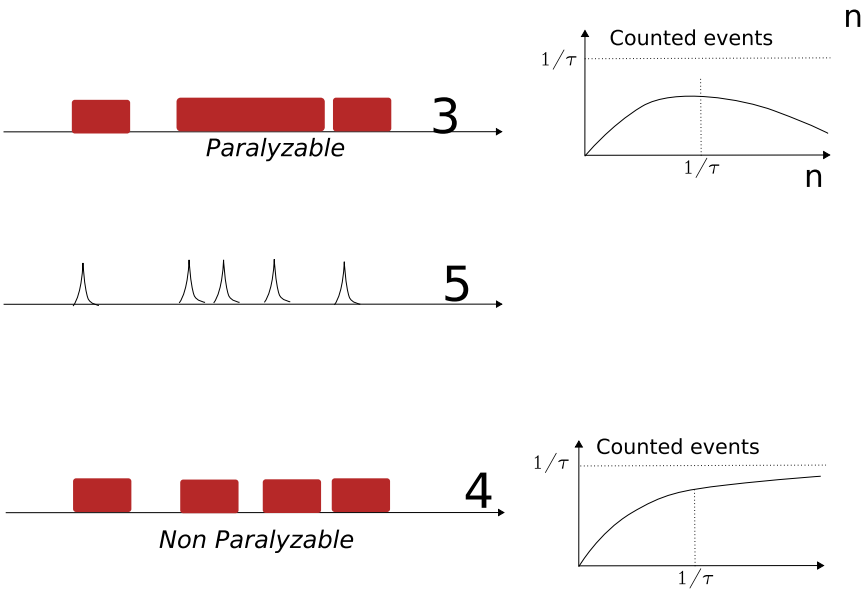

Figure 1.16 : *The paralyzable and non parlyzable behaviors of detectors.*

1.3 Spectroscopy detectors

Spectroscopy detectors focus on high energy resolution. Most often they are position non sensitive detectors, even if some of the technologies used for imaging detectors can offer energy resolution. For the most important characteristics of spectroscopy detectors are their energy resolution and noise, they often come with complex cooling system, which guaranties a minimum noise.
There are various types of technologies for spectroscopic detectors, corresponding to various energy ranges. In X-ray photon science, the most typical detectors are based on technologies such a:

- Solid state detectors such as Silicon Drift Detectors, silicon crystals doped with lithium (Si(Li) detectors) or high purity germanium (HPGe)
- Scintillation based detectors with various scintillation materials depending on the energy range.

Photodiode type detectors

In general, they consist of a p-n depleted region where electron-pairs are created by the incident photons. Then a reverse electric field separates the charges, and a fast current pulse is recorded in the built-in electronics. They offer a very high speed, and a good energy resolution (only 3.5 eV are required for the creation of an electron pair in Si). Unfortunately, the small size of the depletion area and the easy recombination of the charge pairs lower the quantum efficiency of the photodiode to a very small value.
`PIN photodiodes` are an evolution of the photodiodes. They are based on the same principle, except

that the depletion zone is made much larger with the use of an undoped layer between the N and P zones. Still the lack of internal multiplication of the charges makes them unsuitable for low photon flux experiments even if they offer a good quantum efficiency at low energies. Several suppliers of PIN diodes are now available[4].

`Avalanche Photodiodes` (APD) are other cousins of the photodiodes: they combine a thick (130 μm) low field zone combined on both sides with a thin strong electric field p-n-junction. A precise control of the doping levels makes it possible to have a rather large central depletion zone to ensure a good quantum efficiency, and side electric fields strong enough to enable an internal multiplication of the charges with gain up to 10^4. Arrays of APDs making relatively basic 2D detectors are now commercially available (sizes up to 1 or 2 cm^2) [5].

APDs find more and more domains of applications. Unfortunately they cannot be produced in large areas (Si based technology).

Germanium detectors

Germanium detectors are based on the same principle as photodiodes, except that they use germanium instead of silicon as semiconductor. This enables the creation of very large depletion zones (cm vs.mm) and so betters dramatically the efficiency for high energy particles. Their higher intrinsic noise makes the use of liquid nitrogen cooling system almost mandatory[6].

Si(Li) detectors

The introduction of lithium as a dopant is a way to create an intrinsic like zone (donors and acceptors exactly compensate) in the semiconductor. This enables the creation of a much larger zone for pair creation, such increasing the quantum efficiency for high energy rays[7].

Figure 1.17 : *A Photodiode used to monitor the beam intensity in its protecting case.*

[4] Among them, Hamamatsu, Canberra, Eurisys, Centronic, Sintef, Ontrak...

[5] again several suppliers: Perkin-Elmer Corporation, Hamamatsu Photonics, Judson technologies. Arrays by Pacific Sensor, Perkin-Elmer...

[6] Provider of Ge detectors component: Canberra, XIA electronics...

[7] company supplying: e2v scientific instruments...

Scintillator detectors

Figure 1.18 : *A Cyberstar scintillator based spectroscopy detector, and its electronics.*

Scintillation materials convert high energy photons (or the energy deposited by other particles) into visible, UV or infrared light. The intensity of the light produced is proportional to the energy deposited over a wide range of energy (the usual unit is [photons/MeV]), thus enabling a simple intensity measurement to determine the energy of the incoming photon. Yet this approach suffers some limitations, which limit its use for spectroscopy applications:

- For the intensity is proportional to the deposited energy, it is hard to use a scintillator in the case of large numbers of incoming photons.
- Scintillators providing a good yield, also suffer from a long response time, which is another limitation to the dynamic range of those detectors.

Yet, photomultipliers tube, which provide an excellent efficiency to collect the weak light emitted from scintillators, and convert it into an electrical signal, have made this approach a prime choice for spectroscopy applications for a number of decades.

Conclusion

Current spectroscopic detectors mostly suit the current needs of the scientific community. New developments now go in the direction of area detectors, and speed in order to enable new types of experiments.

1.4 Imaging detectors

Imaging detectors include all line or area detectors. They are used both for imaging applications, and to speed up the collection of data (with respect to a dimensionless detector, which would move to cover the same area). This goes beyond a simple speed up of the whole experiment, for a lot of samples, and in particular biological samples, suffer from long exposure into the beam. So imaging detector can be an absolute necessity in certain fields in order to guaranty a good quality of data.

Imaging Detectors are the kind of detectors which need most of the developments in order to satisfy the requirements of the experiments that scientists want to carry out nowadays.

1.4.1 current mature technologies

CCD based detectors

CCD detectors consist typically of a 2 dimensional arrays of silicon wells of a few 10's of μm, which store the charges created by light absorption. After this charge was accumulated, it is read out sequentially with use of an integrated amplifier. They exhibit a very wide spectral sensitivity with attractive quantum efficiency characteristics, but also present a large noise background. They are typically used in photo-cameras, video-cameras, scanners, and other massively produced devices. As such they are rather inexpensive, except in the case of very fast and large area components.
When used with hard X-rays, they are usually coupled with a fluorescent screen, which converts X-rays into visible light. An optical system (based on common optics elements or on optical fibers) is often used to reduce the fluorescent screen size to that of the actual CCD system.
CCD systems[8] are nowadays one of the best way to achieve both large areas (eventually by coupling several systems) with a high speed readout[9]. Unfortunately the optical system, and especially the fluorescent screen largely degrade to resolution of those systems. In addition those systems present an intrinsic high noise as compared to other technologies of detectors, which reduce their domains of application.
Ongoing developments focus on new scintillator materials used to convert X-rays into visible light. Thinner layers would increase the resolution especially with high energy photons, and faster scintillators would enable higher frame rates. Also faster electronics are being developed, as it is also a limitation to the frame rate of cameras.

[8] various systems used in the synchrotron world. Some examples: Dalsa-Medoptics CCD, Hamamatsu Photonics, Philips, GE Medical Systems, The FRELON system developed at ESRF[12]...

[9] Typical systems offer readout speed of a few seconds (up to 15), but new highspeed systems are able to have frame rates as high as 20Hz.

Figure 1.19 : *A CCD camera from the* MAR Company *with its optical coupling system visible.*

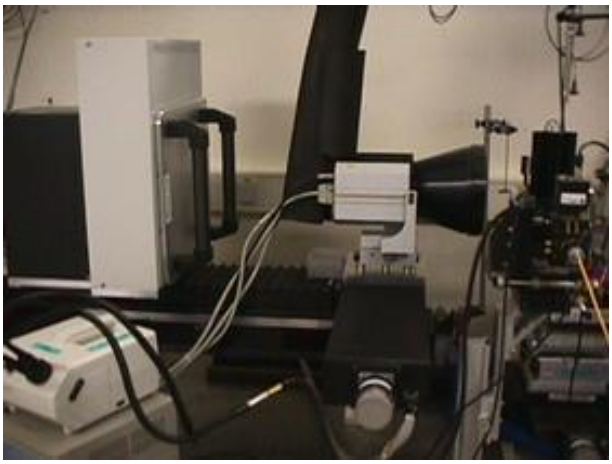

Figure 1.20 : *The image plate* MAR 345 *detector.*

Image plates

Image plates[10] (sometimes called *memory phosphors, storage phosphors or photo stimulated phosphors*) are based on thermoluminescent materials, also referred to as *thermoluminescent dosimeters (TLD)*. In this type of materials, the absorption of the incoming ionizing particle leads to the creation of electron-holes pairs, which are trapped in purposely introduced defects in the crystal. So the material acts as an integrating detector, in which the number of "stored" electrons and holes in the defects of the crystal, reflect the intensity of the incoming beam. To obtain the image, energy has to be provided so that electrons and holes can escape from the traps and recombine, giving a luminescent signal. So classical systems consist of a laser scanning the plate after the acquisition, an optics (usually an array of optic fibers), which collects the luminescent signal and a photomultiplier or a avalanche photodiode to collect the signal.
Image plates are available in very large areas (the mar345 is as large as 300 mm in diameter), and offer a large dynamics. Their drawbacks lie mainly in the presence of noise, and in their very limited speed (the plate has to be scanned to readout the image and typically several minutes are needed per image).

Gas-filled detectors

Gas-filled detectors use a gas both for the absorption of the ionizing radiations, and for the amplification stage of the signal (electron multiplication). This is now a mature technology, which is still interesting because of the major advantages it offers. Unfortunately, gas-filled detectors also suffer from certain drawbacks, which prevent their generalized use nowadays.

A more extensive description of gas-filled detectors is given in the section 2, as well as the description of this project, which aims in overpassing their limitations.

[10] Mar produces the most common image plates used in the synchrotron world, especially in Macromolecular crystallography.

1.4.2 technologies under developments

1.4.2.1 Spectroscopy Detectors under development

Development focus on new technologies such as *Silicon Drift Detectors* in which the created charges drift in a high resistivity, fully depleted silicon wafer. Electrons are collected on the edge of the detector. Those detectors enable the measurement of simultaneous events occurring at different places of the detectors, by being able to distinguish several rise times of the collected charge.
Already used techniques explained in the previous section are also under permanent development.
Also multielement detectors are being developed to offer higher count rates capabilities and larger surfaces.

1.4.2.2 Imaging Detectors under development

CCD detectors and image plates are currently the most common imaging detectors. CCDs are used when high speed is mandatory, while image plates offer large areas as well as a very good dynamic.
To answer the growing needs of the imaging community, strong progress have to be achieved in the domains of dynamics, noise, and readout speed.
So the next step for imaging lies in the use of detectors operated in counting mode with a massively parallel electronics (meaning each pixel is connected to a built in electronics where the first stage of amplification and signal processing is performed, before the image is read out). This new approach is possible thanks to the recent developments in the semiconductor industry, which offers components small enough for this level of integration.

This approach will force the use of other technologies, for current CCD based systems as well as image plates cannot be used in counting mode: the physical processes involved in the detection are too slow to enable this approach (fluorescent materials as well as thermoluminescent materials have decay time constants which are incompatible with single photon counting). So systems using a direct conversion of the photon into the electric signal must be used (instead of a several steps conversion system like in fluorescent+CCD or trapping+luminescence+photomultiplier). The 2 major possibilities are the use of solid materials (Pixel and amorphous selenium detectors) or gas amplification based systems (using the photoelectric effect to produce the initial charge).

Pixel detectors

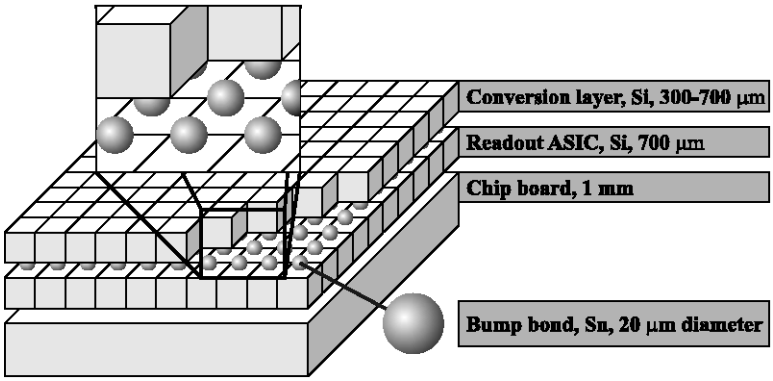

Figure 1.21 : *Schematic of pixel detectors.*

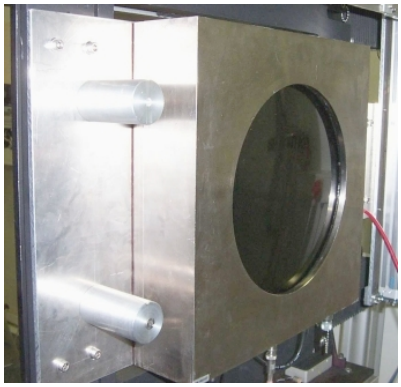

Figure 1.22 : *A large area Gas Filled detector.*

Photon-counting pixel detectors arrays are hybrid devices made of a semiconductor sensor connected to a parallel CMOS readout circuit. The sensor is a Silicon (or another semiconductor) die with a pixel electrode structure connected to the CMOS circuit by bump-bonding flip-chip technology (see 1.21). The sensor is fully depleted by applying a sufficient voltage bias. The photoelectric charge created after X-ray absorption in the sensor is collected to the closest pixel of the CMOS circuit along the bias field. Each pixel acts as an independent particle detector, including a complete pulse processing chain as well as an event counter.
This kind of detectors currently achieves the best performance in terms of speed, and resolution. Unfortunately, only small sizes can be manufactured yet[11], and for large areas, arrays of detectors have to be assembled. This results in inhomogeneities, which have to be compensated and dead zones. The leading projects in this field are *Pilatus* (developed at the Paul Scherrer Institute (SLS detector Group) in Switzerland [13, 14] and the MaxiPix project developed by the Medipix consortium [15]. Here again, the integration of the readout electronics is a challenge!

Amorphous selenium/silicon detectors

Amorphous semiconductor detectors are based on the liquid crystal display technology. Essentially, they are a matrix of capacitances charged (or discharged) by the current generated in the X-ray irradiated amorphous semiconductor (often selenium). The charge is read by the TFT transistor switches present at each pixel capacity. The main difficulty lies in the availability of a good quality material, to permit the drift of the created charges to the transistors.
They are integrating detectors.

Gas-filled detectors

Very few technologies currently offer perspectives for large areas, especially in the case of fast detectors (used in counting mode, with low noise...).

[11] typically $14 * 14\ mm^2$

Gas-filled detectors can offer a solution. More details on gas detectors, and on the link of this project with gas detectors are given in the next section.

Bibliography

[1] ESRF, "European synchrotron radiation facility long-term strategy," tech. rep., ESRF, 2006. http://www.esrf.eu/AboutUs/Upgrade/.

[2] Albert Thompson et al., *X-Ray data booklet*. Lawrance Berckley National Laboratory, available at http://xdb.lbl.gov/ ed., 2001.

[3] G.F.Knoll, *Radiation Detection and Measurement*. Willey, 2000.

[4] G.Zanella et al., "The detective quantum efficiency of an imaging detector," *Nucl. Inst. and Meth. A*, vol. 359, pp. 474–477, 1995.

[5] G.Zanella et al., "The role of the quantum efficiency on the dqe of an imaging detector," *Nucl. Inst. and Meth. A*, vol. 381, pp. 157–160, 1996.

[6] S.M.Gruner et al, "Charge-coupled device area x-ray detectors," *Review of Scientific Instruments*, vol. 73,8, pp. 2815–2842, 2002.

[7] C.Ponchut, "Characterization of x-ray area detector for synchrotron beamlines," *Journal of Synchrotron Radiation*, vol. 13, pp. 195–203, 2006.

[8] C.Ponchut et al., "Experimental comparison of pixel detector arrays and ccd-based systems for x-ray area detection on synchrotron beamlines," *IEEE Trans. Nucl. Sci.*, vol. 52,5, pp. 1760–1765, 2005.

[9] W.Hillen et al., "Imaging performances of a digital phosphor system," *Med.Phys.*, vol. 14,5, pp. 744–751, 1987.

[10] J.P.Moy, "Signal-to-noise ratio and spatial resolution in x-ray electronic imagers: Is the mtf a relevant parameter?," *Med. Phys.*, vol. 27,1, pp. 86–93, 2000.

[11] R.H.Menk et al, "Novel detector systems for time resolved saxs experiments," *J. Appl. Cryst.*, vol. 33, pp. 778–781, 2000.

[12] J.C.Labiche et al., "Frelon camera: Fast readout low noise," *ESRF Newsletter*, vol. 8, no. 25, pp. 41–43, 1996.

[13] C.Broennimann et al., "The pilatus 1m detector," *Journal of Synchrotron Radiation*, vol. 13, pp. 120–130, 2006.

[14] "Pilatus website." http://pilatus.web.psi.ch/.

[15] "Medipix website." http://medipix.web.cern.ch/MEDIPIX/.

Chapter 2

The basics of gas-filled detectors

2.1 historical background

The history of gas-filled detectors starts around 100 years ago when Rutherford and Geiger (working at the Manchester University) discovered electron multiplication gas-filled tube with a thin wire at the axis position.
In 1928, Geiger and Mueller introduced the well known (and still used!) *Geiger Tube*, one of the oldest type of ionizing particle detector. The *Geiger Counter* was the first electronic ionizing particle detector.

Later, in the Manhattan Project [1], the gas-filled detector technology was largely improved. The multiple wire proportional counter (MWPC) was invented. It was later implemented in high energy physics by Georges Charpak, and revolutionized this field of physics.

Figure 2.1 : *A modern Geiger Mueller Counter.*

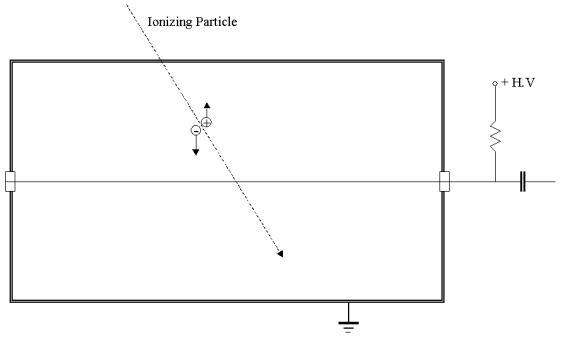

Figure 2.2 : *Schematic of the Geiger Mueller Counter.*

Nowadays, gas-filled detectors are used in a large variety of research fields as well as for various

industrial applications. They are routinely used for the detection of fast and heavy particles (high energy physics), for the monitoring of nuclear facilities and other radioactive environment, for photon detection and imaging (medical applications, non destructive analysis), etc...

2.2 Principle of gas-filled detectors

A detailed description of modern gas-filled detectors can be found in G. C. Smith's article [2]. A deeper analysis of the principles of gas filled detectors (with delay lines) is in A.-M. Petrascu's article [3]. Status of development of gas-filled detectors at the ESRF (giving more details on the specificity of gas-filled detectors used in the synchrotron radiation world) is found in M.Kocsis article [4].
In a gas-filled filled detector, the gas is used for two purposes:

- First it absorbs a fraction of the energy of the incoming photon/ionizing particle. In result of this interaction, one or several electron-ion pairs are created (ionization of one particle of the gas).
- Secondly, an internal multiplication of the electrons. This internal multiplication (typically a gain factor of 10^4 to 10^5) is sufficient to enable each photon to be directly and separately counted by some electronics.

2.2.1 The X-ray absorption in the gas

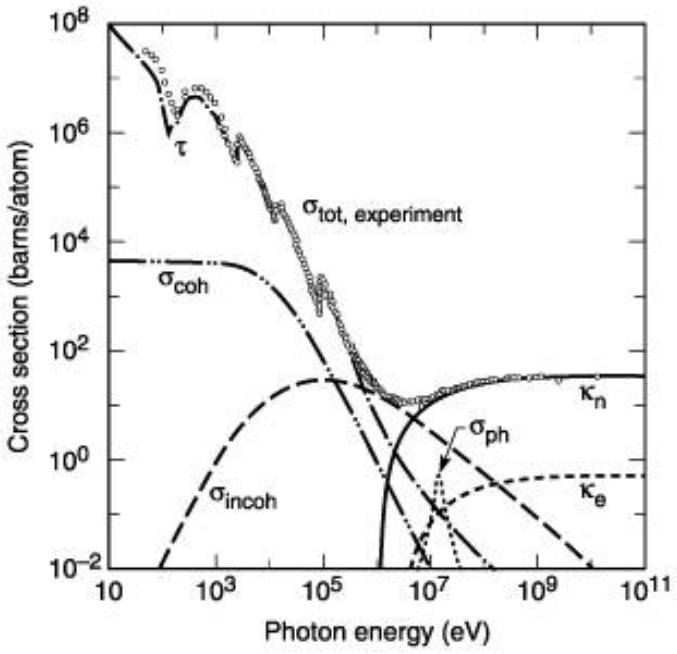

Figure 2.3 : *The cross sections of various interaction processes in the case of Lead.*

In a gas-filled detector, the first function of the gas is to absorb part of energy of the incoming photon to create an electron, as a base of the electric signal.

In the case of the travel of one X-ray photon through matter, several of sorts of interactions can occur between this photon, and the atoms (in our case those of the gas), but mainly three are of importance for photon measurements (see Figure 2.3): *the photoelectric absorption* (τ in Figure 2.3), *the compton scattering* (σ_{incoh} in Figure 2.3), and *the pair production* (κ_n *and* κ_e in Figure 2.3). The later one can occur only in the case of highly energetic photons (more than 1.02 $MeV = 2 * Mass_{electron}$, more often called gamma rays), so it will not play any role in the case of low energy X-rays.
The two other govern the law of absorption of the photon in the gas. Their respective probability is measured by their respective cross sections, which in general depends on the element, the density and the energy of the photon.
The photoelectric effect is dominant for energies up to a few 100s of keV depending on the element atomic number. Then Compton scattering becomes increasingly important, until it is dominated by pair-creation.

Compton Scattering

The interaction process of Compton Scattering takes place between the incident X-ray, and an electron in the gas. It is an elastic scattering process. The photon is deflected through a certain angle θ with respect to its original direction, while leaving part of its energy to the electron, then called *recoil electron*. The energy deposited depends on the angle of deflection, and is increasing with θ.

Photoelectric absorption

The photoelectric process is the very process at the source of the electron production in the gas. When a photon is absorbed by an atom following such a way, its energy is in fully transferred to an electron, ejected by the atom from one of its bound shells. The result is the creation of an electron-ion pair, with the electron energy being $E_{e^-} = h\nu - E_b$, where E_b is the binding energy of the photoelectron in the original shell.
In the case of X-rays, the most probable absorption occurs with electrons from the inner shells. Shortly after the photoemission process, there is a rearrangement of the electrons inside the atom, or the absorption of a free electron from the medium. Either one (or more) characteristic X-ray photons may be emitted, or an Auger electron will be created to enable the excited ion to reach a more stable state. In the case of an X-ray photon re-emission, this photon often is reabsorbed via photoelectric effect, such creating another electron in pair, but with less energy.

2.2.2 The amplification and the modes of operation of gas-filled detectors

The internal amplification of the signal

After the first ionization of a gas particle occurred (by the incoming detected particle), the created electron is thermalized and under moderate fields, the gained energy is lost in collisions with the gas molecules. In the regions where the gained energy *between two collisions* is exceeding a certain level (typically $\sim$ $35eV$), it becomes a ionizing particle, which will later ionize another gas particle, creating a second electron, and finally leading to cascade of ionization (as secondary electrons are

produced).
The amplification of the signal will then depend on several factors such as

- The type of gas,
- its density,
- the accelerating electric field and its shape.

This leads to various *Modes of operation*, which are classified for a certain gas, as function of the applied electric field.

Modes of operation of gas-filled detectors

Depending on the applied accelerating potential, various modes of operations of gas amplification are distinguished. The Figure 2.4 (extracted from [5]) gives the amplitude of the signal collected after the absorption of a particle and the corresponding amplification modes. The two curves correspond to two different amounts of energy deposited in the gas. The result with two X-rays of different energies would be alike.
The different modes of operation of gas amplification are:

Recombination region When the electric field is very low, the field is insufficient to prevent recombination of the ions pairs. The current collected on the electrodes is very low, as only the fraction of the created ions pairs, which did not recombine is collected.

Ion Saturation From a certain value of applied voltage, the electric field is strong enough to effectively separate the charges created after absorption of the energy of the ionizing particle. Then almost all pairs are collected and the intensity corresponds to the rate of creation of charges in the volume of the detector.

Proportional region When the applied tension is further increased, the mean energy gained by electrons between collisions is higher than the ionization energy. From this moment an amplification of the signal occurs. For a certain tension, the intensity collected is *proportional to the original number of ions pairs created*. This is the region of true proportionality.

Limited proportional region and Geiger mode Higher electric field result in the apparition of non linearities: when the electric field becomes very strong, the amount of charges present in the gas becomes high enough to alter severally the electric field resulting from the applied tension. Eventually, this *Space Charge* can become completely dominant and fully determine the pulse shape. This last mode is the Geiger mode of operation of the detector.

In order to avoid a dependence of the amplification on the localization of the deposited charge in the detector chamber, and to improve the stability of the system, the strong electric field is applied only in a thin region of the chamber. In the rest of the chamber, where electrons are created, only a drift field is applied. This also limits the spread of the electron cloud (going exponentially with distance), which occurs during the multiplication and limits the loss of resolution while preserving an absorbing area sufficiently large.

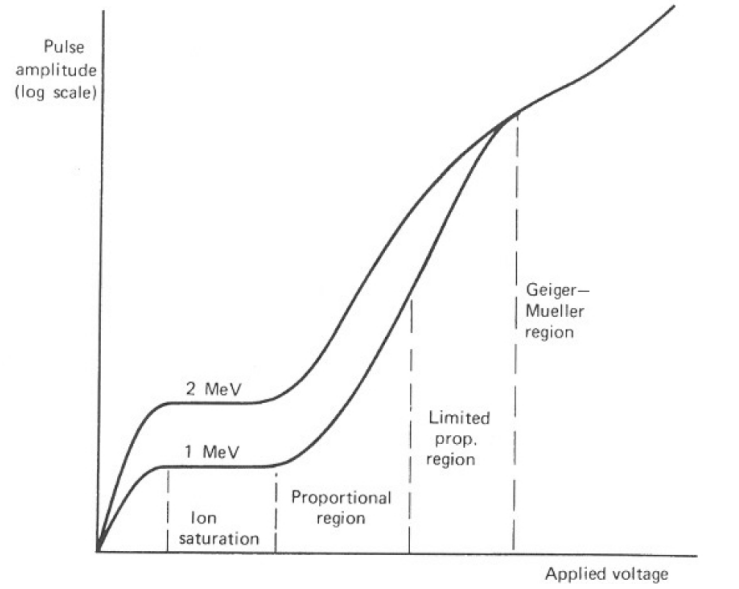

Figure 2.4 : *Regions of operation of gas-filled detectors for two deposited energies.*

Usually the collection of the electrons is performed with a 2D array of wires, which enables proportional amplification mode (the so called *multiwire proportional counters* introduced by Charpak and coworkers in 1968 [6]).
Classical gas mixtures are composed of Xenon, Krypton, Argon, Methane, CF_4 etc... (see [2]).

2.2.3 The benefits of gas-filled detectors

The main advantaged of gas-filled detectors as compared to the previously described types of detectors are:

- their intrinsic speed mainly limited by the electronics
- their dynamic range, also limited by the memory depth
- their available size (among the largest detectors)
- their cost of development and manufacturing
- their easiness of operation, and robustness.

Gas detectors find domains of applications in most fields of photon science. They are some of the very few types of detectors, which can be built in very large areas. In the high energy physics experiments, it is common to find detectors of several square meters, and covering solid angles of almost 4π.

2.2.4 The limitations of gas-filled detectors

Main limitation

As compared to other technologies of detectors, gas-filled detectors suffer mainly from one disadvantage, which made them almost abandoned in whole fields of photon science: `They have an`

`intrinsic low quantum efficiency`, they leave a great number of incoming particles undetected (said another way, they are *photon hungry*).

This is simply due to the very low density of gases, and so very low stopping power. To overcome this, it is possible to increase the pressure of the gas, but this is at the expense of amplification characteristics, which are best at low pressures...

They also suffer from sever parallax error leading to a loss of resolution as soon as the incoming particles do not have a direction perpendicular to the detector (see Figure 2.5).

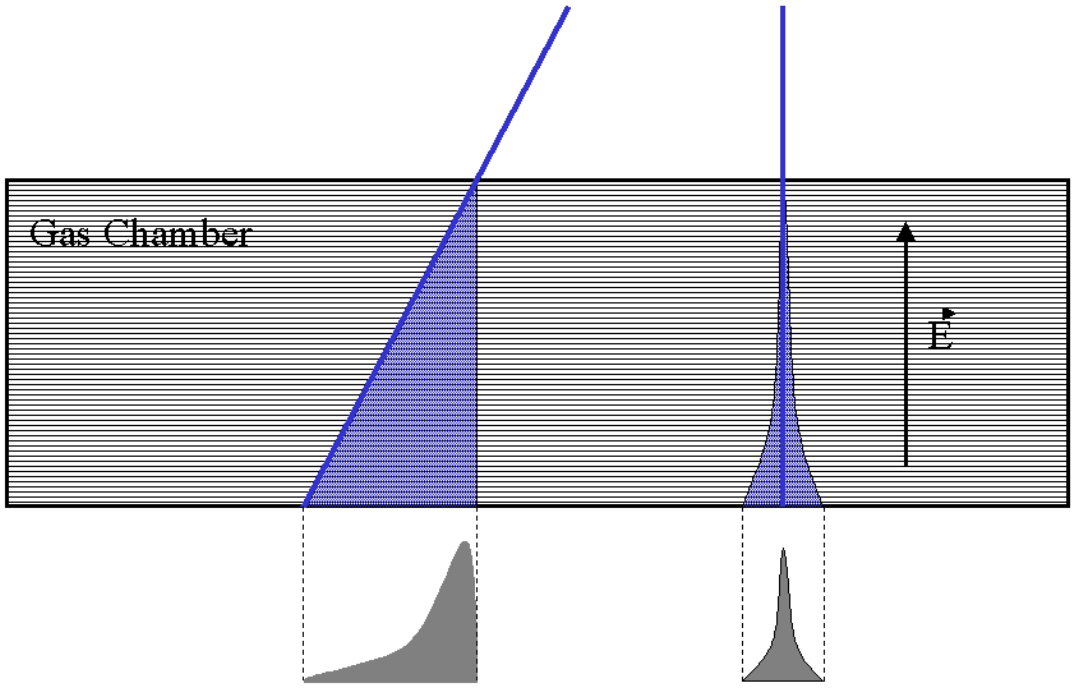

Figure 2.5 : *Parallax error is the loss of resolution due to the absorption of non perpendicular photons all along the depth of the ionizing chamber, thus broadening the position response of the detector.*

So when considering their application in photon research, other technologies less photon hungry are usually used, even if they offer poorer performances in most other characteristics.

other limitations Another weakness is linked to the use of wires to collect the charges after multiplication (MWPC). The small radius of those wires makes them very sensitive to discharges in the detectors (more likely with increasing acceleration voltages/gains). It is indeed very difficult to repair broken wires in the detector. In addition the broken wires are likely to create short circuits and create further damages).

Modern gas-filled detectors overpass this by using microstructures in place of the traditional wires.

2.3 Recent Evolutions of gas-filled detectors

There has been various recent evolutions of the classical gas-filled detectors to overcome their weaknesses and keep their advantages.
The main attempts of improvements of gas-filled detectors over the last few years have been stripped detectors, as well as hybrid gaseous multipliers. Interesting Parallax Reduction Techniques were also introduced.

Parallax reduction techniques

The simplest technique to reduce parallax errors, is to build a curved detector. This technique has been successfully used at ESRF ([7]) and later at the Rutherford Appleton Laboratory ([8]). In addition it largely suppresses the charge spread problem.

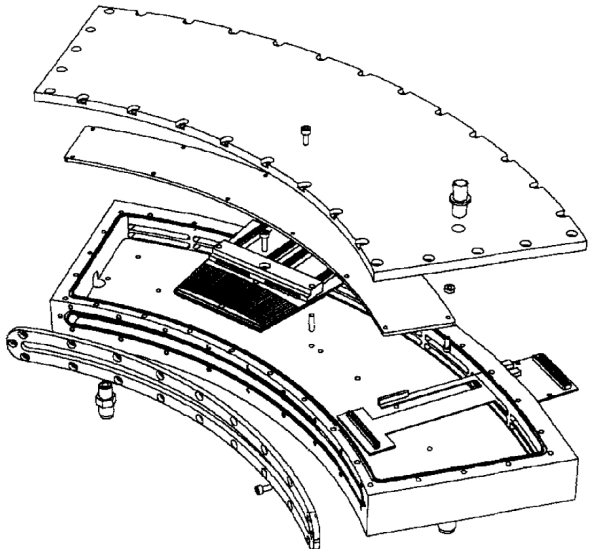

Figure 2.6 : *Curved gas-filled detectors do not suffer from parallax errors.*

Other methods of correction such as off line correction by determination of the X-ray absorption depth were also demonstrated ([9]) but never used in the synchrotron world.
For area detectors, solutions to reduce parallax were offered very early after the idea of MWPC was published. Charpak's group at CERN proposed to add a spherical drift chamber to the front of the MWPC [10]. This idea was successfully applied to a working device, which became the workhorse of the synchrotron LURE in the 80's ([11]). The idea was then bettered in the late 90's [12].

Micro-Pattern

Strip detectors are an answer to the fragility of MWPC's wires and limited amplifications characteristics (limited by space between wires). They also permit to avoid the difficult manufacturing of the chambers (to place the wires of the chamber).
A large number of structures have been proposed over the last 20 years such as micro-strip gas

chambers [13], the microgap chamber [14], the compteur à trous [15], the gas electron multiplier [16], the micro-mesh gaseous structure [17], or the micro-pin array [12].

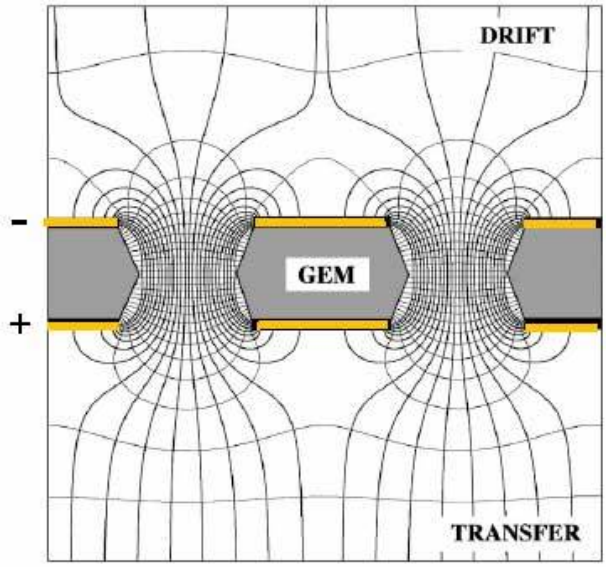

Figure 2.7 : *GEMs are thin metal-clad polymer foils pierced by a high density of holes. On application of a difference of potential, between the two electrodes (sides) electrons drift and multiply in the holes.*

Among those detectors, GEMs (Gas Electron Multiplier) created the largest interest. Introduced in 1996 by F. Sauli and his colleagues from CERN [16], GEM's key feature is a three-layer (metal-insulator-metal) grid which is used both for the amplification of the signal, and for ion feedbacks prevention (to protect the photocathode, used to convert electrons). Several of such grids can be associated to increase the amplification of the system. Working devices were reported in various groups in the world and developments are ongoing to improve this technology. GEMs foils are routinely produced at CERN, and are now commercially available thanks to the company Tech-Etch Inc.[18, 19].

Resolution and speed improvements

The limiting factor of spatial resolution of the detector is the photoelectron range.

The center of mass of the produced electrons during multiplication reflects the position of the original ionization process, and so of the detected particle. Delay-line encoding or charge division methods are naturally determining the center of gravity of the electron cloud below the anode spacing. The speed of the above system is limited to *Mega counts per seconds* (Mcps) range. For example, the RAPID (Refined ADC Per Input Detector) system [20] developed at the Daresbury synchrotron in the UK, is able to determine the position of this center of mass by comparing the amount of charges on the different anodes reached by the cloud of electrons. As a result, the detector is able to position the original impact with a speed of 10^7 counts per second.

2.4 Gas amplification compared to Microchannel plates

Microchannel plates (MCP) are devices able to amplify signal with a very large gain in vacuum.

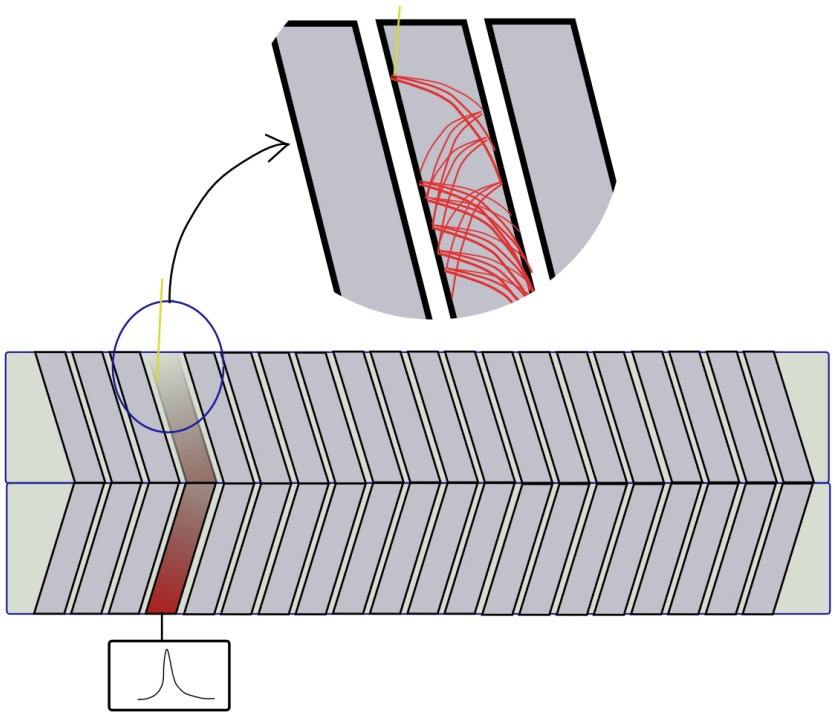

Figure 2.8 : *A two slab Micro Channel Plate (Chevron configuration)*

They consist of a thick slab of highly resistive material (glass, silicates) riddled with small tubes (diameter $\emptyset \sim 10\ \mu m$, and interspace $\leftrightarrow\sim 15\ \mu m$) leading one face to the other: *the microchannels*. The face of the tubes is covered by a continuous-dynode electron multiplier. The application of a strong potential between each face ($\sim 500\ V$) enables the acceleration of electrons in the tubes, which hit the surface of the tube, leading to an amplification of the signal as they create secondary electrons at each impact.
Modern MCPs usually consist of several slabs of MCPs with an angle between the successive tubes (chevron or V-like geometry). This geometry leads to a greater amplification for the same applied voltage, and to an excellent compactness.
Unfortunately, MCPs suffer from major problems:

- Especially for single events, the gain of MCPs is very dispersed. If used in saturation mode, the pulse height is stable and the time jitter small, but the pulse decay is long and not constant. If used in linear mode and associated to a constant fraction discriminator, the pulse shape is assumed to an impulse response with variable height, but fixed shape from a single particle.
- They suffer from a limited speed, meaning they cannot reach high count rates ($\sim 150\ kHz$).
- They can amplify a fix charge during their lifetime, so they need to be replaced frequently.
- They are not available in very large surfaces (diameter area $\sim 10\ cm$).

Compared to gas amplification system, they offer for the same stability in operation, a better gain and a very good compactness. Unfortunately, this is a much slower system, which degrades over time and is less easy to maintain. In addition they cannot be built in very large areas (several 10s of centimeter).
Those reasons, especially their limited count rate capabilities make them a difficult choice for high count rates detectors.

2.5 A promising approach to overcome Gas-filled detectors limitations

A promising approach to overcome the parallax of gas filled detectors (see 2.2.4) is the use of a solid converter called *Photocathode*. The solid state materials density is roughly 1000 times that of a gas. As a result a few microns are enough to absorb the incoming photons and convert them in electric signal. This presents several advantages, including the absence of parallax errors (see Figure 2.5), a better efficiency, and a higher compactness of the detector.

Bibliography

[1] M. P. T. S. National nuclear Series, *Ionization Chambers and Counters. Experimental Techniques.* McGraw-Hill Book Company, Inc, 1949. p97.

[2] G.C.Smith, "Gas-based detectors for synchrotron radiation," *Journal of Synchrotron Radiation*, vol. 13, pp. 172–179, March 2006.

[3] A.-M. P. et al., "A beginners' guide to gas-filled proportional detectors with delay line readout," *Journal of Macromolecular Science*, vol. B37:4, pp. 463–483, 1998.

[4] M.Kocsis, "The status of gas-filled detector developments at a third generation synchrotron source (esrf)," *Nucl. Inst. and Meth. A*, vol. 471, pp. 103–108, September 2001.

[5] G.F.Knoll, *Radiation Detection and Measurement.* Willey, 2000.

[6] G.Charpak et al., "The use of multiwire proportional counters to select and localize charged particles," *Nucl. Inst. and Meth.*, vol. 62, pp. 262–+, 1968.

[7] V.Zhukov et al., "A curved micro-strip gas counter for synchrotron radiation time resolved saxs/waxs experiments," *Nucl. Inst. and Meth. A*, vol. 392, pp. 83–88, 1997.

[8] J.E.Bateman et al., "A gas microstrip wide angle x-ray detector for application in synchrotron radiation experiments," *Nucl. Inst. and Meth. A*, vol. 477, pp. 340–346, 2002.

[9] J.E.Bateman et al., "Improving the performance of the mwpc x-ray imaging detector by means of the multi-step avalanche technique," *Nucl. Inst. and Meth. A*, vol. 239, pp. 251–259, 1985.

[10] G.Charpak et al., "The spherical drift chamber for x-ray imaging applications," *Nucl. Inst. and Meth.*, vol. 122, pp. 307–312, 1974.

[11] R.Kahn et al., "An area-detector diffractometer for the collection of high resolution and multiwavelength anomalous diffraction data in macromolecular crystallography," *Nucl. Inst. and Meth. A*, vol. 246, pp. 596–603, 1986.

[12] P.Rehak et al., "Mipa: A new micro-pattern detector," *IEEE. Trans. on Nucl. Sci.*, vol. ns-44, pp. 651–655, 1997.

[13] A.Oed et al., "Position-sensitive detector with microstrip anode for electron multiplication with gases," *Nucl. Inst. and Meth. A*, vol. 263, pp. 351–359, 1988.

[14] R.Bellazzini et al., "The microgap chamber: a new detector for the next generation of high energy, high rate experiments," *Nucl. Inst. and Meth. A*, vol. 368, pp. 259–264, 1995.

[15] F.Bartol et al., "The c.a.t. pixel proportional gas counter detector," *Journal de Physique III*, vol. 6, pp. 337–347, 1996.

[16] F.Sauli et al., "Gem: A new concept for electron amplification in gas detectors," *Nucl. Inst. and Meth. A*, vol. 386, pp. 531–534, 1996.

[17] Y.Giomataris et al., "Micromegas: a high-granularity position-sensitive gaseous detector for high particle-flux environments," *Nucl. Inst. and Meth. A*, vol. 376, pp. 29–35, 1996.

[18] "Tech-etch inc.." http://www.tech-etch.com/.

[19] B.Surrow et al., "Development of tracking detectors with industrially produced gem foils," *Nucl. Inst. and Meth. A*, vol. 572, pp. 201–202, 2007.

[20] R.A.Lewis et al., "The "rapid" high rate large area x-ray detector system," *Nucl. Inst. and Meth. A*, vol. 392, pp. 32–41, 1997.

Chapter 3

Photocathode for gas-filled detectors

What is a photocathode?

A photocathode is a solid converter: it converts photons into electrons. The energy deposited by the incident particle enables the *creation* of *hot electrons* (more energetic than free electrons), which *exit* the photocathode at a position very close to the entry of the incoming particle.

Photocathodes have to suit the following requirements:

- *Good conversion efficiency*
- *Chemical stability*: as the photocathode has to operate in a gas, it must be reasonably chemically stable

3.1 Basics of Photocathodes

There is currently no theory to describe precisely and predict numerically the characteristics of photocathodes. Only phenomenological models can be made to help predicting the characteristics of materials as good photocathodes.

This comes from the extreme complexity of the physics of electron transport into matter, as the cascade of events varies not only with the type of material (chemical nature and related physical properties), but also with the microscopic structure of the material (most defects, grain boundaries, or impurities act like traps for electrons).

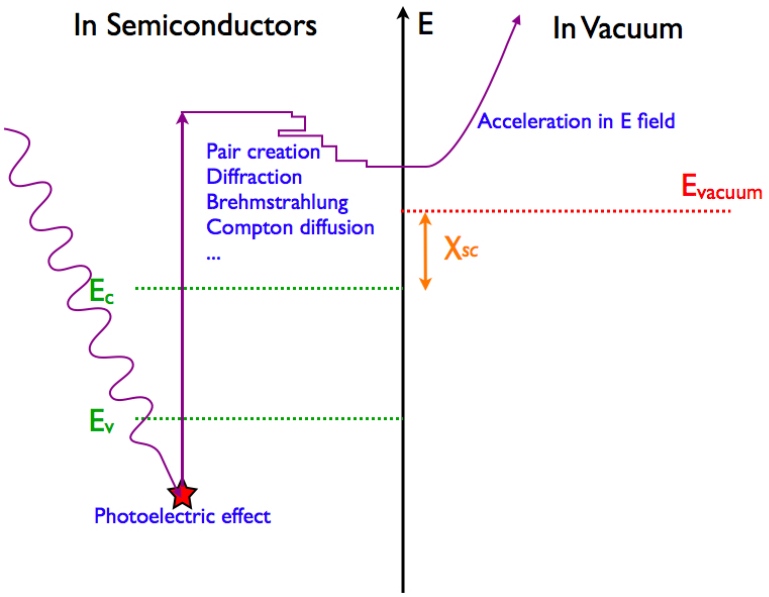

Figure 3.1 : *After its creation, the hot electron rapidly looses its energy because of several interactions with the lattice or other electrons. Few electrons actually reach the surface.*

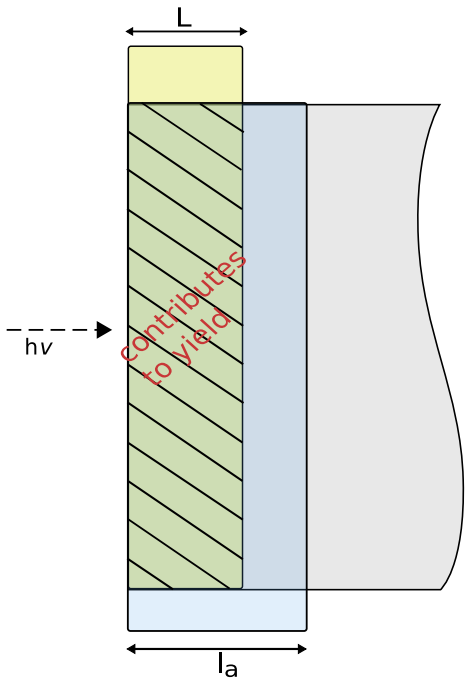

Figure 3.2 : *The region of the photocathode contributing to yield. L is the* scattering length*, l_a is the absorption length.*

As a result only the physics of the absorption of the incoming photon into the matter is well described. To go further, one has to use approximate models, which cannot lead to numerical predictions of the efficiency and speed of the photocathode.
The best (phenomenological) model to describe photocathodes is called the *Spicer Three Step Model*. It was developed approximately forty years ago by William E. Spicer, when he was working for SLAC (The Stanford Linear Accelerator Center)[1].
This model basically separates the process in three major steps:

- Absorption
- Electron transport to the surface
- Extraction from the surface.

More precisely, the model consists in examining the contribution of a slab dx at a distance x from the surface to the emitted electrons.
This contribution depends on:
◇ the amount of photons, which arrive at this depth.
◇ the probability of an electron photoemitted in this slab to join the surface,
The total yield of the photocathode is then obtained by integrating $di(x)$ over the whole volume.
To help comparing materials, the model defines two lengths:

- l_a is the *absorption length* in witch most of the photons are absorbed. It is the *1/e length* where the intensity of the incident beam has dropped to 1/e.

- L is the *scattering length*: the distance electrons can go over before they are thermalized.

The quality of a material can then be examined with the ratio $\frac{l_a}{L}$, which should be as small as possible, and ideally, *inferior to unity.*
The model also enables to define the *active volume* as the portion of the photocathode next to the surface, which is at a distant inferior to both l_a and L (see Figure 3.2 in page 42). This is the region of the photocathode, which is close enough to the surface to enable electrons to escape, and at the same time in the region of absorption of the photons, so contributing to the yield.

Absorption

From the presented model, it is evident that a material with a high stopping power (small l_a) will produce more electrons close to the surface, so more electrons with a high probability to escape the material. In practice, these are materials with a high Z (superior to 50, or ideally to 70), which present the best stopping powers.

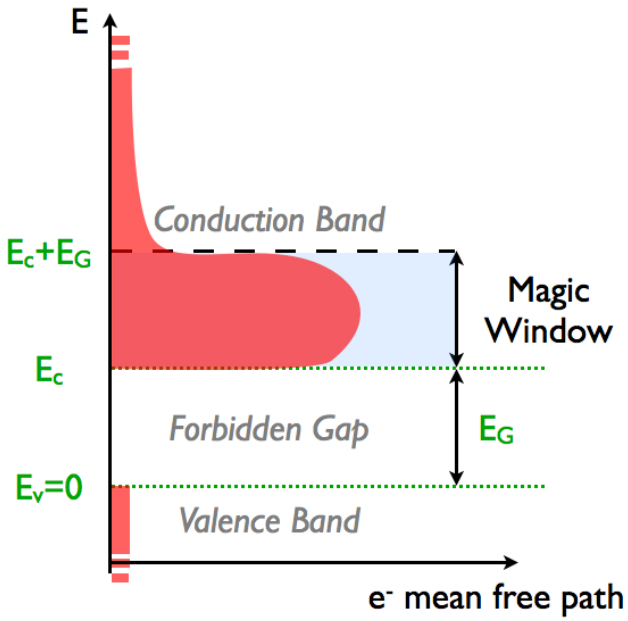

Figure 3.3 : *Electrons with energy $E_C < E < E_C + E_G$ have higher mean free path.*

Electron Transport

The capacity of the Photocathode to transport hot electrons to the surface depends strongly on the type and quality of the material it is made of. This is measured in the Spicer model by the value of the "scattering length" L. This value is closely related to the value of the *mean free path* and that of the *average loss of energy* of electrons in the material.
To maximize the value of L, it is best to have a semiconductor. First because in metals, hot electrons get thermalized very easily by the many free electrons. Secondly, in semiconductors, there is the

appearance of the so called Magic window. The magic window is a region in the conduction band ($E_c < E < E_c + E_G$) where electrons have a much higher mean free path. Indeed, electrons having such an energy cannot excite another electron in the conduction band, for this would result in two electrons in the forbidden gap of energy. The electron ion pair creation being a dominant process at those energies, this results in a much higher mean free path of electrons in the window.

It is also of strong importance to have defect free materials: each defect in the material (vacancy, dislocation, grain boundaries...) acts like a trap for hot electrons, for they often result in dangling bonds.

To have further details, one can look at Henke's papers [2, 3], in which a more precise model for electron transport is given (especially concerning electron-electron and electron-plasmon interactions). Those references also highlight how the efficiency of the photocathodes is closely related to the product $E\mu(E)$, where E is the energy of the incoming photons, and $\mu(E)$ the mass absorption coefficient of the photocathode material.

Extraction

Electrons close to the surface do not necessarily go in the vacuum: they have to overcome a potential barrier called *work function* ϕ_m in metals or *electronic affinity* χ_{sc} in semiconductors (Figure 3.4).

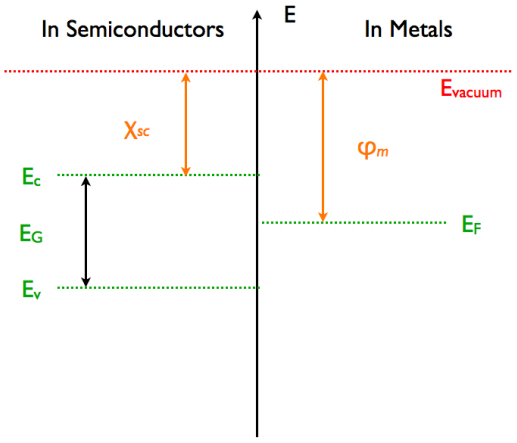

Figure 3.4 : *To exit the solid, e^- have to overcome the workfunction ϕ_m or electronic affinity χ_{sc}*

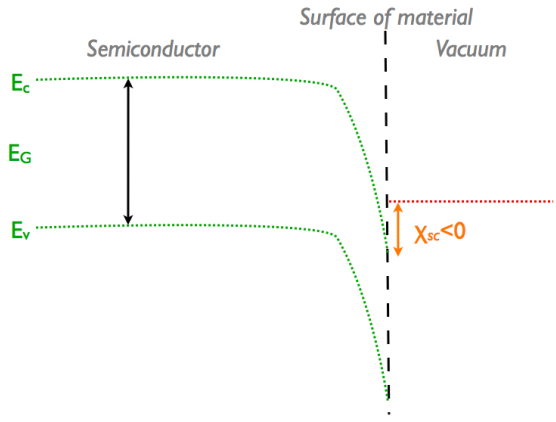

Figure 3.5 : *The Band structure of a* NEA *semiconductor close to the surface*

This barrier is often several eV high, so very few electron can overpass it, leading to a poor yield. To maximize the photocathode efficiency, one must select materials with a very low electronic affinity.

There are materials such as CsI, or hydrogenated diamond, which offer a *Negative Electron Affinity (NEA)*. Those materials are of course of special interest for they act like a kind of `hot electron fountain`: hot electrons close to the surface see an attracting potential, which tends to eject them from the material. The quantum efficiency of this sort of material is of course much better than that

of classical materials.

Their main disadvantage comes from their very high chemical sensitivity. For the potential tends also to attract anions, the negative affinity rapidly disappears as the surface gets polluted. So they require special cleanness of the environment, which is hard to achieve when the photocathode is in a gas chamber. It was also found that the coating of the surface with materials like caesium or TMAE can improve this efficiency (see adding details in the following section, or see [4] published in 1936 !). This effect is usually explained by the appearance of dipoles at the surface of the materials, which lower the electronic affinity.

The Contradictions

Already several contradictory requirements appear for the photocathode :

- The photocathode must be *thick* to absorb the incoming particles, but *thin* to let electrons escape.
- It should be made of high Z materials, but should be defect free. In terms of availability, there are very few high Z materials (especially in the case of semiconductors), which can be processed with a good purity and few defects.
- It would better be *NEA* but has to be chemically very stable.

So one has to choose the best compromise to finally achieve an optimal quantum efficiency in a certain energy range.

3.2 Improved Models of Photocathodes

Obviously the model presented in the previous section is very simple, and it cannot be used for quantitative analysis. It is yet the only general model.
Yet more accurate models were developed to predict quantitative secondary emission yield, as well as the energy distribution of both photoemitted electrons, and secondary emitted electrons.
Unfortunately all those models are material specific (they usually study CsI, considered as the most interesting material for photocathode application [5, 19, 7]), for they use extensively fitted parameters. Most of them were developed for Monte Carlo based analysis. So it is difficult to use this sort of models for prediction of efficiencies of new materials.
More details will be given in the section dedicated to the Monte Carlo Analysis.

3.3 Major technologies of photocathodes currently available

Most materials now used as photocathodes have been known for a long time. A compilation by P. Miné then at Ecole Polytechnique in 1993 [8] is still valid (this publication deals with photoemissive materials in the UV, but the state of knowledge in the X-ray energy range is not really different). Jochen Teichert, Rong Xiang, Guy Suberlucq and Jeroen W.J Verschuur also made a Report on

Photocathodes in 2004 but again, mainly focused on photocathodes in UV and Visible range for electron injection system applications [9]. Focus was given on a better control of the fabrication process to ensure the best quality of cathodes.

3.3.1 Metallic Photocathode

Metallic photocathodes are the oldest type of photocathodes.
Classical materials include gold, copper, and silver. Gold is of all those materials the best, for it offers the best efficiency (highest atomic number so excellent stopping power), an excellent speed, as well as the best chemical stability (noble metal) .
Gold is used for photocathodes in a wide range of application where high chemical stability, high conductivity and speed are mandatory. This is especially the case for photo-injectors in synchrotrons and X-fels (injectors made of photocathode excited with pulsed UV-laser to create the packets of electrons) where high quality pulses of electrons (in terms of intensity and shortness) are mandatory. The photocathode is often used in RF cavities coupled with the pulsed laser to enable the creation of extra short/very high intensity electron packets.
NB. RF cavities cannot be used to improve the efficiency of gas-filled photodetectors, because they work exclusively under ultra high vacuum (discharge problem) so are incompatible with gas amplification.

Past studies of metallic photocathodes

Metallic photocathodes were mostly studied during the 70's and early 80's (though, some older references can be found). Classical references include:

- for **Gold, Copper and Silver**: [10, 11, 3, 12, 13].
- for **Aluminum and** Al_2O_3: again [3, 13, 12].
- other materials such as **Tungsten, Molybdenum, Silver, and Palladium** are presented in [10]

For the X-ray energy range as well as for the UV energy range, gold is the most suitable metallic photocathode. Recent measurement using synchrotron radiation facilities [14, 15] report all with good agreement efficiencies of a few tenths of a percents in the 1-10 keV energy range. [16, 17] also provide interesting results even if the quantum efficiency is not directly measured. Lastly H.Henneken *et al.* reported measurements of the efficiency of gold in the case of the specific Au(111) surface [15].

3.3.2 Semiconducting Photocathode

As previously discussed, semiconductors are theoretically much better materials in terms of quantum efficiency. Their availability in excellent purities and almost defect free bulk materials make them a very attractive choice.
In practice several compounds offer excellent efficiencies in the visible or infrared ranges (Alkali antimonides such as Cs_3Sb, K_3Sb, Na_2KSb, K_2CsSb). Unfortunately they all present a high

reactivity to moisture and oxygen, which makes their manipulation difficult, and also completely unsuitable for gas amplification based systems.
Other systems were studied because of their insensitivity to visible photons, and high efficiency in the UV range (*solar blind* photocathodes for spatial application). Those photocathodes reacting to wavelength smaller than 380nm, often exhibit a negative electron affinity (eventually after an activation with Cs or another material).
Theoretical analysis of secondary emission by semiconductors can be found in [3, 2].
Materials, which created interest include

- **boron nitrides** BN reported to present NEA characteristics [18]
- **Gallium Arsenide** GaAs also reported to present NEA when Cs activated (see [19], which compares GaAs with other semiconductors, as well as [20, 21]
- **Gallium nitride, Indium Gallium Nitrides and Aluminum Gallium Nitrides** GaN, INGaN and $Al_xGa_{1-x}N$ were extensively studied because of their potential for solar blind detectors ([22, 23, 24, 25]).

Unfortunately when it comes to X-rays, common semiconductors such as gallium arsenide, silicon or germanium are completely inefficient. Indeed those materials do not have the stopping power suitable for energetic photons, for electrons cannot reach the surface before they are thermalized. In addition, those materials are available only in small dimensions.
Heavier materials being much harder to process in good quality, there are very few materials, which are actually used as photocathodes. CsI is the exception, and it will be later described.

3.3.3 Organic Photocathode

Organic photocathode such as $TMAE$ (tetrakis dimethyl-amino!ethylene), or C_6H_5, have created great interest in the 80's for they exhibit a negative electron affinity. They were also used as activator (like Cs). Unfortunately, they are of no interest in the X-ray energy range, because of their very low stopping power. The interested reader can find information in P. Miné's [8].

3.3.4 CsI

Since its first discovery by Taft and Philipp in 1957 [26] and its further studies by J. Edgecumbe and E. L. Garwin in 1965 [27, 28], CsI has probably been the material, which was the most widely studied. This comes from several advantages it offers:

- Excellent quantum efficiency: the material exhibit NEA properties, and an excellent stopping power (high Z).
- A rather good chemical stability, at least if compared to most other materials with similar characteristics. Still the material is hygroscopic and suffers from degradation with time.
- Easiness of synthesis and deposition.

From the beginning, a lot of efforts were put in attempts to reduce its sensitivity to moisture and need for cleanness (UHV conditions) [29, 8, 13, 32, 11, 34, 35][1].
Efficiencies measured vary among authors. This is probably due to the high reactivity of the material, and the importance of the deposition/synthesis conditions.

- [32] report a quantum efficiency of 2 to 4% in the 5 to 10 keV energy range.
- [13] report a quantum efficiency of 1 to 5% in the same range of energies.

The ALICE collaboration made a systematic study of the effect of water and oxygen on the quantum efficiency of CsI [36]. [32] provides information on the effect of heating to resorb the loss of efficiency after exposure to moisture.
Effects of electric field [12], Gas amplification with various mixtures [38, 39], polarization of X-rays [40], as well as various Monte Carlo dedicated codes [38, 5] were also studied. This shows the wide interest and hopes that this material created.
Now, CsI is still considered as a reference, and a lot of projects are still based on the use of this material. Unfortunately, the sensitivity of CsI as a photocathode is still an issue, and few success were recorded.
Lastly, a sensitivity of CsI to radiation was recorded [8, 41]. This is of course an issue regarding the stability in time of a detector using CsI. Fortunately, this sensitivity seems to be limited in the X-ray energy range [41].
The key feature of CsI is its negative electron affinity. This NEA is explained by the appearance of dipole charges at the surface of the material, leading to a bending of the band structure, and the presence of an attractive potential to electrons at the surface.
Those dipoles are of course very attracting to all sorts of impurities, which easily form chemical bounding with the surface charges, so destroying the NEA of the surface.
As a result, CsI photocathodes usually loose their high quantum efficiency after a few hours of exposure to moisture, and even much faster in an unclean environment.
There were a lot of attempts to protect the CsI from degradation in unclean environment. Another approach was to try developing online cleaning processes (like [32] already cited). But none of these approaches were able to provide a solution acceptable in terms of robustness and efficiency.
It remains that CsI offers an attractive efficiency, and in addition it is widely available (it was also successfully used as a scintillator material by addition of dopants like Tb or Na).

3.3.5 Conclusions on available technologies of Photocathodes and the issues related to their use

A wide variety of photocathodes is available on the market. But most of them are suitable only for low energy applications (visible, ultra-violet and infrared applications).
There are mainly two families of photocathodes suitable for the hard X-ray energy range:

- *Metallic photocathodes*, mainly gold, which offers a poor efficiency but an excellent robustness

[1] It should be noted that a number of those publications come from A.Breskin's group from the Weizmann Institute of Science in Israel, which has been very active in developing this technology.

	Gold	CsI
Efficiency	few $\frac{1}{10}$'s of a percents [16, 17]	few percent [32, 13]
Sensitivity	none	To moisture, impurities in gas

Table 3.1 : *Technologies of photocathode*

- CsI photocathodes, which offers the best efficiency, but a sensitivity to moisture and contamination leading to huge technological problems, especially in the case of gas-filled detectors.

Recapitulation tabular (Table 3.1):
Other classical photocathodes such as *tetraminoethylene (TMAE)*, the organometallics ($(C_2H_5)Cr$, $(C_2H_5)Fe$...), are not suitable for X-rays for their stopping power is not good enough and so do not achieve a good efficiency (this is mainly due to their low Z).
The same restrictions apply to GaAs and parents (InGaAs, InGaAsP) usually used after activation with Cs. In addition, those materials can be used only with gases of very high purities.
TMAE was successfully used to increase to quantum efficiency of CsI and other photocathodes, but no good stability could be achieved.

Bibliography

[1] W.E.Spicer, "Photoemissive, photoconductive, and optical absorption studies of alkali-antimony compounds," *Phys. Rev.*, vol. 112, no. 1, pp. 114–122, 1958.

[2] B.L.Henke et al., "Soft x-ray induced secondary-electron emission from semiconductors and insulators: Models and measurements," *Phys.Rev.B*, vol. 19, pp. 3004–3021, 1979.

[3] B.L.Henke et al., "0.1-10kev x-ray induced electron emissions from solids-models and secondary electron measurements," *J.Appl.Phys.*, vol. 48, pp. 1852–1866, 1977.

[4] L.Malter, "Thin film field emission," *Phys.Rev.*, vol. 50, pp. 48–58, 1936.

[5] A.Akkerman et al., "Monte carlo simulations of secondary electron emission from csi, induced by 1 10 kev x rays and electrons," *J.Appl.Phys.*, vol. 72(11), pp. 5429–5436, 1992.

[6] A.Gibrekhterman et al., "Characteristics of secondary electron emission from csi induced by x rays with energies up to 100 kev," *J.Appl.Phys*, vol. 74, pp. 7506–7509, 1993.

[7] A.Gibrekhterman et al., "Spatial characteristics of electron- and photon- induced secondary electron cascades in csi," *J.Appl.Phys*, vol. 76, pp. 1676–1680, 1994.

[8] P.Miné, "Photoemissive materials and their application to gaseous detectors," *Nucl. Inst. and Meth. A*, vol. 343, pp. 99–108, 1994.

[9] J.Teichert et al., "Report on photocathodes," tech. rep., CARE/JRA-PHIN, 2004. http://www.fzd.de/projects/CARE/index.files/reports/report.pdf.

[10] W.C.Walker et al., "Photoelectric yield in the ultraviolet," *J.Appl.Phys.*, vol. 26(11), pp. 1366–1371, 1955.

[11] W.F.Krolikowski et al., "Photoemission studies of the noble metals. ii. gold," *Phys.Rev.B*, vol. 1(2), pp. 478–487, 1970.

[12] R.H.Day et al., "Photoelectric quantum efficiencies and filter window absorption coefficients from 20ev to 10kev," *J.Appl.Phys.*, vol. 52(11), pp. 6965–6973, 1981.

[13] B.L.Henke et al., "The characterization of x-ray photocathodes in the 0.1-10kev photon energy range," *J.Appl.Phys.*, vol. 52(3), pp. 1509–1520, 1981.

[14] G.W.Fraser et al., "The characterization of gold x-ray photocathodes," *Nucl. Inst. and Meth. A*, vol. 321, pp. 376–380, 1992.

[15] H.Henneken et al., "Absolute total yield of au(111) and cu(111) surfaces," *Journal of Electron Spectroscopy and Related Phenomena*, vol. 101-103, pp. 1019–1024, 1999.

[16] M.Hirata et al., "X-ray detection characterization of gold photocathodes and microchannel plates using synchrotron radiation (10ev-82.5 kev)," *Nucl. Inst. and Meth. B*, vol. B66, pp. 479–484, 1991.

[17] S.Gosavi et al., "Stability improvement at high emission densities for gold thin film photocathodes used in advances electron beam lithography," *J. Vac Sci. Technol. B*, vol. B19(6), pp. 2591–2597, 2001.

[18] M.J.Powers et al., "Observation of a negative electron affinity for boron nitride," *Appl.Phys.Lett*, vol. 26, pp. 3912–3914, 1995.

[19] G.A.Allen, "The performance of negative electron affinity photocathodes," *J. Phys. D*, vol. 4, pp. 308–317, 1971.

[20] S.H.Kong et al., "Photocathodes for free electron lasers," *Nucl. Inst. and Meth. A*, vol. A358, pp. 272–275, 1995.

[21] K.A.Elamrawi et al., "Preparation and operation of hydrogen cleaned gaas(100) negative electron affinity photocathodes," *J. Vac Sci. Technol. A*, vol. A17(3), pp. 823–831, 1999.

[22] F.S.Shahedipour et al., "Efficient gan photocathodes for low-level ultraviolet signaldetection," *IEEE Journal of Quantum Electronics*, vol. 38(4), pp. 333–335, 2002.

[23] M.P.Ulmer et al., "Progress in the fabrication of gan photocathodes," *Proc. SPIE*, vol. 4288, pp. 246–253, 2001.

[24] P.Sandvik et al., "$al_xga_{1-x}n$ for solar blind uv detectors," *J. Cryst. Grow.*, vol. 231, pp. 366–370, 2001.

[25] D.J.Leopold et al., "High quantum efficiency ultraviolet/blue algan/ingan photocathodes grown by molecular epitaxy," *J.Appl.Phys.*, vol. 98, pp. 043525–1,5, 2005.

[26] E.A.Taft et al., "X-ray induced radiation damage in csi, gadox, y_2o_2s, and y_2o_3 thin films," *Phys. Chem. Solids*, vol. 3, p. 1, 1957.

[27] J.Edgecumbe et al., "Attenuation length for secondary electrons in bulk-density kcl and csi," *J.Appl.Phys.*, vol. 37, pp. 2916–2917, 1965.

[28] J.Edgecumbe et al., "Csi as a high-gain secondary emission material," *J.Appl.Phys.*, vol. 37, pp. 3321–3322, 1966.

[29] V.Dandendorf et al., "Progress in ultrafast csi-photocathode gaseous imaging photomultipliers," *Nucl. Inst. and Meth. A*, vol. A308, pp. 519–532, 1991.

[30] E.Shefer et al., "Photoelectron transport in csi and csbr coating films of alkali antimonide and csi photocathodes," *J.Appl.Phys.*, vol. 92(8), pp. 4758–4771, 1993.

[31] A.Breskin et al., "New ideas in csi-based photon detectors: Wire multiplication and protection of the photocathode," *IEEE Trans.Nucl.Sci*, vol. 42(4), pp. 298–305, 1995.

[32] J.E.Lees et al., "Thermally annealed soft x-ray photocathodes," *Nucl. Inst. and Meth. A*, vol. 381, pp. 453–461, 1996.

[33] H.S.Cho et al., "A columnar cesium iodide (csi) drift plane layer for gas avalanche microdetectors," *IEEE transaction on Nuclear Science*, vol. 45(3), pp. 275–279, 1998.

[34] L.Periale et al., "Evaluation of planar gaseous detectors with csi photocathodes for the detection of primary scintillation light from noble gases," conference paper *Presented at the 1st Topical Symposium on Functional Breast Imaging with Advanced Detectors*, 2001. http://arxiv.org/pdf/physics/0106070.

[35] E.Schyns et al., "Status of large area csi photocathodes developments," *Nucl. Inst. and Meth. A*, vol. 494, pp. 441–446, 2002.

[36] A.Di.Mauro et al., "Study of the quantum efficiency of csi photo-cathodes exposed to oxygen and water vapour," *Nucl. Inst. and Meth. A*, vol. 461, pp. 584–586, 2001.

[37] A.Breskin et al., "Electric field effects on the quantum efficiency of csi photocathodes in gas media," *Nucl. Inst. and Meth. A*, vol. 344, pp. 537–546, 1994.

[38] T.H.V.T.Dias et al., "The transmission of photoelectrons emitted from csi into xe, ar, ne, and their mixtures: a monte carlo study of the dependence on e/n and incident vuv photon energy," *J.Appl.Phys.*, vol. 37, pp. 540–549, 2002.

[39] R.Aleksan et al., "Measurement of csi photocathode quantum efficiency in methane," *Nucl. Inst. and Meth. A*, vol. 343, pp. 173–191, 1994.

[40] S.Hanany et al., "Measeurement of the electron yield of csi with polarized x rays," *Phys.Rev.B*, vol. 48(2), pp. 701–709, 1993.

[41] A.S.Tremsin et al., "X-ray induced radiation damage in csi, gadox, y_2o_2s, and y_2o_3 thin films," *Nucl. Inst. and Meth. A*, vol. 459, pp. 543–551, 2001.

Chapter 4

The Simulations by Monte Carlo Method

This chapter presents the study by Monte Carlo of the photocathodes performed in this work.
The chapter is divided into four parts :

1. A general introduction to the Monte Carlo Method,
2. a description of the Monte Carlo code developed in this work is given,
3. a detailed analysis of the limits of Monte Carlo methods in the case of particle tracking into matter is given, and the reason why these limitations forbid the use of this method in the case of photocathode analysis
4. Conclusions on this part of the work.

4.1 A first approach to Monte Carlo

4.1.1 History

Figure 4.1 : *Monaco's Casino*

The Monte Carlo Method is called after the city of the Principality of Monaco, because of the *roulette* (and similar games), seen as a random number generator. This name and the systematic development of the Monte Carlo Method date from about 1944.

Before, there had been several isolated instances of this method, some of them on much earlier occasions (see the examples given in B.1). Those methods were only rarely actually used for scientific purpose. A reason for this is the necessity to make a large number of repetitive operations to achieve "a good precision". This is the arrival of computers, which created a greater interest for this sort of simulations.

The principles of the Monte Carlo Method are due to the polish mathematician *Stanislaw Ulam*, when he was working in Los Alamo for the Manhattan Project[1].
Those developments were implied by the work on the atomic bomb, which needed a direct simulation of the probabilistic problems of neutron diffusion in fissile materials. But even at an early stage of the project, Stanislaw Ulam and John von Neumann refined the method to a more general theory[2].

Finally, the systematic development of the method occurred only in 1948 with the work of Harris and Herman Kahn. From this moment, the method had a fast development, and already in 1948, Fermi, Metropolis, and Ulam obtained estimations for the eigenvalues of Schrodinger's equation. The Method became intensively used in extremely various fields from 1970, thanks to the new generation of computers.

4.1.2 Description of the Monte Carlo Method

A possible definition: *The Monte Carlo Method, as it is understood now, encompasses any technique of statistical sampling employed to approximate solutions to quantitative problems.*
Said another way, the Monte Carlo Method gives an approximate solution to a problem using a statistical approach. The method consists in performing statistical sampling experiments, and applying the central limit theorem[1] to determine the general behavior of the studied system. It applies to problems with no probabilistic content, as well as to those with inherent probabilistic structure.

The progress in terms of performance of modern computers has enabled the use of the Monte Carlo Method in an increasing number of problems, and it has now several fields of applications: the most common problem treated via a Monte Carlo approach are:

- Particle Transport through matter (detailed in 4.1.3),
- Astrophysics models,
- Molecular studies ("classical", "quantum", "path-integral", "volumetric", molecular dynamic, etc...),
- Evaluation of multi dimensional integrals (see example in annex B.1.1),
- solving the integro-differential equations defining the radiance field.

All those applications have lead to new development in various areas, for example the last application has been used in global illumination computations, which is a way to produce photo-realistic images. As a Result, Monte Carlo Methods have been usefully employed in industries as various as that of Graphics industry (in the case of ray tracing softwares, see the case of the *Radiance software* [3]), Finance [4], or Search And Rescue and Counter-Pollution, where models are used to predict the drift of a life raft or of an oil slick on the sea.

[1]The Central Limit Theorem states that if the sum of *independent random variables* has a finite variance, then it will be approximately normally distributed.
said another way: Given a population with a mean of μ and a deviation σ, then the sampling distribution of the mean has a mean of μ and deviation of $\frac{\sigma}{N}$ (N being the sample size).

4.1.3 The Monte Carlo Method in Particle Transport

There are mainly two different approaches to study the transport of particles through matter:

- The deterministic methods, in which the transport equation is solved.
- The Monte Carlo approach, in which single particle transports are computed.

It is said sometimes that, while the deterministic approach consists in solving the *integral transport equation*, the Monte Carlo approach consists in solving the *integro-differential transport equation*. This statement (which is incorrect, for the `integral` and `integro-differential` equations, are actually a single one put in two different forms) illustrates the difference between the two approaches: The deterministic methods return a general law of behavior of the particles, and a complete set of information (flux, penetration, etc...).
In contrast, the Monte Carlo Method does not solve an explicit equation, but obtains the solution by simulating individual particle transports and interactions with matter and by recording all the information along the trajectories of the particle. Then the *central limit theorem* enables to determine the general behavior of the particles by making a statistic analysis of the recorded information.

The particle transport simulation consists in tracking the particles one by one, by evaluating at each *step* the probability of interaction with matter. The probability densities of interaction (calculated according to various parameters such as the particles energy, type, bias... and the material type, density...) are used in addition to a random number generator to determine the step length, and the interaction type, which will happen. Thus, the particle behavior is not deterministic but governed by probabilistic laws, following the quantum nature of fundamental interactions.
The interaction laws used in the simulation are obtained from the quantum mechanics theory (for their analytical form), and from experimental measurements (the *cross sections*, which describe "the probability of interaction").

The major problem of the Monte Carlo Methods for particle tracking is the need of computer power to achieve simulations with an acceptable precision (*i.e.* enough particles tracked to achieve a good statistics). Only modern powerful computers are able to perform the simulations in an acceptable time (a few hours).

4.2 The Geant4 toolkit for particle transport into matter

The development of a Monte Carlo code is a very ambitious project, especially if it is meant to study many materials. So it was preferred to use a general toolkit with proven capacities at low energies. Several codes were considered (Penelope, MCNPX, EGSnrc, Geant4). **Geant4** was chosen because of various reasons, including:

- It has become a standard among Monte Carlo codes.
- It is well documented and open source, thus it gives straighter access to code and physics verification.

- It is provided with numerous tools, which simplify data analysis.
- It has a series of libraries dedicated to low energies.

Among the disadvantages of Geant4 when compared to other codes:

- It is harder to program, as the user has to make the program himself (no script language to command Geant4). It is written in C++. So the user needs basic notions of object-oriented programming.
- Complex setup of the program (compilation, configuration settings...)

Those difficulties are also the strength of Geant4, for they find their origin in the very high versatility of the toolkit, and in its cross-platform nature.

Geant -for `GEometry ANd Tracking`- is a simulation toolkit developed for the tracking of particles through matter. It has been developed by more than 100 scientists from 10 institutions and has now become a worldwide reference.
The first version was developed at CERN and dates from 1974. Up to version 3.21, Geant was made in Fortran, and was mainly dedicated to high energy physics. From 1994, a new version completely written in C++ and with modern object oriented structure was developed.

The toolkit includes facilities for handling complex geometries, tracking particles, simulating detector response, handling run management and the user interface.
Its possibilities were also expanded, and Geant4 is now routinely used in fields as various as:

- High energy and nuclear physics,
- Medical applications,
- Space industry development,
- Accelerator physics,
- *Lower energy physics* ...

The reference article for Geant4[2] was published in *Nuclear Instrument and Methods in Physics Research A*: [5].

4.2.1 The way Geant4 computes particle propagation

4.2.1.1 The tracking of the particles

The core of the method consists in tracking the particles one by one, letting them having all possible physical interaction with matter[3]. It takes into account:

- the particle intrinsic properties, its direction, energy...

[2]The reference webpage of Geant is currently : *http://cern.ch/geant4/*

[3]Geant uses a combination of the *composition* and *rejection* Monte Carlo Method . The exact description of those two methods will not be done here, but those who have interest can have a look at the book from H.Messel and al. [6], at the article from J.C.Butcher and al. [7], and at the EGS4 Code System Manual [8].

- all physical processes applicable to the current particle (ex. for a photon the photoelectric effect, for an electron the bremsstrahlung ...).
- the volume boundaries, the material characteristics (geometrical information),
- the electromagnetic fields.

One usually makes the difference between the *primary particles*, which are generated by the programmer with defined type, momentum, position, etc... and the *secondary particles*, which are generated by previous interactions of other particles with the matter or their disintegration (unstable particles). Of course the secondaries can generate other secondaries. In Geant4 any created particle is tracked until it has a zero energy (absorption).

In Geant4, the basic element of the tracking is the **Step**. It consists of two points (*start* and *end* point) and the "delta" information of the particle:

- step length,
- energy loss during step,
- change in elapsed time,
- change of direction, etc.

A step can be summarized the following way (see table 4.2):

→ The particle velocity is calculated,

→ A step length is associated to each physical process:
The probability of interaction weighed by a random number is computed, and converted into a distance.
The minimum of all computed distances (ie. the limiting physical process) defines the *physical step length.*

→ The navigator finds "*safety*": the distance to nearest boundary in the direction of the particle.

→ the minimum of *physical step length* and *safety* is kept as the step length

→ If the physics process has limited the step, the interaction is done (interaction before the boundary of the volume). Otherwise the particle is transported to the next volume.

→ If the particle was not killed during the track, it is ready for the next step. Eventually, secondary particles are stored for later tracking.
Before the following step is performed, *Along step physical processes* are applied (for example scattering).

→ Last, the track properties are updated (momentum, position, time, etc...).

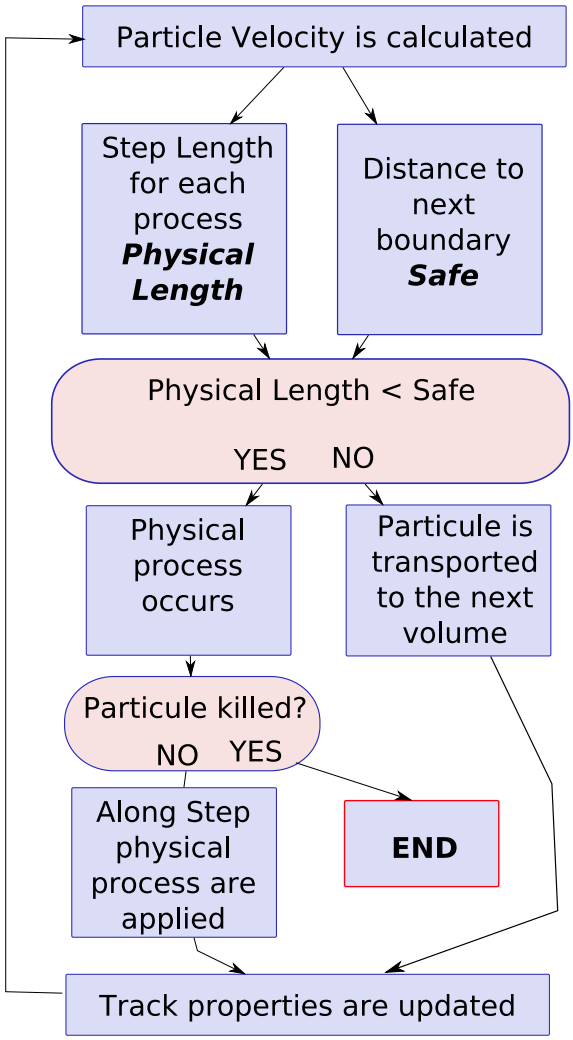

Figure 4.2 : *Tracking procedure of particles in Geant4*

At the end of the tracking process of one particle, one can eventually store the *trajectory*, which is the compilation of steps, which happened when tracking the particle.

To have a better description of the tracking processes[4], the interested reader should refer to chapter 5.1 of the *Geant4 Users Guide* [9]. Alternatively, the reference publication of Geant4 published by the Geant4 community in Nuclear Instrument and Methods in Physics Research A: [5] gives a rapid overview of the way particles are tracked.

[4]Especially to have a proper description of the way discreet and continuous processes are taken into account, and the way boundaries are treated.

4.2.1.2 The physical interactions in Geant4

The sets of physical processes

Geant4 offers two sets of processes describing particle interactions with matter:

- The historical one, dedicated to the high energy physics.
- The low energy extension of electromagnetic process, which has been developed since 1997, intends to extend the validity of Geant4 down to low energy. It can now simulate physical process down to 250 eV (and up to 100 GeV) with atomic numbers between 1 and 99.
  This extension is described both in the User Guide [9] and in the *Physics Reference Manual* [10] [5]

In addition, Geant4 also enables the user to use the set of processes from the *Penelope Monte Carlo toolkit* [11]. This way the users are offered two flavors of Low Energy physical processes, and rapid comparison can be obtained.

Cross Sections

The physical processes involved in particle transport through matter have a quantum nature, meaning that they do not follow a deterministic behavior.
On the other hand, their behavior is very well described by a probabilistic approach: the probability of interaction of a particle with a material is fixed. It is measured by the *cross section* σ and expressed in unit of area (usually in $barn \equiv 10^{-28}\ m^2$). The cross section can be understood as the apparent surface as seen from an incoming particle of an atom. In the case of a thin foil, the probability of interaction of the incoming particle is $n\ \sigma/S$ with S the surface of the foil and n the number of atoms contained in the foil.

In practice σ varies greatly with the nature of the particle, and its energy.
The various sorts of interactions of the particle with matter have corresponding cross sections.
The differential cross section $\frac{d\sigma}{d\Omega}$ describes the probability to observe a scattered particle per unit of solid angle Ω.

Cross sections used in Geant4 result from measurements as often as possible. When those data are unavailable, then only an analytic formula is used to build the cross section data. For the data are provided as series of discrete values, an interpolation formula is used to have access to any value of the energy:

$$\log(\sigma(E)) = \frac{\log(\sigma_1)\log(E_2/E) - \log(\sigma_2)\log(E_1/E)}{\log(E_2/E_1)}. \tag{4.1}$$

The set of data used in Geant4 for the determination of the cross sections and for sampling of the final states are extracted from a set of publicly distributed evaluated data libraries (for the low energy extension):

[5] The low energy extension has its website here http://www.ge.infn.it/geant4/lowE/index.html

- EPDL97 (Evaluated Photon Data Library) : [12]
- EEDL (Evaluated Electron Data Libraries) : [13]
- EADL (Evaluated Atomic Data Libraries) : [14]
- stopping power data : [15, 16, 17, 18]

Those sets of data are well described in their reference manual which can be obtained from *Lawrence Livermore National Laboratory's website*[6].

4.2.1.3 Analysis and Representation tools

The Geant4 toolkit offers numerous interfaces to access all physical parameters while the simulation is running. It has also dedicated libraries for trajectories and other data storing. So the user can record the information it has interest for later analysis.

But Geant4 is also *AIDA compliant*, meaning it has access to all the functionalities AIDA offers for online data analysis and histogramming/tuppleing.
AIDA is a set of abstract interfaces and formats for data representation. There are various implementations of AIDA, offering all sorts of tools for data analysis (filtering, combination, etc...), and representation (histograms, ntupples/data trees...).
For Geant4 possesses a direct interface with AIDA compliant tools, it is possible to make the analysis of the simulations performed online and to store the results of those simulations. This is of particular importance, as Monte Carlo simulations produce enormous amounts of data, which can be very long to analyze.
Of course the data recorded can be further studied and exported thanks to dedicated softwares, which are also AIDA compliant.

In addition, Geant4 possesses interfaces for 3D representation of the geometry and particles trajectories in the volume. This is of strong help for complex geometries definitions.

4.2.2 The simulation tool developed

4.2.2.1 Description and Functionalities

The code developed was expected to

- help understanding the physics of the photocathodes in the X-ray energy range,
- compare various geometries of photocathodes,
- help predicting the efficiencies of unstudied materials.

For the description of the physical processes is rather straightforward in the Geant4 toolkit, the hardest part was the implementation of the tools to perform detailed analysis of the simulations.
The following libraries of Geant4 or common associated tools were chosen for the implementation:

[6] http://www.llnl.gov/cullen1/photon.htm

Concerning the Physics

The Low Energy Extension was used to perform all the simulations.

All processes involving photons were activated except the *pair creation*, which has no sense for simulations of photons having energies lower than 100 keV.

So the following processes were activated:

- *The Photoelectric effect* (G4LowEnergyPhotoElectric library).
  Both *Fluorescence* and *Auger* de-excitations of photoionized atoms were activated.
  By default, the photoemitted electron has the same direction as the incident photon. Instead, the use of the standard electron angular emission generator was forced. Unfortunately, this angular distribution corresponds only to electrons emitted *from the K-shell*. For most interactions of X-rays in the targeted energy range occur with electrons from the K-shell, this limitation is not a real problem.
- *The Compton Scattering process* (G4LowEnergyCompton Library).
- *The Rayleigh Scattering process* (G4LowEnergyRayleigh).

Concerning electrons, all the processes were also activated:

- *Electron Ionization* (Library G4LowEnergyIonisation).
  Here again *Auger* and *Fluorescence* desexcitations of the ionized atom were activated.
- *The Bremsstrahlung* continuous loss of energy of electrons (Library G4LowEnergyBremsstrahlung).
- *Electron scattering*, which corrects path lengths and lateral displacements after each step for charged particles (Library G4MultipleScattering). Identically *Auger* as well as *Fluorescent* desexcitations were activated, for accurate simulations.

Cut Lengths (corresponding in Geant4 to energies under which no secondary particles are created), were always set to their minimum values ($\equiv$ 250 eV).

Concerning the data analysis tools

To calculate the overall efficiency of the photocathode (calculated as $Qu_{eff} = \frac{Nb\ emitted\ e^-}{Nb\ incoming\ photons}$), a direct implementation was used. A csv (comma separated value file format) file was happened after each simulations with Quantum Efficiency, and the photocathode parameters (Material, geometrical information...).

All other information extracted from the simulations were recorded thanks to the AIDA interface. A global Tupple Manager was created and linked to the various manager of the code (RunManager, EventActionManager...), in order to enable information to be grabbed in the proper instances of the code[7].

More than 20 histograms, 2D clouds... were created to enable a proper track of the simulations.

[7] For example, Information regarding physical processes in the StepManager,
Information regarding the deposition of the photons/electrons in the EventActionManager...

4.2.2.2 The test of the code, comparison with experimental values

Various tests were made to confront the code with experimental data. Unfortunately, it turned out that the code is not able to simulate properly the photocathodes.
In this part, success and failures of the code are exposed, and an explanation is given to those limitations.

The aim of the simulations

Various authors were able historically to create codes based on the Monte Carlo Method calculating successfully the efficiencies of photocathodes (especially for CsI, [19, 20] already cited in section 3.2). So it was natural to try to develop a code based on the latest technologies to help studying new materials for photocathode applications.

The code was expected to provide reasonable predictions of the efficiency of one material, the influence of the geometry, and the influence of an electric field.

It was planed to use it to study novel sorts of photocathodes, with materials and geometries untested so far.

In none of those expectations, an exact value was considered as mandatory, but **an error of less than** 10 % can be considered as **a minimum requirement** to be able to use the code for predictions on the efficiency of new materials.

Unfortunately, it turned out rapidly that this precision could not be reached with the code developed: the calculated values were always largely underestimated and with an error for some materials of more than one order of magnitude !

It is likely that this error can be bettered by a refinement of the code for each material studied. But this process is long and uncertain, and it involves several experimental tests to adjust the physical model used for each material.

This study was out of purpose in the scope of this work, which aims in testing several materials.

Examples of results returned by the code and discussion

Gold and CsI were taken as reference materials to test the code. As both materials were intensively studied, it was easy to find reliable measurements of their absolute efficiencies.
For Gold, the measurements made by B. L. Henke *et al.* at the *BESSY-I* and *II* light sources [21] were taken as a reference (Figure 4.4, and for CsI, the measurement by G.W.Fraser were taken (Figure 4.3).

In the simulation, the photocathode thickness is 1 μm, and the efficiency is calculated from the electrons escaping the photocathode on the side of the incident photons (following the corresponding measurements in the cited publications).

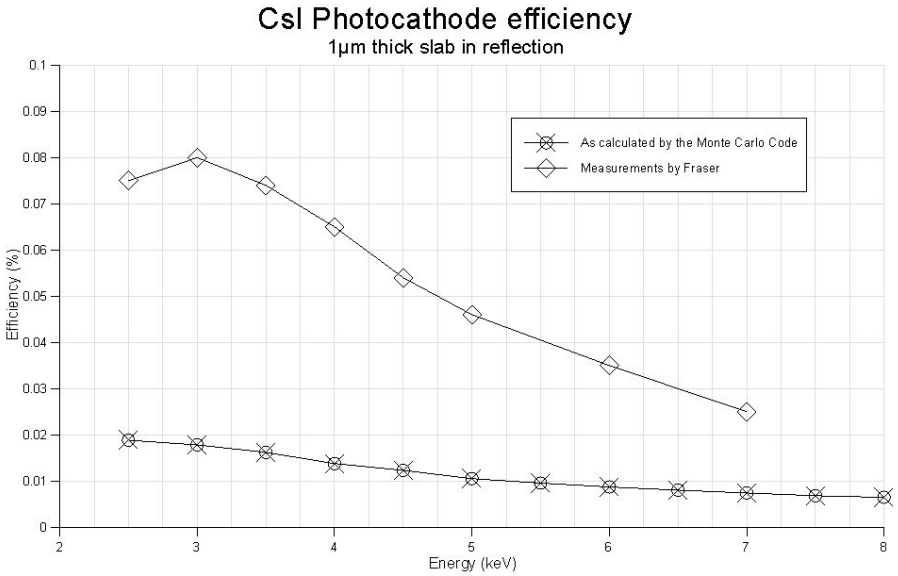

Figure 4.3 : *Quantum Efficiency of CsI as computed by the code, and measured*

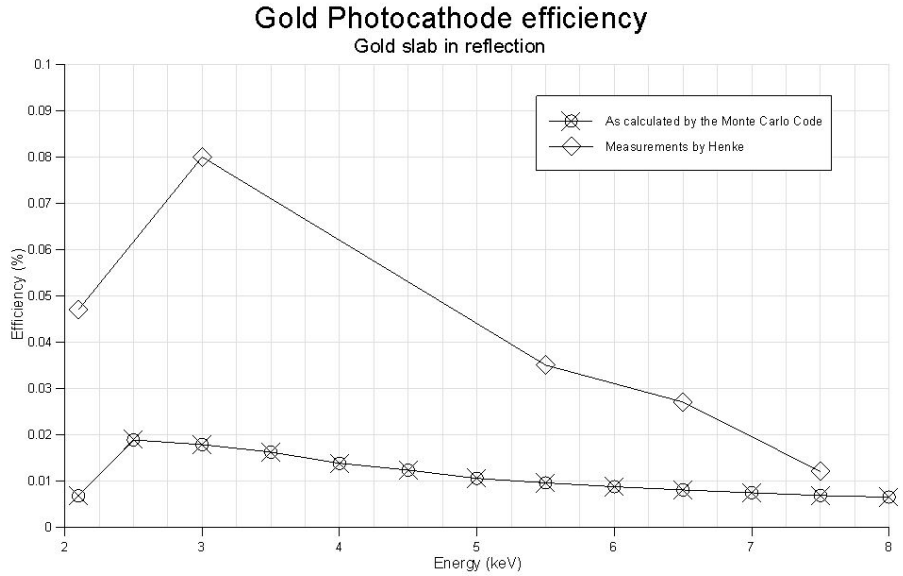

Figure 4.4 : *Quantum Efficiency of Gold as computed by the code, and measured*

4.2.2.3 The limits of the Monte Carlo Method

A deep investigation of the code and of the Monte Carlo Method was performed to understand why the simulations were providing such bad results.

First the Geant4 toolkit was compared with another well known code: **Penelope**, developed mainly at the University of Barcelona (PENetration and Energy Loss Of Electrons and Positrons in matter, [22, 23]). This toolkit did not give better results. The same toolkit was also tested through its implementation into Geant4.
After some investigation it became clear that several problems could explain why the code would return wrong results:

- **A problem of Approach**: The Monte Carlo Method is based on a *particle/nucleus* interaction approach. The models do not include *a priori*, differences between the various chemical states and physical structures, which coexist in one material (chemical bounding, crystalline structure, grain joins, etc...). Yet those states can have a large impact on the dynamic of electrons in the material, for any defect in the crystallinity of the material corresponds to a trap. In particular, a semiconductors and metals are treated mainly the same way.
  In the case of X-rays and energetic electrons, this approximation can be considered as not too rough for at high energies, most interactions occur with electrons of the core shells of the atoms. Those inner shells being practically unperturbed, the corresponding cross sections do not vary sensibly.
  But when it comes to lower energy electrons, most interactions occur with the outer shell electrons or with free electrons, so the result becomes largely affected by the precise form of the material (chemical state, bounding to neighboring atoms, etc...), as well by its purity and its structure (change of band structure, traps, etc...). This is the main limiting factor for simulations at low energies[24] .

Unfortunately, concerning photocathodes, the key phenomenons occur at this energy, for most escaping electrons have an energy of only a few eV.

In addition, a number of other difficulties appear at small energy:

- **The quality of experimental data at low energies**. Experimental cross sections at low energies are extremely hard to obtain with a good precision. Actually, only some indirect data can be used, like *the stopping power for electrons through a thin slab*, *characteristic energy losses (plasmon excitations)*, and *the total mean free path for inelastic scattering*.
  On the other hand it is not possible to theoretically determine the values of the cross sections, as this implies solving the *many-body interaction* problem in solids.
  In practice, while cross sections are provided down to very low energies, their precision is considered as extremely poor.
- **The infrared divergence**. As explained previously, at low energies, particles tend to create large numbers of secondaries, which in turn create an even greater number of daughter particles.

To avoid this, the Monte Carlo codes block the creation of secondary particles under a certain *cut off* energy. This is extremely bad for the simulation of photocathodes, as it turns out that secondary electrons are the main contributors to the total yield (from 80 % for materials like gold to more than 99.5 % in the case of CsI[21]).

- **The specific problem of electron extraction from the material**. As emphasized by the Spicer model, the extraction of the hot electrons from the surface is a key problem, for the electrons have to overpass a barrier of potential to reach vacuum. Those potentials are of the order of a few eV high, so they are far too small to be properly simulated by Monte Carlo codes. Moreover, according to B.L.Henke *et al.*[21], most secondary electrons have an energy inferior to 10 eV. The interested reader can also read the publication by A.Gibrekhterman *et al.*, which details the proportions of primary to secondary electrons contributing to the emitted current in [19] in the case of CsI. Also B.L.Henke *et al.*[25] detail how the conditions of cleanness of the surface can have a major impact on the emission efficiency.

So the major difficulties arise from the strong dependence of the photocathode quantum efficiency on physical effects, which occur at energies unreachable by conventional general purpose Monte Carlo codes.
The few codes, which succeeded to overcome this difficulty are based on analytical formula with free parameters such as *the probability of loss of an energy $\hbar\omega$ per unit energy, momentum, and path.*
This method enables to obtain codes in very good agreement with experimental data, but they are *material specific* and cannot be extended to other materials in general (see the very interesting work by T. Boutboul *et al.*[20] in the specific case of CsI).

In conclusion, if the transport of the X-rays is well simulated by the Monte Carlo codes, the simulation of the very low electron dynamics in solid state materials is far from being enough refined to enable a proper simulation of the photocathodes.

4.3 The simulation performed

Despite of the bad performance of the code to reproduce quantitatively the efficiency of the photocathodes, simulations were performed to study the possibility of a qualitative description of the enhancement of the efficiency by varying the geometrical structure of the photocathode.
The result of those simulations is presented in this section.

4.3.1 The simulations performed

The simulation of flat photocathodes was performed to check the validity of the code. The results were presented in the section 4.2.2.2. They serve as the basis to compare with the efficiency of structured photocathodes.
Different types of structures were simulated:

- Structures with "pillars"

- Structures with "pyramids"
- Chevron like structures
- Structures randomly or periodically placed...

Those studies enabled to optimize the thickness of the photocathodes as function of the energy of the incoming photons. Indeed, the most energetic electrons are those, which exit the photocathode from the deepest places, and they are also those which are correctly simulated by the code, for their energy is high.

For example Figure 4.5 shows the position of photoemission of the electrons, which reached the vacuum in the simulation for two different energies. It clearly appears that, from the point of view of the escape length of the electrons, a photocathode of thickness 0.5 μm is too thick for low energies (here 10 keV) but well adapted for higher energies (50 keV). Both the pillar structures and the underlying layer are made of the photoemissive material (gold).

Figure 4.6 shows the simulation of a pyramidal structure with only the outer layer being photoemissive. This corresponds to the case of structures, which are covered with the photoemissive material (gold). The underlying structure would be made of a low absorbing material (like capton), which is not simulated.

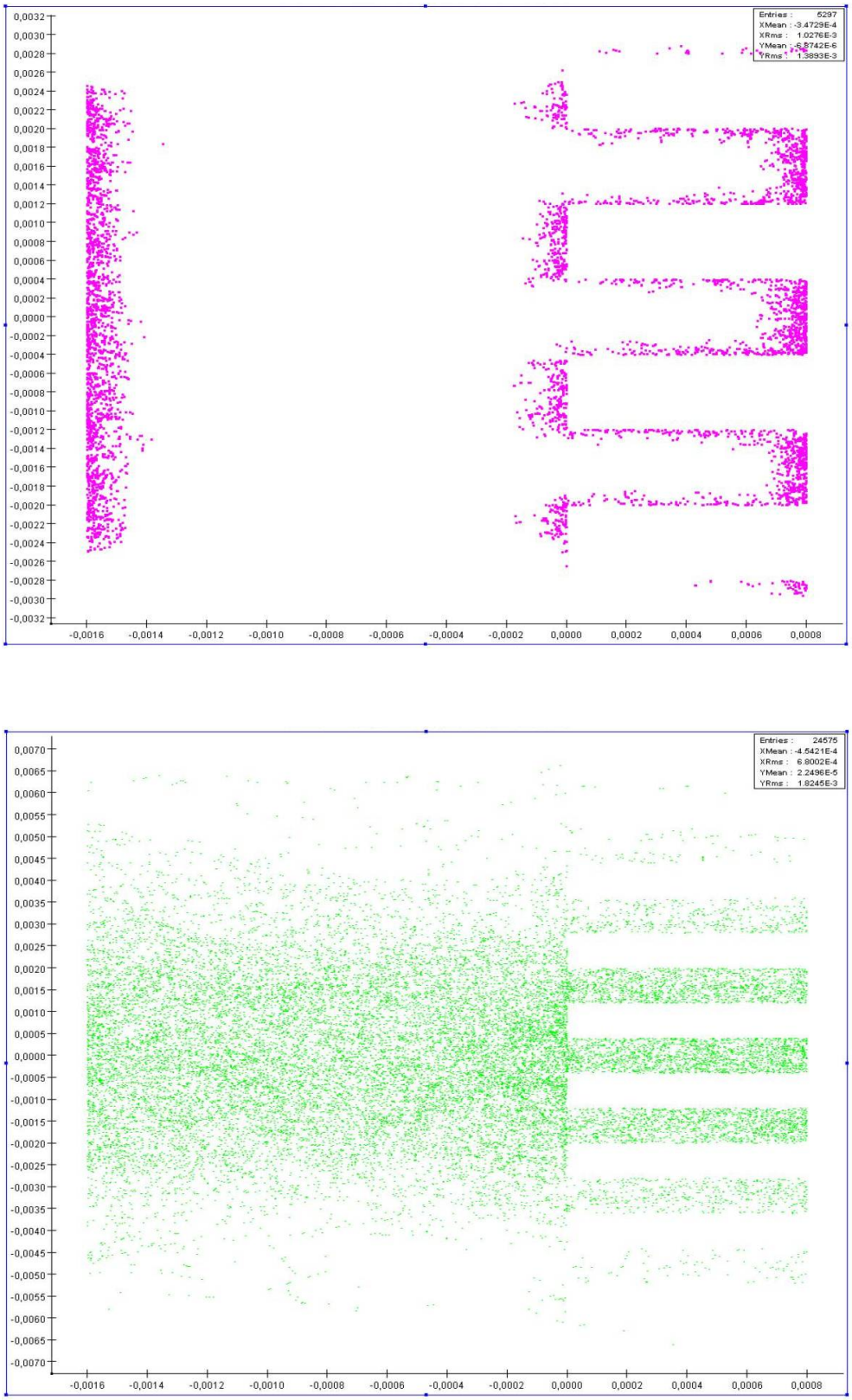

Figure 4.5 : *Simulation of Pillars structures on a photocathode of sizes* 0.8 μm *height and* $0.4 * 0.4$ μm^2 *size. Each dot corresponds to the creation of one electron, which exited the bulk.* ***Top*** *Picture corresponds to a photon energy of* 10 keV*, and* ***Bottom*** *picture to photon energy* 50 keV*.*

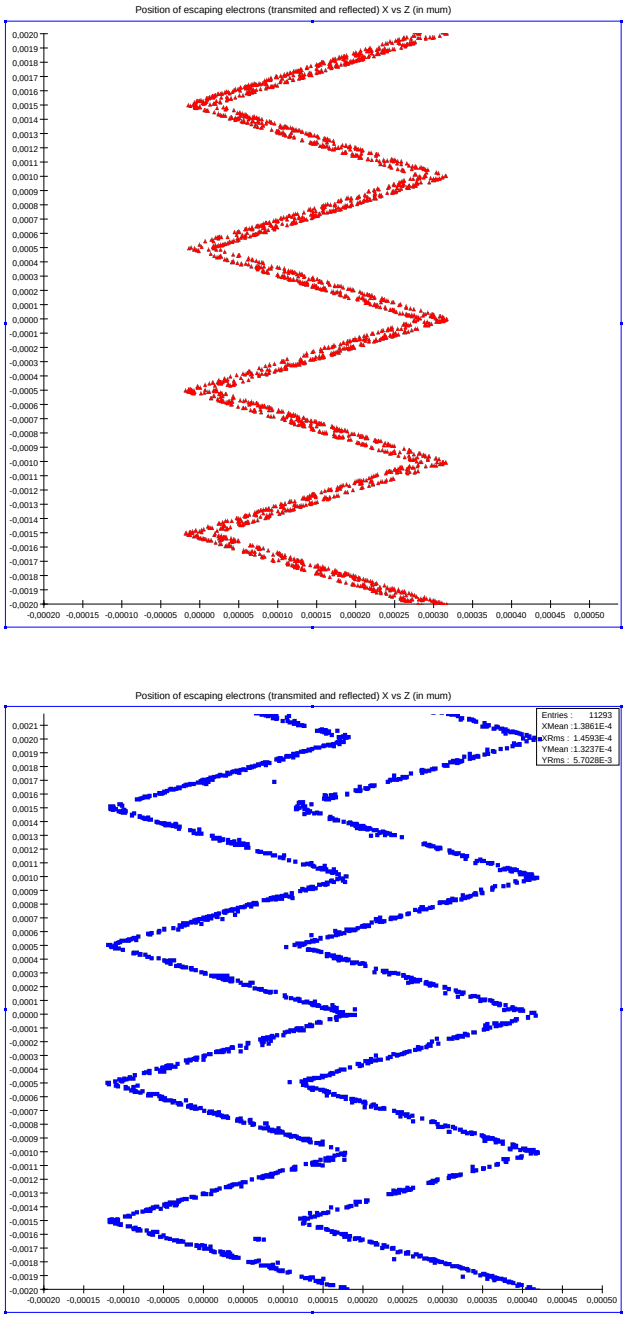

Figure 4.6 : *Simulation of periodically placed pyramidal structures with a photon energy of* 5 keV. *The* ***top*** *picture is a photocathode of thickness* 0.1 μm *and height* 3 μm. *The* ***bottom*** *picture is a photocathode with the same parameters except the thickness:* 2.5 μm.

4.3.2 Use of the simulations for thickness optimization

The simulations performed enabled to confirm that the electrons photoemitted have a very short mean free path in the photocathode. No quantitative differences in terms of efficiency could be extracted for the different thickness. Only a qualitative analysis thanks to diagrams like on figures 4.5 or 4.6

enabled to define optimized thickness.
According to this analysis, for energies in the order of a few keV (as the main target of energy range in this application), thickness of the order of a fraction of a micron seem to be the most suitable, for all tested material. Larger thickness indeed result in dead zone in the middle of the photocathode, and imply larger structures, which corresponds to a smaller surface of the photocathode, and so to a lower efficiency.
This result was predictable from the known mean free paths of electrons in photoemissive materials.

4.3.3 Simulation of the impact of structures on the photocathode

Even if the code cannot simulate properly the quantum efficiencies of photocathodes for X-ray detectors, it is *a priori* not out of hope that it can help to evaluate the effect of structures on the photocathodes.
To test the validity of the code for this, after the first experimental test of structures had been done, the simulations were compared to the experimental results.

The measurements to perform this verification are detailed in section 7.1.2. The sample *Trizact 143* is constituted of periodic square pyramids of sizes 500 μm length and height $\sim$ 160 μm (see Figure 7.4 and 7.5). The faces form an angular of 57^oC with respect to the base plane. The sample was covered with a gold layer of thickness 0.3 μm.

The measurement indicate an increase of quantum efficiency of a factor $\sim$ 1.9 in good agreement with the theoretical value of $\frac{1}{\cos(57)} = 1.9$ (see section 6.2.1).
The simulation by Monte Carlo of the flat surface calculated a quantum efficiency of 0.088 % (cf Figure 4.4) for an energy of 5 keV.
With the geometry of the trizact sample, the code returns a quantum efficiency of 0.12 %. This corresponds to a gain of a factor: $\sim$ 1.4.

So here again, the code fails to predict correctly the increase of quantum efficiency due to the structures on the surface.

4.4 Conclusion on this part of the work

Use of the code for photocathode simulations

Unfortunately, the application developed cannot be used to predict theoretically the quantum efficiencies of novel photocathodes.

The limits of the Monte Carlo Method for Photocathodes Simulations.

The impossibility to simulate properly the photocathodes properties, lies in the poor simulation of the particles interactions with matter. **This is due to the incomplete cross section knowledge for very low energy particle-matter interaction**.

More precisely, in the case of the photocathode simulations, the electrons behavior could not be simulated with a sufficient precision (while the simulation of the photons interaction were precise enough).
So, in order to use a monte carlo approach to simulate X-ray photocathodes, one must first determine precisely cross sections at energies down to a few eV.
To obtain those cross sections at such energies, it is not possible to study each material and combine the obtained cross sections to simulate mixtures of them like it is usually done at high energy for such an approach cannot take into account the chemical state of the atoms.
So each material has to be studied one by one.

Is is possible to use Monte Carlo codes for photocathode simulations ?

It is possible to overcome the lack of knowledge of the cross sections at low energies by introducing free parameters, which are then fitted on experimental data. This approach was successfully used to study CsI [20] and enabled a much better understanding of the material.
Of course this sort of method is material specific and cannot be used for general purpose photocathodes simulations (to study a great number of photocathode material).

This sort of analysis being out of the scope of this thesis work, the code was not further used, except for trivial thickness optimization analysis.

It should also be noted that the developped application would likely have been more successful in simulating the photocathode properties used with more energetic photons.
As with increasing photon energies, the fraction of energetic electrons contributing to the yield increases [21], the code is more capable of simulating the photocathodes properties.
The lack of experimental data at higher energies did not permit to test further the code, and here again it was not in the scope of this thesis work to investigate further the limits of the code.
So it is not hopeless to use a Monte Carlo code to simulate the efficiency of photocathodes in the case of photocathodes used with more energetic photons.

In particular, Geant4 offers all the needed flexibility to implement cross sections with better precision, and to adapt the Monte Carlo method to the specific case of very low energies particles.
The only limitation would be the power of the computer, as the number of secondary particles would increase dramatically (infrared divergence).

Possible other methods for the simulations of photocathode simulations with low energy photons.

Other methods to simulate photocathodes properties are analytical methods like the three step model introduced by Spicer (see section 3.1) or more simply an evaluation of the efficiency by considering the product $E\mu(E)$ (with E the energy, and μ the photoionization cross sections).
Those methods do not provide quantitative evaluations of photocathodes quantum efficiencies Yet.

It remains that *this part of the work was of great help to understand the various processes and parameters, which are key for the quantum efficiency of photocathodes in the hard X-ray energy range. This has proven to be of great help for the following research of new materials for photocathode applications.*

Bibliography

[1] S. U. et al., "Statistical methods in neutron diffusion," *LAMS-551, Los Alamos National Laboratory*, 1947.

[2] S. U. et al., "The monte carlo method," *Journal of American Statistical Association*, vol. 44, p. 335, 1949.

[3] G.Ward et al., "The holodeck ray cache: An interactive rendering system for global illumination in nondiffuse environments," *ACM Transactions on Graphics*, vol. 18(4), pp. 361–98, 1999.

[4] P.Jaeckel, *Monte Carlo Methods in Finance*. John Wiley and Sons, 2002.

[5] Agostinelli et al., "Geant4-a simulation toolkit," *Nucl. Inst. and Meth. A*, no. 506, pp. 250–303, 2003.

[6] H.Messel et al., *Electron-Photon shower distribution*. Pergamon Press, 1970.

[7] J.C.Butcher et al., "Electron number distribution in electron-photon showers in air and aluminum absorbers," *Nucl. Phys.*, no. 20, 1960.

[8] R.Ford et al., "The egs4 code system," Tech. Rep. 265, Slac, Stanford, 1985.

[9] Geant4 Community, *Geant4 User Guide-for application developers*.

[10] Geant4 Community, *Physics Reference Manual*.

[11] F.Salvat et al., "A code system for monte carlo simulation of electron and photon transport," *Workshop Proceedings, Barcelona, Spain, 4-7 July 2006: OCDE NEA*, p. http://www.nea.fr/html/dbprog/peneloperef.html, 2006.

[12] D.Cullen et al., "Epdl97: the evaluated photon data library, 97 version."

[13] S.T.Perkins et al., "Tables and graphs of electron-interaction cross-sections from 10 ev to 100 gev derived from the llnl evaluated electron data library (eedl), z=1-100."

[14] S.T.Perkins et al., "Tables and graphs of atomic subshell and relaxation data derived from the llnl evaluated atomic data library (eadl), z=1-100."

[15] H.H.Andersen et al., *The stopping and ranges of ions in Matter*, vol. 3. Pergamon Press, 1977.

[16] J.F.Ziegler et al., *The stopping and ranges of ions in Matter*, vol. 4. Pergamon Press, 1977.

[17] H.H.Andersen et al., *The stopping and ranges of ions in Solid*, vol. 1. Pergamon Press, 1985.

[18] A.Allisly et al., "Stopping powers and ranges for protons and alpha particles," tech. rep., ICRU, 1993.

[19] A.Gibrekhterman et al., "Characteristics of secondary electron emission from csi induced by x rays with energies up to 100 kev," *J.Appl.Phys*, vol. 74, pp. 7506–7509, 1993.

[20] T.Boutboul et al., "An improved model for ultraviolet- and x-ray- induced electron emission from csi," *J.Appl.Phys*, vol. 86, pp. 5841–5849, 1999.

[21] B.L.Henke et al., "The characterization of x-ray photocathodes in the 0.1-10kev photon energy range," *J.Appl.Phys.*, vol. 52(3), pp. 1509–1520, 1981.

[22] J.Barba et al., "Penelope: An algorithm for monte carlo simulation of the penetration and energy loss of electrons and positrons in matter," *Nucl. Inst. and Meth. B*, vol. 100, pp. 31–46, 1995.

[23] F.Salvat et al., "Penelope, a code system for monte carlo simulation of electron and photon transport," in *Proceedings of a Workshop/Training Course, OECD/NEA 5-7 November 2001*, vol. 19, 2001. ISBN:92-64-18475-9.

[24] J.M.Fernández-Varea, "Private communication during hands on session of the workshop on use of monte carlo techniques for design and analysis," 09 2006.

[25] B.L.Henke et al., "0.1-10kev x-ray induced electron emissions from solids-models and secondary electron measurements," *J.Appl.Phys.*, vol. 48, pp. 1852–1866, 1977.

Chapter 5

Experimental Setup and Sample Preparation

5.1 Design of the measurement setup

5.1.1 A few general considerations

The measurement of the quantum efficiency of a photocathode is not a trivial task. The actual efficiency varies greatly with the experimental conditions, and with the material quality and the shape of the photocathode material.

The main factor is the cleanness of the photocathode surface, as it has a strong impact on the work function of the material, which is the main parameter determining the quantum efficiency.
To reach the maximum quantum efficiency of one material, one has to deposit it in an ultra clean environment (ultra-high vacuum), and to perform the measurement in situ without any vacuum break.

Yet, in this work a perfect environment was not targeted as this does not enable to test the photocathode in real conditions (gas-filled detectors). Indeed maintenance operations often require to open the detector.
The preparation and mounting conditions of the samples are those typical for the preparation of gas-filled detectors (clean room environment, special care in cleaning...).

The main requirements for the photocathode quantum efficiency measurement setup are:

- Adaptability to all available sources (synchrotron, but also X-ray tube and radioactive sources). This implies the ability to work with very small X-rays flux.
- The possibility to work with samples of various sizes and shapes.
  This requires a system to keep a constant distance between the photocathode and the polarizing grid.
- The possibility to use the system both in reflection and transmission modes (electrons collected on the side of incident X-rays or on the opposite side).

Parameters	Value
Electrons acceleration	20 kV
Current Intensity	20 mA
Slits 1 aperture	7 mm
Slits 2 aperture	7 mm
Filter	Ø

Table 5.1 : *X-ray tube source parameters*

The main difficulty arises from the necessity to work with very low currents. Indeed, a ^{55}Fe radioactive source of activity $30\mu Ci$, encapsulated in the protection case typically offers a flux of $\sim 10^6$ $photons/s/4\pi$ (an avalanche photodiode measurement gives $4 \cdot 10^6 counts/s$). If the photocathode has a quantum efficiency of 1% at the k_α line of ^{55}Mn (5.9keV), then the expected current is of $10^6 * 0.01 * 1.6 * 10^{-19} \equiv 10^{-15} A \equiv 1\ fA$.
So the setup must be able to measure currents of less than a femtoamper.

The source used to perform the measurement was mainly an X-ray tube, mounted with a copper anode. Apart from measurements made for calibration purposes, the tube was used with the parameters indicated in table 5.1.

The setup was also tested on the ID15c ESRF synchrotron radiation beamline, which has a fixed energy of 39.5keV. For the signal to noise ratio was not actually better than the one obtained with the X-ray tube (flux $\sim 10^{10}$ $photons/s$, but in the meantime much lower quantum efficiencies of the photocathodes), the beamline was not often used.

5.1.2 The chamber and the ammeter

5.1.2.1 The Photocathode holder, the electrical shielding

The electrical scheme used to perform the measurements is given in figure 5.1.
It was chosen to bias the photocathode at a negative potential and to place the collection grid at ground potential, rather than polarizing the collection grid. This presents several advantages:

- a smaller sensitivity to the geometrical parameters,
- no contribution to the measured current of electrons photoemitted by surrounding materials at ground potential,
- a better use of the ammeter, which has a dedicated mode for such mounting (see later for a description of the ammeter).

Indeed, some earlier tests with the grid being polarized showed higher leakage currents (typically several fA), any other parameters being identical.

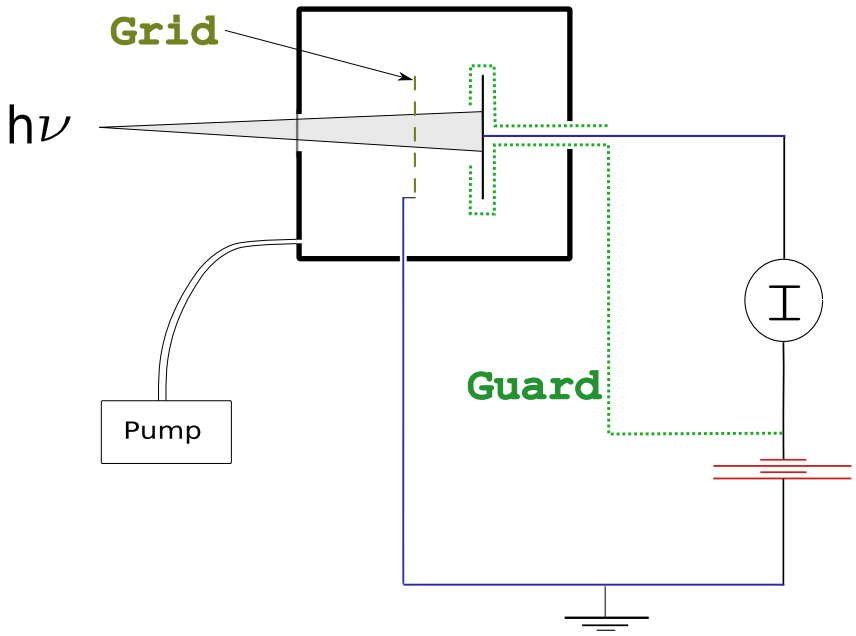

Figure 5.1 : *Schematics of the experimental setup used to make the measurements*

The holder is mainly made of PEEK, a UHV compatible, hard plastic. It also shows a high electrical resistivity (around 10^{14} Ωm at room temperature). To reduce as much as possible the surface conductivity, a cleaning with ethanol (and eventually acetone to remove traces of glue due to the copper tape -see next) was systematically performed.

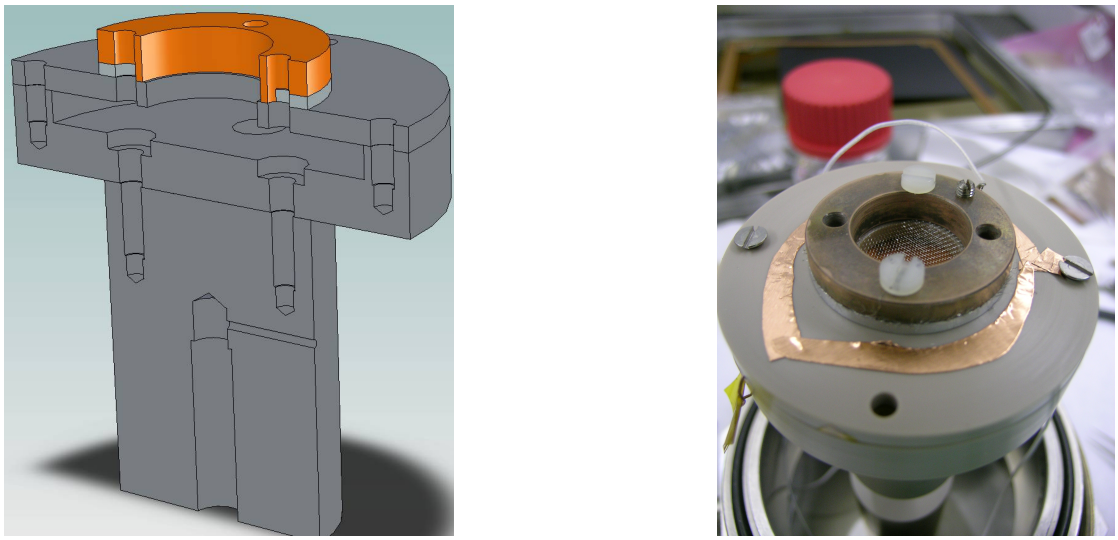

Figure 5.2 : *The photocathode peek support*

The circuit is fully shielded with guard rings. A copper tape was used to adapt the shielding to each photocathode. Special care was taken to hide the copper from the X-Rays (to avoid contribution from the copper).

The grid used to polarize the photocathode (actually it is at ground potential) is mounted on a copper holder, with an iron ring to put it under voltage.
After mounting and cleaning of the photocathode, the resistance between the photocathode and the other parts of the circuit (guard-rings and collecting grid) was typically of a few 100s $G\ \Omega$ to a few $T\ \Omega$ (as measured by the Keithley 6430, see later). When applying a voltage of $-100\ V$, typical measured leakage currents were inferior to $0.4\ fA$.

5.1.2.2 The Chamber

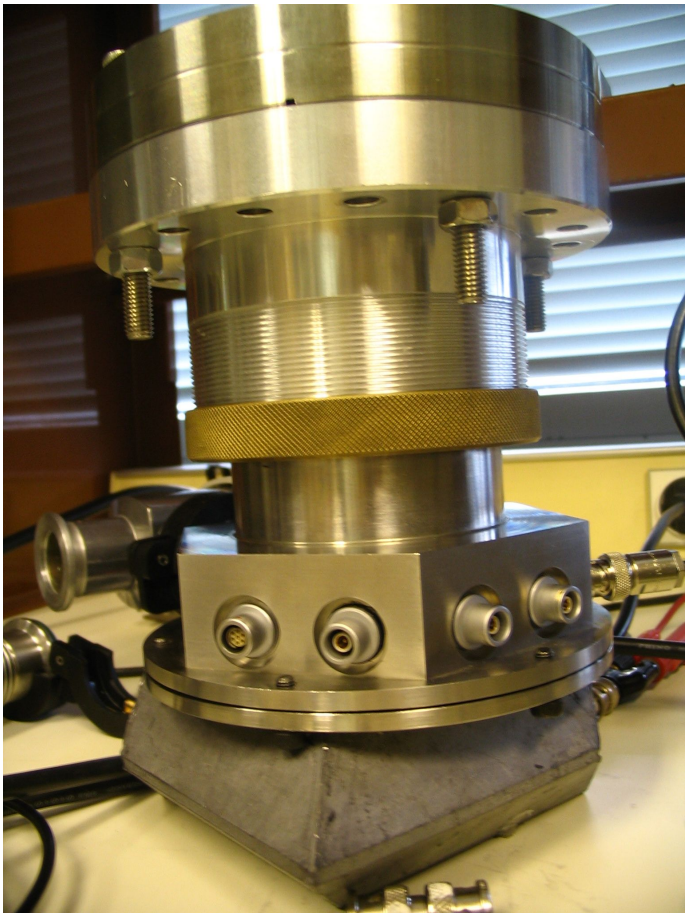

Figure 5.3 : *The chamber with some of the connectors*

The chamber has a volume of $2.5\ dm^3$. It is made of standard and custom components. It has various coaxial and triaxial connectors, as well as a KF-connector for pumping. The entrance window is a thin Beryllium window of $2 * 1\ cm^2$ size.
Connections with the ammeter are performed with triaxial feedthrough connectors (by *Pomona*)[1].

[1]For the connectors to the ammeter are 3 slot-male triaxial connectors, while the *Pomona* feedthrough are 2 slot-male triaxial male connectors, 2 to 3 slot-female triaxial connectors made by *Trompeter*.

The preamplifier of the ammeter (see later) was directly connected to the chamber (via the adaptors) without any adding extra wire.

The chamber was pumped thanks to a turbo-molecular pump. Yet no precaution was taken to reach ultra high vacuum. Only high vacuum was used to perform the measurements (to suppress any contribution of gas molecules to the measured quantum efficiency). This is justified by the need to develop photocathodes for gas-filled detectors, which have to work effectively in unclean environments.

5.1.2.3 The Keithley 6430 ammeter

The *Keithley 6430 sub-femto ammeter* is a high end electrometer by Keithley, whose main characteristic is the presence of a remote pre-amplifier with triaxial connectors, which reduces as much as possible the contribution of the leading cable to the measured signal.

Figure 5.4 : *The Keithley 6430 ammeter*

The 6430 possess several ways of operation, including the possibility to measure very small currents while polarizing the sensor to a voltage in a range $-210\ V < U < 210\ V$ (*Source-Measure Concept*). This mode was used to polarize the photocathode according to the schematic on figure 5.1. This mode is also the one providing the best internal precision of measurement [1, 2].

The 6430 can also be used to measure electrical resistances up to $20T\ \Omega$ (the measurement is performed between the guard and the source). This mode was used to check the quality of the insulation ($\sim$ *cleanness*) of the setup before each measurement.

5.1.3 Results of calibration and test of the chamber

To ensure that the setup provides reliable measurements of the photocathode quantum efficiency, a tests were performed with the X-ray tube (all tests performed with a copper cathode, acceleration parameters being 20 mA current, and 20 kV accelerating voltage).

First the setup was tested without any photocathode. This enabled to measure the contribution of the grid (parasitic photoemission). For this, the schematics presented on figure 5.1 had to be inverted, so that the ammeter would actually measure the current emitted from the grid (as a negative contribution to the measures intensity). This intensity I_0 was $I_0 < 2\ pA$. This contribution is superior to the typical leaking currents, but can be considered as negligible when compared to typical measured photo-currents (typical measured currents are of the order of 20pA to several hundred pA, see 7.1.2).

In addition, this measurement corresponds to the absence of any electric field (no photocathode). In presence of electric field, the amount of grid photo-emitted electrons is reduced to its most energetic fraction. Other electron cannot escape the attracting potential.

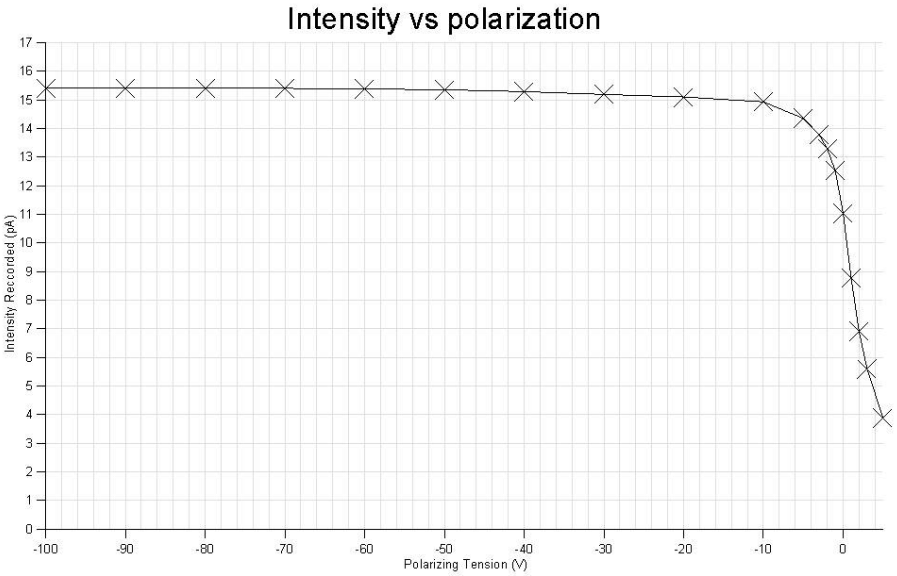

Figure 5.5 : *Current-Voltage (I-U) characteristics of the experimental setup in presence of X-rays with a gold photocathode.*

With the same configuration (*ammeter connected to the grid*), tests were performed with a "non emitting photocathode": a thick kapton foil with copper on the back layer to bias it. This was used to measure an hypothetical contribution of the surrounding materials (from the PEEK made holder). Again this contribution was extremely small, for no current could be recorded (contribution inferior to the intrinsic noise of the system $\sim 0.1\ fA$).
This measurement also confirms according the previous measurement (no bias, ammeter connected to the grid) that the contribution of the grid is very small.

Last a reference system (gold deposited on a kapton foil by sputtering) was used to study the dependence of the electrons collection quantum efficiency on the bias voltage. The result is depicted in figure 5.5.
A current saturation clearly appears for voltages inferior to $-40\ V$. The non zero intensity for positive bias can be explained by the proportion of photoemitted electrons with high kinetic energy (see [3]). Electrons emitted with energies superior to 100 eV (theoretically up to 20 keV for the tube was used with an acceleration of 20 kV) have a sufficient energy to escape the attractive potential of the photocathode and so are counted. The small current value at positive voltages highlights the small proportion of photoemitted energetic photons.

Photoemitted currents as function of the electron intensity on the cathode also follows a very good

linearity with the X-ray tube current in the range [10 mA; 40 mA]: the photoemission is proportional to the flux of X-rays. This indicates that there is no saturation effect at those intensities (like charging of the surrounding material, which would affect the extraction electric field).

5.1.4 Conclusion concerning the setup

The test of the setup was a success: the setup shows very good characteristics for the measurement of very low currents. Its intrinsic noise is inferior to the fA, and can measure the typical currents emitted by the photocathodes ($pA \leftarrow nA$). The Keithley ammeter guaranties $5\frac{1}{2}$ digits at those currents.
Its high modularity enables the test of photocathode samples of very diverse sizes and characteristics. The setup can be used with various sources of X-rays: radioactive sources, X-ray tubes, and synchrotron beamlines.

Bibliography

[1] keithley Instruments Inc., *Private Communication with Keithley*, 2004.

[2] keithley Instruments Inc., *Keithley 6430 Manual, Chapter 5*, 2000.

[3] B.L.Henke et al., "The characterization of x-ray photocathodes in the 0.1-10kev photon energy range," *J.Appl.Phys.*, vol. 52(3), pp. 1509–1520, 1981.

Chapter 6

The different concepts to make a photocathode

Different approaches were taken to try to increase the photocathode quantum efficiencies. Some ideas were explored only theoretically, while others -more promising- lead to the fabrication of test-samples to compare them with reference photocathodes.

6.1 Indirect conversion

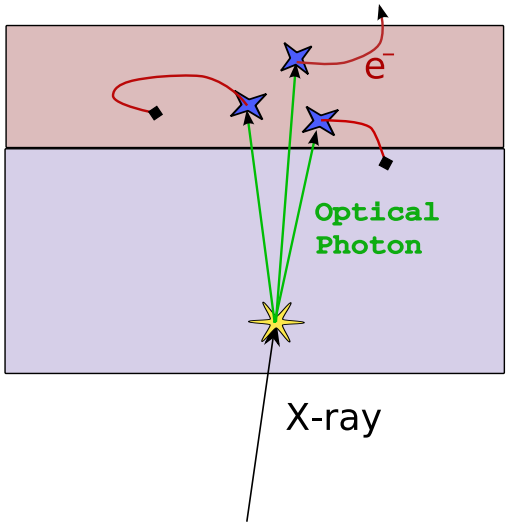

Figure 6.1 : *A two step photons to electron conversion*

In this section, an *indirect conversion* of the X-rays into electrons is evaluated. The X-rays are first converted into lower energy photons thanks to a scintillating material, and then the photocathode converts those photons into electrons.
The origin of this idea is the availability of photocathodes offering good quantum efficiencies in the visible or UV energy range (infra-red sensitive photocathodes were not considered as they involve

cooling systems to suppress their intrinsic noise -due to thermal emission), while one can benefit from the yield of scintillators (several UV/visible photons created per incoming X-ray). In addition with this technique one can hope to convert 100 % of the X-rays into visible/UV photons, and so avoiding the presence of X-ray photons in the back-end electronic, which can be problematic (for the noise of the system mainly).
If a fluorescent material can produce low energy photons with yields as high as $50,000\ photons/MeV$, if about one hundredth of those photons hit the photocathode (the solid angle corresponding to angle without total reflections is small), and if this photocathode has a quantum efficiency of 10 %, then for 10 keV incoming photons, the expected yield is:

$$50,000 * 0.01 * \frac{1}{100} * \frac{1}{10} \sim 0.5\ e^-/photon.$$

This is of course only a theoretical value.
Several aspects have to be considered when making such a system, including the predictable time response, which has to be compatible with high count rates and the resolution of the system, which must be compatible with the targeted pixel size.
Some prototypes (like [1, 2, 3]) exploiting such an approach were already made for PET application (so with much higher photon energies), but none of them could provide good results until now. This study explore the principle in the case of lower energy X-rays.

6.1.1 Photocathodes in visible and UV

The requirement for the photocathode to work in the visible range are the same as for those working in the X-ray energy range. Yet, because of the difference of energy, one does not have to limit the research to high Z materials, so providing a much wider range of possibilities. This is very interesting as in general there are more materials with well controlled physical and chemical properties. Lastly, photocathodes working at low energies find a lot of applications in astronomy, photo-injectors (coupled with short-pulse lasers). At those energies they are typically found in photomultipliers and phototubes.
The most common photocathodes in the visible/UV energy range (available industrially) are:

Bialkali photocathodes such as $Sb-Rb-Cs$, $Sb-K-Cs$. They feature a spectral responses in the optical and close UV. They are usually not very stable, and so their use cannot be envisaged.

Multialkali photocathodes especially $Na-K-Sb-Cs$, which exhibit a very wide spectral response, from ultraviolet to wavelength as long as 930 nm.

GaAs also with a very wide spectral response. Eventually GaAs photocathodes are covered with Cs to make them NEA (negative electron affinity), but this is at the cost of a higher sensibility to pollution.

Solar Blind Photocathode especially GaN, KBr, $CsBr$, $InGaN$ and $Al_xGa_{1-x}N$. Most were developed for space applications (UV cameras, insensible to light pollution due to the sun). Those photocathodes often exhibit quantum efficiencies of more than 30 %, at wavelength inferior to 350 nm. Among those photocathodes, GaN is the material which offers the most promising characteristics.

Diamond (**C***) is a relatively new photocathode, which offers several advantages: it is rather stable [4] and NEA[5, 6] when plasma-hydrogenated. In addition in principle it suffers less than other materials from pollution due to organic gases such as methane (which is a good gas for amplification). Diamond photocathodes are obtained by *CVD*[1], or by *low energy ion deposition* of carbon. They are amorphous materials, which exhibit a mixture of sp^2 (graphite like) and sp^3 (diamond like) bonds (CVD deposited diamonds are usually better as they exhibit a higher proportion of diamond like bonds, and a better crystallinity). The surfaces are then treated by plasma hydrogenation in order to make the surface NEA. The problem comes from its sensitivity limited to wavelength inferior to 210 nm (large band gap semiconductor: 5.47 eV).

6.1.2 Scintillation materials

There are various materials able to provide fluorescence photons at various energies. They are characterized by four main parameters:

- The fluorescence yield, usually given in *photons / MeV*. The linearity of the yield is excellent for energies up to a few MeV.
- The energie(s) of emitted photons.
- The time response of the scintillator, often there is a fast response corresponding to few photons and a slower one corresponding to a much higher yield, and to an energy slightly different.
- The achievable resolution with the scintillator. This is strongly related to the thickness of the deposited layer. But in average, with a resolution of a few μm, most materials can absorb 100 % of the photons with wavelengths inferior to 30 keV.

To obtain a competitive quantum efficiency, as shown in the calculus made in the introduction, a minimum yield of $10,000$ $photons/MeV$ is necessary.
As said previously, it would be best to have a photocathode sensible to UV light. So the fluorescent material needs to have a good yield at those wavelength (typically less than 350 nm).
Also, the aim of the project is to build a detector able to work in counting mode, and with a typical count rate of the order of 1 MHz. This means the *decay time constant* of the fluorescence must be at least one order of magnitude smaller, so of the order of 100 ns.

Here is a list of the most commonly used scintillation materials with high yields, small decay times, and maximum of emission at energies inferior to 500 nm [7]:

$NaI(Tl)$ is one of the most common scintillators. Pure NaI offers a maximum yield of $76,000$ $photons/MeV$ at $\lambda_{max} = 303$ nm, and with a scintillation decay time constant of 60 ns. It is more often used doped with thallium, and then has the following parameters: $\lambda_{max} = 415$ nm, with yield $38,000$ $photons/Mev$ and a decay time constant of 230 ns.

BaF_2 is interesting because it emits very energetic photons: the fast component, which is 25 % of the total yield is at 220 nm with a yield of 2500 $photons/MeV$ and a decay time constant of 0.6 ns. The main maximum is at 310 nm with a decay time constant of 630 ns.

[1] CVD stands for Chemical Vapor Deposition

$CsI(Na)$ has a maximum emission at 420 nm, with a total yield of $38,000$ $photons/MeV$ and a decay time constant of 630 ns.

$CaF_2(Eu)$ has its maximum at 435 nm, a yield of $19,000$ $photons/MeV$, and a decay time constant of 630 ns.

$K_2LaCl_5(Ce)$ has its maximum at 380 nm, with a yield of $30,000$ $photons/MeV$, and a decay time constant of 80 ns.

$LaCl_3(Ce)$ has its maximums at $330 - 352$ nm with a yield of $49,000$, with several components, which have all a decay time constant inferior to 200 ns.

$LaBr_3(Ce)$ has its maximums at $358 - 387$ nm, a total yield of $61,000$ $photons/MeV$, and 90 % of the emission occurring before 90 ns.

$Lu_2Si_2O_7(Ce)$ (LPS) has a total yield of $23,000$ $photons/MeV$, with maximums of emission at $380 - 385$ nm, and a decay time constant of 38 ns.

$LuI_3(Ce)$ has a maximum emission at 465 nm, with a yield of $33,000$ $photons/MeV$, and a decay time constant of 34 ns.

$RbGd_2Br_7(Ce)$ has a maximum of emission at 420 nm, with a yield of $56,000$ $Photons/MeV$, and a decay time constant of 43 ns.

BrilLance® 350 *and* 380 of formula $LaCl_3(10\%)$ and $LaBr_3(5\%)$ by the Company St Gobain are also very interesting: BrilLance®350 for example offers a maximum of emission at 350 nm, with a yield of $49,000$ $photons/MeV$, and a decay time constant of 28 ns.

In conclusion, there are a lot of materials providing maximums of emissions in the close ultra-violet energy range, with acceptable decay time constants, and good yields. Unfortunately, all high yield materials are limited to wavelengths superior to 300 nm, which is a problem as shown next.

6.1.3 Possible combinations

To obtain a good quantum efficiency, it is of course mandatory that the maximum of emission (and more generally, the whole spectrum of emission) of the scintillation material be contained in the spectrum of sensitivity of the photocathode.
For the same reasons as previously exposed, it is also necessary that the photocathode exhibits a good robustness to pollution and to irradiation damages. The robustness to pollution of the scintillator is less important, as it can be well protected if enough care is taken by the photocathode and the substrate.

This leaves few choices of photocathode.

Diamond

In spite of its very interesting characteristics of quantum efficiency, diamond cannot be chosen, for its sensitivity starts at energies unreachable by scintillation processes. In addition, diamond is not yet well known as a material, and only a few groups can produce diamond with a sufficient quality (in terms of crystallinity, hydrogen activation quality, purity of the material). Yet diamond is now

a subject of great interest for applications in the field of photocathodes (solar blind, for space applications), so it might become an interesting alternative in the future, also if suitable scintillation materials are discovered in the future.

Bialkali and Multialkali

Bialkali and Multialkali are very interesting because they offer a good sensitivity at the emission peaks of high yield scintillators. Unfortunately they are also extremely sensitive to pollution and moisture, and even protective layers do not prevent loss of yield after short exposure to polluting environments [8].

GaN and relatives

Those photocathodes have been the subject of a lot of studies for they offer a very good quantum efficiency below the long-wavelength cut off (typically $Q.E. \sim 0.4$) while having a very low quantum efficiency above this cut-off. This is of special interest for solar-blind detectors in space applications. In our case this means that they could be coupled to high-yield scintillators to form a two step X-ray photocathode. In particular an association of a NaI scintillator and GaN photocathode seems to be a promising combination.

Alas, those photocathodes also require a good vacuum to work effectively. So for the same reasons as previously, they cannot be used in detectors using gas amplification.

Protected photocathodes

Studies have been made to try protecting UV and visible photocathodes for the specific case of gas-filled detectors [8]. The possibility exists to effectively reduce the sensitivity of the photocathodes to moisture and oxygen (the main contributors to the degradation of the photocathodes in unclean environments), but at the cost of a highly-reduced quantum efficiency (at maximum 10 %, the protection depending on the thickness of the protecting layer).

6.1.4 Conclusion

It appears clearly that in spite of its promises it will be difficult to build a 2 steps photocathode for X-ray detection.

Diamond seems to be the most promising material, for it is a robust material (yet no real studies of the stability of the hydrogenated surface -by plasma activation or else- could be found), but short wavelength scintillators have still to be found. Otherwise carbon does not offer the stopping power mandatory to enable a good quantum efficiency with X-rays without a first conversion stage.

The other materials unfortunately do not offer a stability good enough to guaranty a good reliability when used in gas-filled detectors.

6.2 Direct conversion

As an indirect conversion does not seem to be a good way of designing a photocathode for gas-filled detectors, a direct conversion has to be used.
There are various possibilities to better the quantum efficiency of the photocathodes presented in section 3.3. Three approaches were studied theoretically and experimentally in the scope of this work to try bettering the quantum efficiency of photocathodes in the X-ray energy range:

- Modify the geometry of the photocathode in order to maximize the yield of a material,
- Use of sharp tips to profit from a field emission phenomena,
- Investigate new materials in order to find one with better properties.

All three approaches are detailed in the following subsections:

6.2.1 Modify the geometry to increase the yield of one material

As explained in section 3.1, the yield of the photocathode depends directly on the ratio $\frac{l_a}{L}$, where l_a is the *absorption length* and L is the *scattering length*.

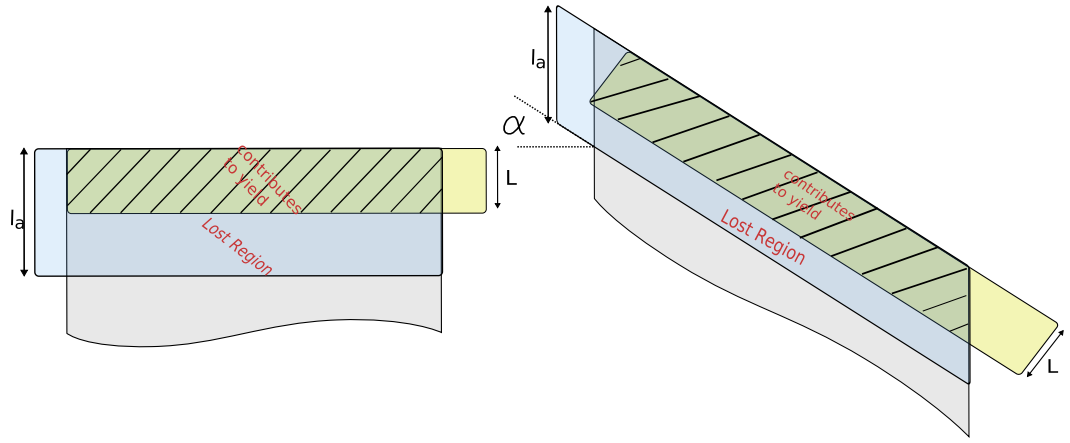

Figure 6.2 : *The impact of the incidence angle of photons on the active area (contributing to the yield).*

This formula is valid in the case of photons with a direction perpendicular to the surface. Indeed in the case of photons with slanted directions, the apparent thickness is increased, leading to more photons absorbed in the *active area* (distance to the surface inferior to L). With the definition of the angle α of Figure 6.2, the theoretical increase of quantum efficiency is a factor $\frac{1}{\cos(\alpha)}$:

$$Efficiency \propto \frac{l_a}{L} \cdot \frac{1}{\cos(\alpha)}. \tag{6.1}$$

This was measured by D.P.Lowney *et al.* in [9] in the case of CsI, and the measurements show a good agreement with the formula.

To use this effect, the classical way is the use of a grazing incidence. Unfortunately, this leads also to technological problems, and to the impossibility of making large areas detectors. So in this work the possibility to use microstructures was investigated.
More generally this approach consists in increasing the surface to volume ratio of the material, as this increases the *active area*. In fact the best available photocathodes have a controlled microstructure, which maximizes this surface to volume ratio (often a columnar structure obtained during the deposition of the material).
The main requirement for the microstructures concerns their size: they should be much smaller than the pixel size (collecting anodes in the case of a gas amplification), which means **structures with typical sizes of less than a micron**.
Various ways of playing with the geometry were tested during this study, as will be shown in the coming subsections. Only systems which can be obtained on large surfaces for a reasonable price were used during this study.

6.2.1.1 Porous Photocathodes

The most straightforward way of creating a structure is the use of a porous material. Indeed this enables the creation of a much larger surface (so a greater active area) actually reached by the photons (then the *absorption length* becomes $\frac{l_a}{Porosity}$, where $Porosity$ is the fraction $\frac{V_{pores}}{V_{total}}$ in the material). But as explained in the previous section, with increasing porosity, the probability that emitted electrons reach the actual surface of the photocathode also decreases for the electrons have to find their way through the connected pores or even through thin walls between pores to then exit the photocathode. While M.P Lorikyan [10] published interesting results using this sort of materials, the measurements could not be later confirmed, and doubts subsist concerning a possible amplification inside the pores, which would affect the measurement of the quantum efficiency (as several electrons would be detected per single detected photon).
Still a similar approach was used for some of the samples prepared, and results are given in the next chapter.

6.2.1.2 Regular Structures

Modern photocathode always have a microstructure, which maximizes the surface to volume ratio, in order to have a maximum active area. Yet the structure is not fully controlled as it is most often obtained by carefully controlling the deposition parameters so that the photocathode material adopts a columnar growth [11]. So there is little control on the actual structure of the deposited material.
Another approach can be the use of a patterned substrate or a process able to imprint the desired structure in the material. So that the geometry of the deposited material is well controlled and optimized.

The main problem of structured photocathodes lies in the lack of escape path for electrons reaching vacuum (or the gas) at a point far from the surface of the photocathode. The solid angle is indeed

inversely proportional to the square of the aspect ratio of the structure[2]

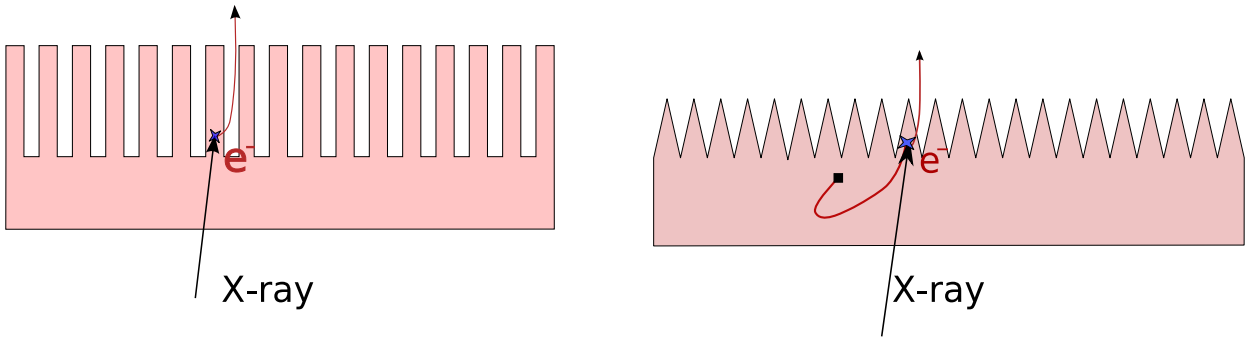

Figure 6.3 : *Two examples of regular Structures.*

There are some requirements to respect to guarantee a minimum quantum efficiency of the photocathode:

- For the photocathode has to work in transmission, special care must be taken to guaranty an excellent transparency to X-rays of the substrate. Ideally the substrate is thin, made of low Z material, and flexible in order to guarantee a good mechanical robustness. Organic materials like kapton or some sorts of polymers are good candidates.
- The process used to create the structures must be adaptable to large surfaces at an acceptable price. In particular, etching technologies or holographic-based technologies, which are common in the semiconductor industry should be avoided, for their costs increase dramatically with large surfaces. On the other hand, physical engraving technologies are well adapted (see the example of the *Trizact Sample* in the next Chapter).
- The uniformity of the pattern has to be good enough to guaranty a good homogeneity of the conversion efficiency.

As said before, typical sizes of the structures must be small enough to ensure that they will have no impact on the uniformity of the image.
In addition, in theory it would be best to match the typical escape length[3] of the emitter material. Indeed smaller sizes will not enable to minimize the transparency and larger sizes will result in a loss of flux in the active area of the photocathode.
But in practice the typical values of L are very hard to obtain (for example $L(Gold) \approx 2\ nm$ and $L(CsI) \approx 50\ nm$), and as the photocathode works in transmission, it is better to deposit a thin layer of the high yield material (thus high stopping power) on top of a low stopping power structured material, so that a maximum flux of photons reaches the active area of the material.
Concerning the shape, a trade-off must be done between two different requirements:

[2] For example, in the case of a square well of surface l^2 and deepness h, the solid angle from the bottom of the well is $\frac{l^2}{4\pi h^2} \propto \frac{1}{(Aspect\ Ratio)^2}$).
[3] the escape length is inferior to the scattering length because of the work-function/electron affinity of the material.

1. The higher the aspect ratio, and the higher the angle with the surface of the structure, the larger the active area,
2. The smaller and the more separated the structures are, the higher the electron escape solid angle is, and so the higher the escape probability.

It is also better to have non rectangular like shapes, as the active area is very thin. Pyramidal, or conic like shapes, offer a larger surface of the photocathode with an oblique surface with respect to the X-rays.

Those shapes also enable a better penetration of the electric field between the structures, and offer a larger solid angle for electrons allowing exit from the bulk of the material far from the top of the structures. Indeed, the surface of the material often exhibits an attractive potential to electrons in the gas (except in the case of NEA materials), so electrons are likely to return back in the material again before reaching the surface of the photocathode.

To increase the escape probability of the electrons, one has to use an electric field. Unfortunately, also the efficiency of the electric field is limited: Figure 6.4 depicts the result of the simulations of the electric field in the case of metallic structures with rectangular and triangular shape by means of a Finite Element Method (the simulations were performed with *Comsol Multiphysics*). The back surface (flat) of the structure was at ground potential, while a "collecting plane" above the structures was at a potential of 100 V.

It appears in the simulation, that the electric field penetrates more into the triangular structures. In both cases yet, the values reached are very small. Fortunately, most electrons exit the bulk material with energies of only a few eV, so even a small electric field can have a strong impact on the collection of the electrons.

In conclusion, the simulations show that the *aspect ratio* ($\frac{Height}{Width}$) of the structures cannot be very high, otherwise the electrons created far from the surface will be not extracted.

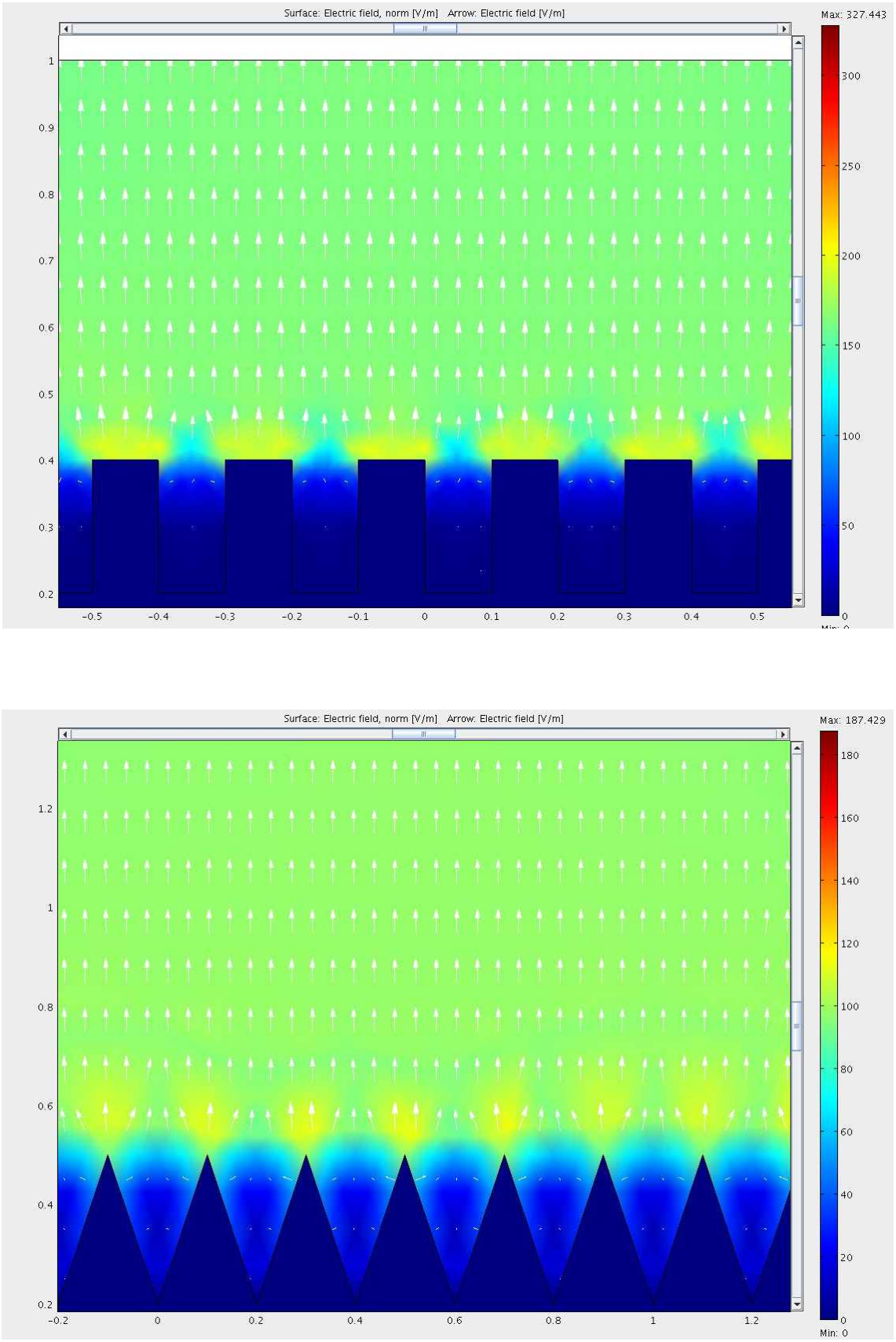

Figure 6.4 : *Simulations of the electric field in triangular and rectangular structures.*

6.2.2 Field emission

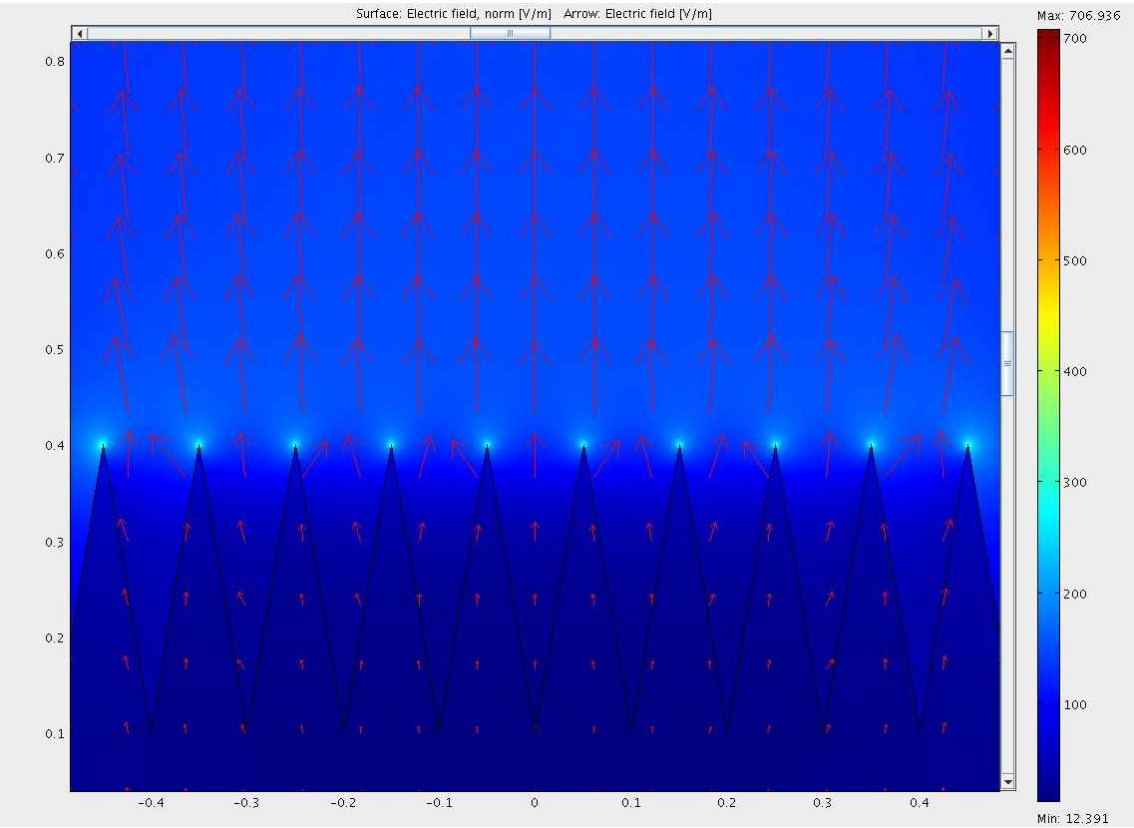

Figure 6.5 : *Simulation of the electric field in the case of silicon sharp tips.*

As explained in section 3.1, the most important parameter for photocathode quantum efficiencies concerns the electrons extraction of the material. Several studies [12, 13, 9] were performed to evaluate the effect of an electric field to diminish the potential barrier electrons have to overpass to reach vacuum (the electron affinity/work function). Those studies showed that strong electric field is needed to have a real impact on the quantum efficiency of the photocathodes. This can be explained by the much higher value of the *dielectric permittivity* in solid materials (ex. $\varepsilon(CsI) = 6.3$ and $\varepsilon(Si) = 12$) than in gas/vacuum ($\varepsilon(vac.) = 1$): in the case of two dielectrics superposed, the proportion of the energy stored in both materials is the inverse of the ratio of the electric permittivities. As a result the electric field has a very small value inside the material, and does not effect much the dynamics of the electrons in the material (see the simulations by finite elements of metal microstructures on Figure 6.4). To create a strong field inside the material, one has to connect electrodes to the photocathode, which is of course not possible in the case of electro-emitters (the electrode would take the role of the emitter).

In order to improve the electric field, it was envisaged to use sharp tips to profit from the concentration of the electric field around sharp tips (*Tip effect*), and so create a field emission system.
Figure 6.5 depicts the result of the simulation by the finite element method of such sharp silicon tips.

Indeed, a strong electric field appears at the top of the tips.

Such arrays were already successfully used in association with short pulse UV-lasers for photo-injectors systems [14], and could be interesting for photon-detection systems. Tests were performed with silicon-made tips arrays in order to test the efficiency with X-rays.

6.2.3 A new material: CsI_3

In parallel to the work made to enhance the emission properties of known materials by changing the geometry of those materials, new materials were investigated. Following the example of CsI, which is currently the best material in terms of quantum efficiency, various iodide were studied.
In particular, CsI_3 as a derivative material of CsI was found to share some interesting physical properties with CsI, while solving some issues specific to CsI.

Bibliography

[1] G. Charpak et al., "Some studies of the application of csi photocathodes in gaseous detectors," *Nucl. Inst. and Meth. A*, vol. 333, pp. 391–398, 1993.

[2] J. Van der Marel et al, "A microgap photomultiplier for the read-out of a $laf_3 : Nd(10\div)$ scintillator," *Nucl. Inst. and Meth. A*, vol. 410, pp. 229–237, 1998.

[3] F.Garibaldi et al, "A pet scanner employing csi films as photocathode," *Nucl. Inst. and Meth. A*, vol. 525, pp. 263–267, 2004.

[4] A.Laikhtman et al., "Absolute quantum photoyield of diamond thin films: Dependence on surface preparation and stability under ambient conditions," *Nucl. Inst. and Meth. A*, vol. 73,10, pp. 1433–1435, 1998.

[5] J.Roberston et al., "Band diagram of diamond and diamond-like carbon surfaces," *Diamond and Related Materials*, vol. 7, pp. 620–625, 1998.

[6] D.Vouagner et al., "Photoemission properties and hydrogen surface coverage of cvd diamond films," *Diamond and Related Materials*, vol. 13, pp. 969–974, 2004.

[7] M.Globus et al., *Inorganic Scintillators For Modern And Traditional Applications.* National Academy of Sciences of Ukraine., 2005.

[8] E.Shefer et al., "Photoelectron transport in csi and csbr coating films of alkali antimonide and csi photocathodes," *J.Appl.Phys.*, vol. 92(8), pp. 4758–4771, 1993.

[9] D.P.Lowney et al., "Characterization of csi photocathodes at grazing incidence for use in a unit quantum efficiency x-ray streak camera," *Review of scientific instruments*, vol. 75,10, pp. 3131–3137, 2004.

[10] M. P. Lorikyan, "Study of counting characteristics of porous dielectric detectors of radiations," *Nucl. Inst. and Meth. A*, vol. 515, pp. 701–717, 2003.

[11] H.S.Cho et al., "A columnar cesium iodide (csi) drift plane layer for gas avalanche microdetectors," *IEEE transaction on Nuclear Science*, vol. 45(3), pp. 275–279, 1998.

[12] A.Breskin et al., "Electric field effects on the quantum efficiency of csi photocathodes in gas media," *Nucl. Inst. and Meth. A*, vol. 344, pp. 537–546, 1994.

[13] A.Breskin et al., "New ideas in csi-based photon detectors: Wire multiplication and protection of the photocathode," *IEEE Trans.Nucl.Sci*, vol. 42(4), pp. 298–305, 1995.

[14] e. J. M. Nation, "Advances in cold cathode physics and technology," *Proceedings of the IEEE.*, vol. 87, 5, pp. 865–889, 1999.

Chapter 7

Experimental tests and discussion of the results

Not all the different approaches to improve the photocathodes were experimentally tested. In particular, the indirect conversion photocathodes were not actually fabricated, for no good combinations of scintillators and emitters could be found. Otherwise, most ideas to improve the photocathode quantum efficiencies were tested. This section follows the structure of the previous one and gives the experimental results obtained.

7.1 Modify the geometry to increase the yield of a material

As previously explained, the approach of modifying the geometry of one material consists in benefiting from the increasing of the quantum efficiency in the case of an oblique incidence of photons on the surface of the photocathode material. Only samples potentially manufacturable as large surfaces were used.
Mainly two types of structured photocathodes were tested:

Random Structures were actually *sand paper* materials normally used for the coarsing of surfaces. The different *grades* of papers enabled to test further the impact of the structure sizes on the quantum efficiency.

Periodic Pyramidal Structures were special sorts of sand paper available in a very special and periodic shape. They are normally used for highly demanding polishing applications (in terms of uniformity, and robustness of the paper).

The reference sample was a flat Kapton foil.
Those samples were covered with $0.2-0.4\ \mu m$ of gold by argon ion sputtering (the thickness could not be precisely controlled, so the thickness was evaluated thanks to the given deposition characteristics of the machine). This thickness was sufficient to ensure a maximum yield (thickness greater than the escape length) while not changing radically the structure shapes.

7.1.1 Analysis of the microstructures characteristics

Several samples were created and their structures were analyzed both with an optical and a scanning electron microscope (SEM).

First a flat kapton foil was taken as a reference photocathode.

For the random structures, the samples were the following (SEM images):

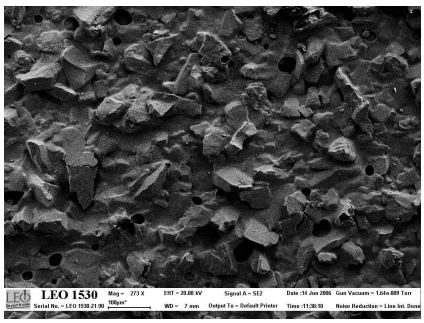

Figure 7.1 : ***Grade 280 sample****: Random structures of sizes* $\sim$ 100 μm.

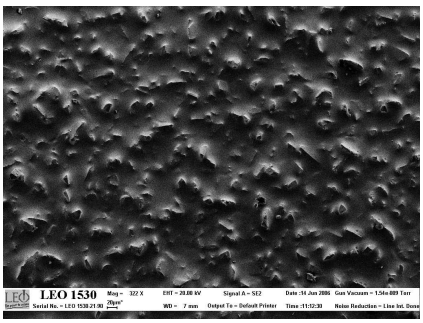

Figure 7.2 : ***Grade 800 sample****: Random structures of sizes* $\sim$ 20 μm.

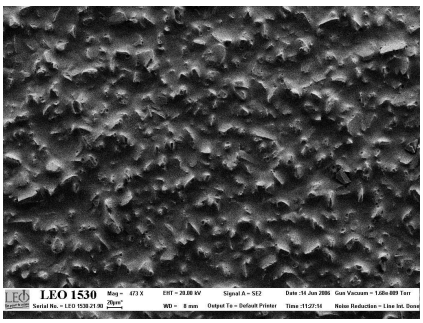

Figure 7.3 : ***Grade 1200 sample****. Random structures of sizes* $\sim$ 10 μm.

Those samples were made with normal sand paper, normally used for grinding of surfaces. Higher grades correspond to a finer smoothening, so structures are smaller and more numerous. The sizes indicated under each pictures (7.1, 7.2, 7.3) are those of the largest structures (covering most of the surface), and are always surrounded with smaller structures.

For the periodic structures, the special Trizact 143 paper by the company 3M was used. Those structures are obtained by positive engraving in a special polymer and are available in large areas.

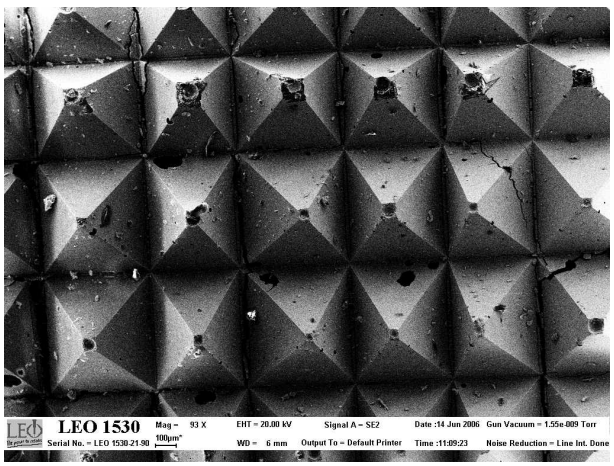

Figure 7.4 : ***Periodic Structures seen from top*** *SEM image, size of structures* $\sim$ 500 μm

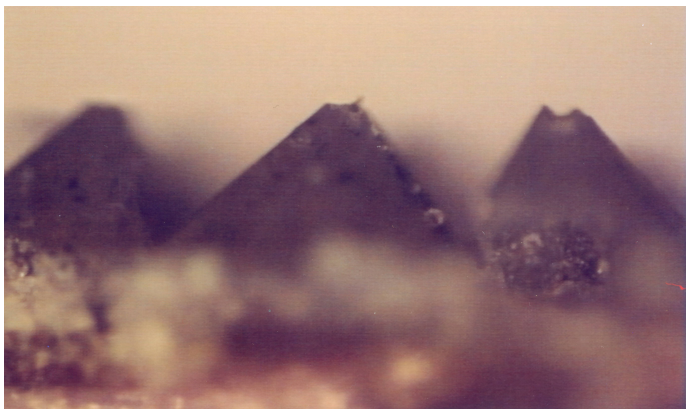

Figure 7.5 : ***Periodic Structure seen from the side*** *Optical Microscope.*

The side surfaces form an angle of $\sim 57^o$ with respect to the base plane (averaged on several pyramids).

7.1.2 Efficiency measurements

The different samples presented were all covered with a layer of gold of thickness $\sim 0.3\ \mu m$. This thickness is far bigger than the escape length of gold (a few nm), so there is no contribution to the yield from the substrate. The structures are much larger than the gold thickness, and there was no attenuation observed of the quantum efficiency due to a "smoothening" of the surface by the deposited layer (different thickness of deposited gold gave the same results).

The results are presented compared to a flat surface of gold obtained in the same conditions in table 7.1 (X-ray tube parameters: 20kV acceleration voltage, 20mA intensity, with Cu anode):

Substrate	Gold Thickness (μm)	Measured Current (pA)
Kapton	0.3	18.5 ± 0.9
Sand Paper Grad 280	0.3	22.4 ± 1.1
Sand Paper Grad 800	0.3	20.8 ± 1.0
Sand Paper Grad 1200	0.3	19.4 ± 0.9
Trizact 143	0.3	34.65 ± 1.7

Table 7.1 : *Results intensities of gold covered structured paper*

The best sample is the Trizact 143, which indeed offers the largest inclined surface (so a higher active area). It should be noted that with respect to the flat Kapton sample, there is a factor

$$1.87 = \frac{34.65}{18.5} \approx \frac{1}{\cos(57)} = 1.83$$

as predicted by the formula in section 6.2.1.

Sand Paper do not give results as good as the periodic trizact samples, probably because the structure covered surface is much smaller than that of the trizact samples.

7.2 Field Emission

Silicon sharp tips were obtained and tested to evaluate their potential in the case of X-ray photocathodes.

7.2.1 Analysis of the microstructure characteristics

The sample is formed of a periodic array of 4.5 μm separated tips, engraved in a silicon wafer.

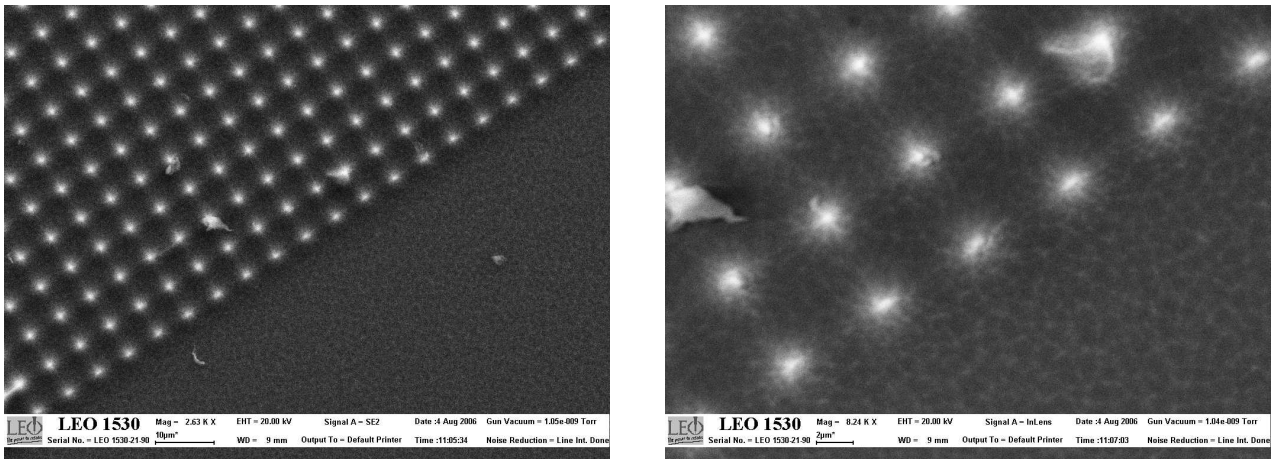

Figure 7.6 : ***Si Tips Array*** *SEM images at* 10 μm *and* 2 μm *resolution. No better image could be obtained because of space charge effects.*

Due to the small dimension of the tips, neither the SEM images nor the optical ones enabled us to obtain detailed information about their shape. Yet the SEM images do show an effect of emission enhancement at the tips tops (Figure 7.6).

7.2.2 Efficiency Measurements

The measurement of the quantum efficiency of silicon tips as X-ray photocathodes showed that silicon tips are not a good choice for *no signal could be detected*. This demonstrates that the yield is very small.

This can be explained by the small stopping power of silicon in the case of X-ray photons. For photons penetrate deeply in the material before being stopped, the electrons are created too far from the surface to drift and exit the bulk (in the case of moderate electric field as presented in the simulations detailed in section 6.2.2).

It is likely that a strong electric field could enhance the yield, but such a field is not compatible with gas amplification.

7.3 CsI_3 as a new photocathodes material

7.3.0.1 Physical and chemical characteristics

CsI_3 is a dark reddish-brown solid material, with a standard density of 4.51 g/cm^{-3}, and melting point of 207.5^oC. Its crystal structure was first studied in 1925 by Bozorth *et al.*[**?**], and later refined by H.A.Tasman *et al.* and by J.Runsink *et al.*[**?**, **?**] and belongs to space group $Pmcn$.

Extensive studies (complete phase diagram) on the manufacturing of polyiodides of caesium can be found in [**?**] ; the material is also available from major chemicals companies such as *Sigma-Aldrich* or *Alfa Aesar* or can be easily synthesized from CsI and I_2 [**?**].

It is not stable under vacuum at room temperature but it releases I_2. L.E.Topol indicates in [**?**] that the partial vapor pressure can be obtained from the formula

$$\log(P_{CsI_3}[Torr]) = \frac{-4269 + 0.20(T - 273)}{T} - 2.013 \log T + 16.2548. \tag{7.1}$$

In particular, at a temperature of 25^oC, $P_{CsI_3} \approx 10^{-3} Torr = 1.33 \cdot 10^{-3}\ mBar$ and at 40^oC: $P_{CsI_3} \approx 4.14 \cdot 10^{-3}\ Torr = 5.51 \cdot 10^{-3}\ mBar$.

More detail (including $(E - E^o)$, ΔG associated to the system $CsI - CsI_3$) can be found in [**?**]. The differential free enthalpy is $\Delta_f^o = -358\ kJmol^{-1}$.

Indeed when CsI_3 was left on the photocathode holder in vacuum, a layer on surroundings metals appeared, which is a sign of reaction with I_2 (the layer showed the same aspect as when exposed to vapors of I_2 obtained from solid iodide). Also the color of the sample rapidly changed to a brighter one (yellowish, after a few hours in vacuum), which is also a sign of the appearance of CsI at the surface (CsI is white or transparent, depending on its crystallinity). After 1 week in vacuum at a pressure of $\sim 10^{-5}$ the sample had lost as much as 12 % of its weight. Unfortunately we could not leave it under vacuum for a longer time to test further the stability of solid blocks (to check whether there is only surface transformation, which acts like a passivation layer, or deeper degradation and if a denser block would degrade the same way). The scanning electron microscope (SEM) analysis confirms an evolution of the material microstructure (see figures 7.7 and 7.8):
Kept in air at atmospheric pressure, there was no visible evolution after several months, apart from the plastic box, which turned into red (like it did with other compounds such as AuI, known to release I_2), which indicates that the evolution is slow, as soon as the equilibrium pressure of I_2 is reached.

7.3.1 The CsI_3 samples

Different flavors of CsI_3 samples were obtained and tested. For each the analysis of the microstructure and the quantum efficiency measurements were performed. CsI_3 is unstable under vacuum, so an analysis of the microstructure evolution under vacuum was performed.
Samples of CsI_3 were created following two ways:

1. CsI_3 was ordered from the company Sigma-Aldrich, and pressed into a pellet with a die-press set. A pressure of 3.5 GPa was enough to obtain a solid sample.
2. CsI samples were exposed to I_2 vapors (CsI with solid I_2 in a closed bottle in a furnace at 30^oC). The solid state reaction is very slow. We had to wait several days to observe a reaction of the bulk of the material. This method has the advantage that it is possible to compare directly nearly identical CsI and CsI_3 samples.

CsI_3 samples obtained were tested and compared with CsI and gold. CsI is an isolator, therefore it is hard to test due to charging effects. To overcome the space charge, conductive $CsI(C)$ samples were made, and compared with $CsI_3(C)$.

7.3.1.1 Preparation of the different samples

Samples obtained from CsI_3 as supplied

CsI_3 was obtained from the company *Sigma-Aldrich* (the vendor guaranties a purity better than $99.99x$ %).

The product came as a fine powder, which was then pressed into a pellet in an hydraulic press die, at a pressure of 4GPa for 5 minutes.

Samples obtained from a CsI crystals, in presence of I_2 vapors

Samples of $CsI(Tl)$ crystals grown for fluorescence applications were obtained from the company *Saint-Gobain*.

The samples come in the form of a polished crystal (transparent to light, colorless). It was then exposed to I_2 vapors at a temperature of $\sim 40^oC$ for several days. Already after a few minutes, the color of the crystal had changed into one very close to that of CsI_3. After several weeks in presence of I_2, the sample is hard to distinguish from the one obtained from the CsI_3 powder.

CsI was also tested. To do this, it was placed rapidly after opening (less than 5 minutes in air) on the experimental setup in vacuum and tested. Unfortunately, this test was not relevant, as explained later.

Samples obtained from a powder of CsI mixed with carbon in order to reduce the space charge

The CsI crystals from St Gobain could not be tested directly because of charging effects. So high purity CsI powder (from the company *Sigma-Aldrich*) was mixed with graphite in order to increase its conductivity. Those samples enabled to have a direct comparison of CsI and CsI_3.

Because CsI is an hygroscopic material, all manipulations were done under protecting atmosphere, in a glove box. The sample was then rapidly mounted on the experimental setup (less than 5 minutes) and put under vacuum for testing.

The received CsI was grained and mixed with graphite in a mortar. The sample composition was 0.5 % of graphite-carbon and 99.5 % high purity CsI.

It was then removed from the glove box, put in a die and pressed at 6 GPa for 2 minutes. Immediately after it was mounted and put under vacuum. Such a way, the sample stayed less than 5 minutes in air between its removal from the glove box, and the start of the pump.

A second sample prepared the same way, was treated in iodine vapors in order to transform it to $CsI_3(C)$ (left in a furnace at a temperature of 40^oC for one week).

Porous CsI Photocathodes

Porous CsI photocathodes by the company *Luxel* were tested for comparison purpose. Those photocathodes have a microstructure, which is optimized for a use in X-ray cameras. They give an indication of the maximum yield obtainable with CsI. Those photocathode are shipped in a sealed flask filled with an inert gas to protect them from moisture. As for the previous samples, they were mounted in the clean room and evacuated in less than five minutes.

7.3.1.2 Analysis of the microstructures of the samples and their evolution

The CsI_3 samples were stored in the clean room, in non hermetic plastic boxes. No visible change of aspect could be observed after several months, and no evolution of the microstructure was visible with the scanning electron microscope.
However, under vacuum a clear evolution was observed. Details of the sample evolution under vacuum are the following:

Samples obtained from pure CsI_3

The evolution of the microstructure of the sample was observed by SEM (a *Gemini Leo 1530*):
The surface microstructure of the pressed sample is depicted in the Figure 7.7.

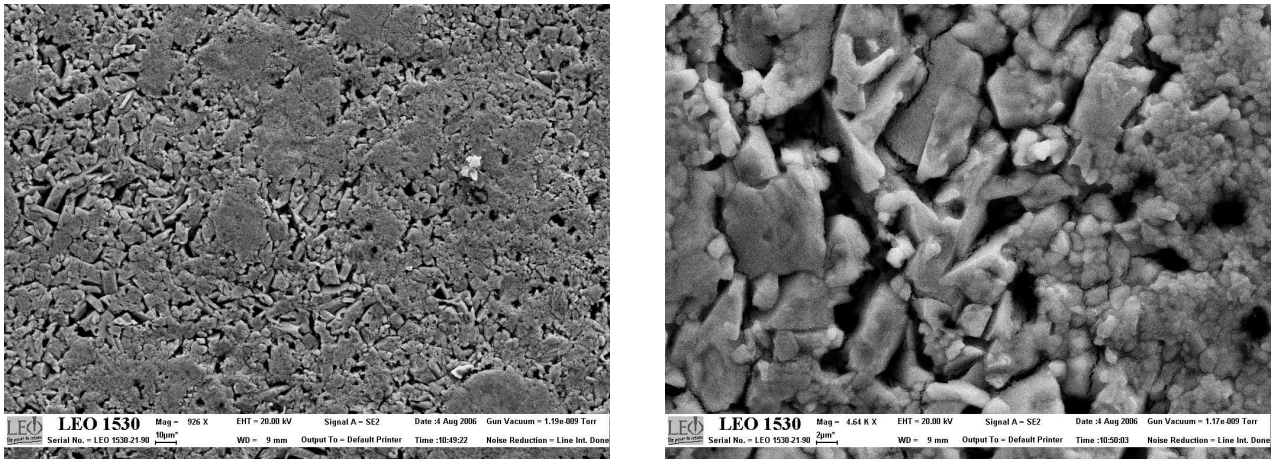

Figure 7.7 : *CsI_3 **as pressed** SEM images. Left image is a large field picture with resolution ~ 10 μm, right image is a closer view with resolution ~ 2 μm.*

This sample was left for one week under vacuum at a pressure of $\sim 10^{-6}$ $mbar$. The sample was then re-examined by SEM. The result is depicted in Figure 7.8.

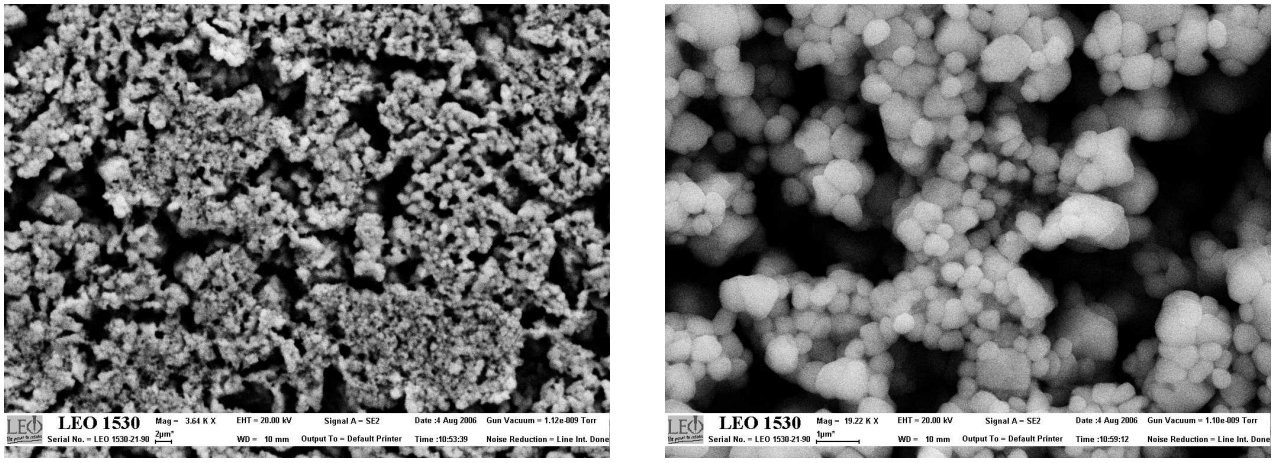

Figure 7.8 : *CsI_3 **samples** SEM images, after the sample was placed for one week in vacuum. Left image is a large field picture with resolution ~ 2 μm, right image is a closer view with resolution ~ 1 μm.*

There is a clear evolution in the microstructure, which has become much more porous. In the mean time, the color of the sample changed from dark to a white yellowish one (close to the color of CsI). This is further indication of the reaction

$$CsI_3 \rightleftharpoons CsI + I_2. \tag{7.2}$$

Samples obtained from CsI exposed to I_2

The study of the samples made from CsI_3 enabled to study the microstructure evolution of the material in vacuum. It is also interesting to study the evolution of microstructure of samples of CsI after they were exposed to I_2 and then placed in vacuum.

The following pictures depict the evolution of the samples made of pure CsI mixed with 0.5 % of carbon: "$CsI(C)$".

As pressed, the microstructure of this sample is depicted in Figure 7.9.

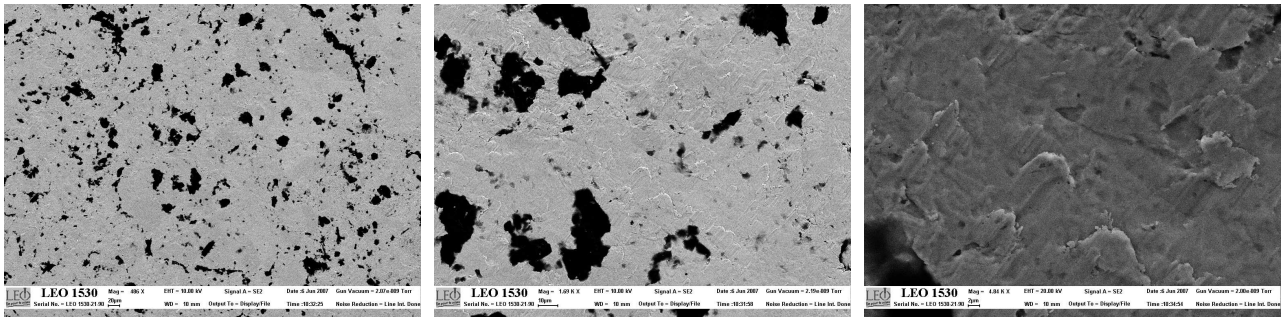

Figure 7.9 : ***CsI(C)*** *at 20 (left), 10(center), and 2 µm resolution (right).*

After exposure to I_2 for two days, no visible evolution of the microstructure was observed.

But after one night in vacuum, the structure becomes the following (Figure 7.10).

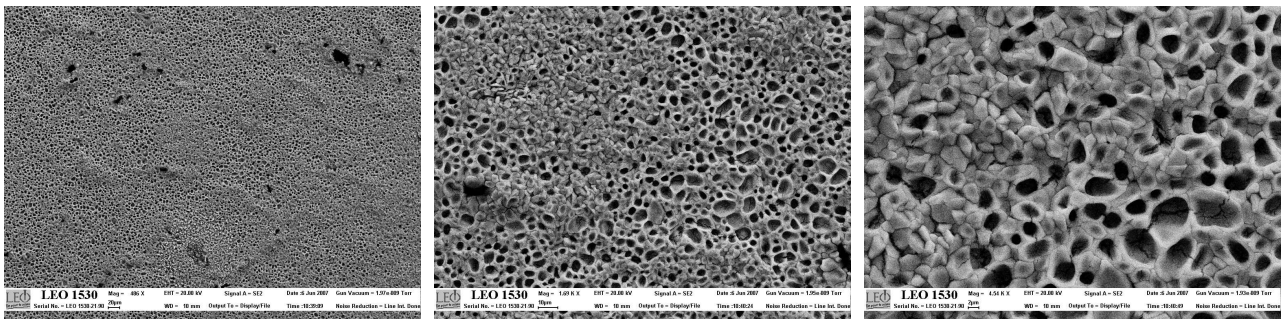

Figure 7.10 : ***CsI(C)*** *at 20 (left), 10 (center), and 2 µm resolution (right) after the sample was exposed to I_2 and placed one night in vacuum.*

The samples obtained from the $CsI(Tl)$ crystals show the same evolution (visible on Figure 7.11).

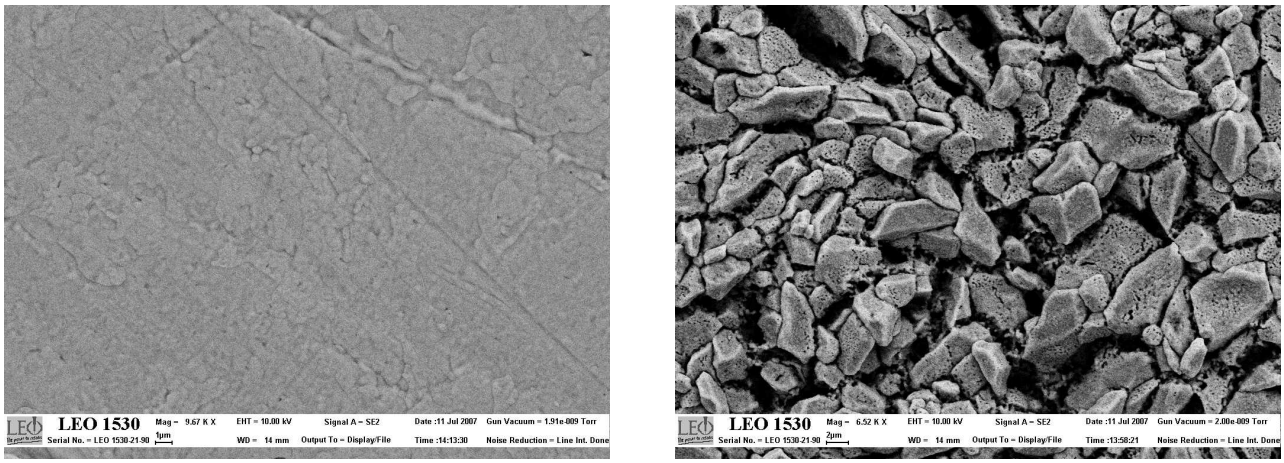

Figure 7.11 : *$CsI(Tl)$* ***Crystal by St Gobain Before*** *any treatment (left),* ***and after*** *it was exposed to I_2, and placed one night in vacuum (right).*

Before any treatment, most of the surface is flat like on picture 7.11 left (polished sample). The right picture highlights the complete change of the surface after the exposure to I_2 and vacuum. This evolution follows the same trend as for the compacted CsI_3 samples. The difference of obtained microstructure can be explained by the difference of the CsI microstructure before exposure to I_2. When the structures are left in vacuum for longer periods, no visible change occurs at the surface.

Porous samples of CsI

Those samples are obtained from the company Luxel and have a microstructure optimized for the detection of X-rays in streak cameras.
Indeed they show a spongy structure as depicted in pictures 7.12.

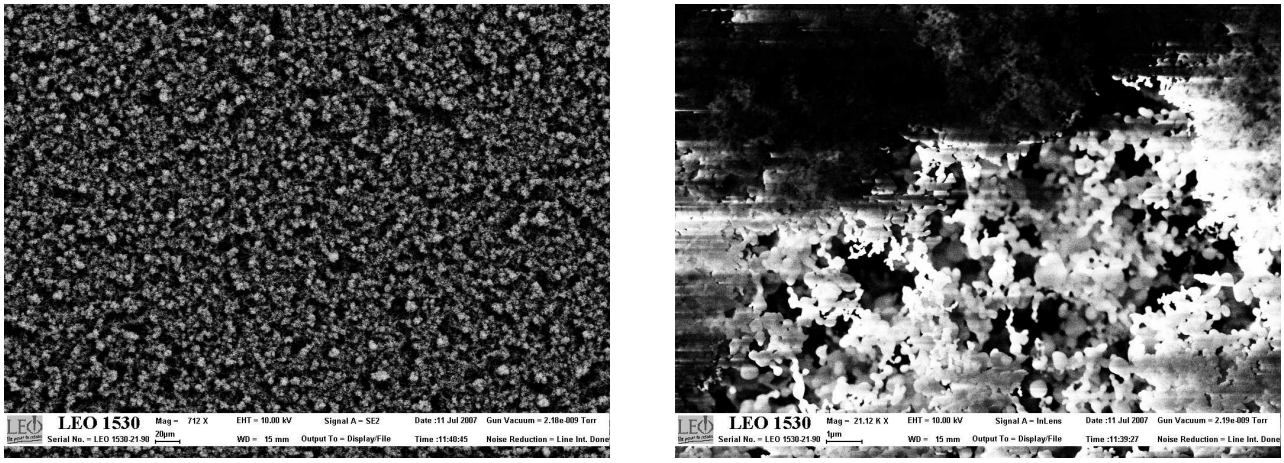

Figure 7.12 : *CsI* ***optimized for streak cameras*** *from the company Luxel. The left SEM image is shot with a resolution of $\sim$ $20\mu m$, the right one with a resolution of $\sim$ $1\mu m$. Space charges on the sample prevented us from obtaining a better image.*

As presented in section 6.2.1.1, this sort of structure is a way to obtain a large surface of the material

and then, a large active area (cf. 6.2.1).
It should be noted that this sample has a microstructure which is similar to that of the CsI samples exposed to I_2 and then placed in vacuum.

So the exposure to I_2 appears as a way to obtain a granular microstructure of the CsI.

This is an important result, as this method is much easier than the complex deposition processes normally used to obtain such materials.
This result will be further detailed in the conclusion concerning the use of CsI_3 as a photocathode material.

7.3.2 CsI_3 quantum efficiency and comparison with CsI.

The quantum efficiency of CsI_3 was evaluated and compared to that of CsI, both before and after exposure to air. See chapter 5 for details concerning the experimental setup.

7.3.2.1 The quantum efficiency of CsI and its evolution in air

measurement of the quantum efficiency of clean CsI

Those measurements were done for calibration and comparison purpose, as this subject was already widely studied in the past.
Yet, few authors provide results of the quantum efficiency after exposure to air (at best short exposures and techniques to recover the virgin quantum efficiency [29, **?**, **?**, **?**, 32]).
The best quantum efficiency one can obtain is measured in our case by the quantum efficiency of the samples provided by the Luxel company. Those samples are optimized for a very high quantum efficiency: thick deposited layers, with an adapted microstructure.

The best quantum efficiency, was obtained right after introduction of the sample in the chamber. With our setup, **a maximum current of** 1144 ± 57 pA was recorded. The second sample gave 1115 ± 55 pA (3% difference, can be attributed to a slight degradation of the sample during its manipulation, or to a difference in the sample itself).

Those results were compared with the samples obtained from the CsI mixed with 0.5 % of carbon. The **intensity obtained was** 144 ± 7.2 pA.
While this lower intensity can be explained by an effect of the structure of the sample (as explained before, prior exposure to I_2, the surface of the $CsI(C)$ sample was very flat), it is likely that the condition of cleanness during the preparation of the chamber cannot guaranty a maximum quantum efficiency of the CsI photocathode prepared this way: the quantum efficiency of CsI as a secondary emitter depend strongly on the state of cleanness of the sample surface (cf. section 3.3.4). For the CsI used to prepare the sample was grained and pressed during the preparation process (see sec-

Time in air	Intensity measured (pA)
0	1144 ± 57
1 day	736 ± 36
30 days	113 ± 5.6

Table 7.2 : *Evolution of the current of the porous CsI sample after it was left in air.*

tion 7.3.1.1), it can have been polluted, despite of the care taken to clean the mortar and the die used.

Evolution of the quantum efficiency of the porous CsI in vacuum and after exposure to air

CsI is known for being sensitive to pollution, and in particular to moisture. Tests were performed in order to compare its stability with that of CsI_3.

- Evolution of the quantum efficiency of CsI in vacuum.

The vacuum in which the measurements were performed is not ultra high. The measured pressure next to the chamber was in the range 10^{-5} *to* 10^{-4} *mbar*. This pressure is high enough to cause contamination of the surface on the long-term.
Under such conditions, a degradation of the quantum efficiency of the porous CsI was recorded only after a few days: the quantum efficiency **after 2 days** was at a value of 1040 ± 52 pA. This corresponds to a **drop of quantum efficiency of 9%**.
This highlights the necessity to keep the photocathode in a very clean environment, as already reported.
In the same time, no drop of intensity was recorded in the case of the sample $CsI(C)$.

- Evolution of the quantum efficiency of CsI in air.

The evolution of the quantum efficiency after exposure to air is just a way to study the evolution of the quantum efficiency of the photocathode when it is left in a more aggressive environment.
The different samples of CsI were just left in a protecting box, inside the clean room. So the samples are still in a controlled environment, but in particular there was no protection against moisture, which is known as the worst enemy of CsI photocathodes.
It turns out the evolution of the quantum efficiency is much more dramatic, than when the photocathode is kept in vacuum (table 7.2):
After **one night in air**, the intensity was 736 ± 36 pA, which corresponds to a relative **drop of 35 %** of the quantum efficiency.
After **one month in air**, the intensity was only 113 ± 5.6 pA. So only **10%** of the original quantum efficiency was left.
No change of intensity was recorded for the sample of $CsI(C)$ in the same time. This is a further indication that the sample was already degraded at the time of the first measurement.

Time (in hours)	Intensity measured (pA)
Introduction	160 ± 8
0.5	188 ± 9.4
1	217 ± 10
2	230 ± 11
∞	did not increase further

Table 7.3 : *Evolution of the current returned by the sample $CsI_3(C)$ when placed in vacuum.*

7.3.2.2 The quantum efficiency of CsI_3, its evolution in air and comparison with CsI.

The quantum efficiency of CsI_3 was evaluated the same way as CsI, except that in addition to those measurements, after exposure to air, CsI_3 samples were eventually put back in an atmosphere saturated with I_2 and then they were tested again.
Following the evolution of the microstructure presented in the last section, there is an evolution of the CsI_3 photocathode quantum efficiency when left in vacuum.
For all the samples of CsI_3 prepared do not have the same microstructure, all the quantum efficiencies of the various samples are not equal. Yet they all follow the same trend concerning the evolution of their quantum efficiencies.
First, the sample made of "$CsI_3(C)$" is detailed here. Then a comparison of the maximum intensities of the different samples is given.

The sample "$CsI_3(C)$"

- Evolution of the quantum efficiency after introduction in the chamber under vacuum.

The sample made of $CsI(C)$ after it was tested as a CsI sample was put in presence of I_2 vapors for two days, at a temperature of 40^oC. The obtained $CsI_3(C)$ was then tested.

At the introduction in the chamber, the intensity was $160 \pm 8.0\ pA$ and rapidly evolved (table 7.3). The maximum intensity was then $\sim 230 \pm 11\ pA$. The microstructure then corresponds to Figure 7.10.
No further evolution of the intensity was recorded, so the sample was removed from the chamber.

- Evolution of the quantum efficiency when left in air.

The sample was then left for a long period (1 month) in air in the clean room (storage in a plastic box). After only one day the sample had lost a great part of its quantum efficiency, for the measured intensity was then $93 \pm 4.6\ pA$. This evolution did not go further, and after one month, the quantum efficiency was still $92 \pm 4.6\ pA$ (table 7.4).

Time in air	Intensity measured (pA)
Introduction	230 ± 11
1 day	93 ± 4.6
30 days	92 ± 4.6

Table 7.4 : *Evolution of the current of the sample $CsI_3(C)$ sample after it was removed from vacuum, and left in air.*

Time (in hours)	Intensity measured (pA)
Introduction	160 ± 8
0.5	260 ± 13
1.5	299 ± 14
3	314 ± 15
4	320 ± 16
15	340 ± 17
∞	did not increase further

Table 7.5 : *Evolution of the quantum efficiency of the sample $CsI_3(C)$ in air after re-exposure to I_2.*

- Evolution of the quantum efficiency after re-exposure of the sample to I_2.

Lastly the sample was put back in presence of I_2 for a few days, and the quantum efficiency was retested. The quantum efficiency then evolved according to the data of table 7.5.

In conclusion, the history of this peculiar sample can be plotted like on Figure 7.13.

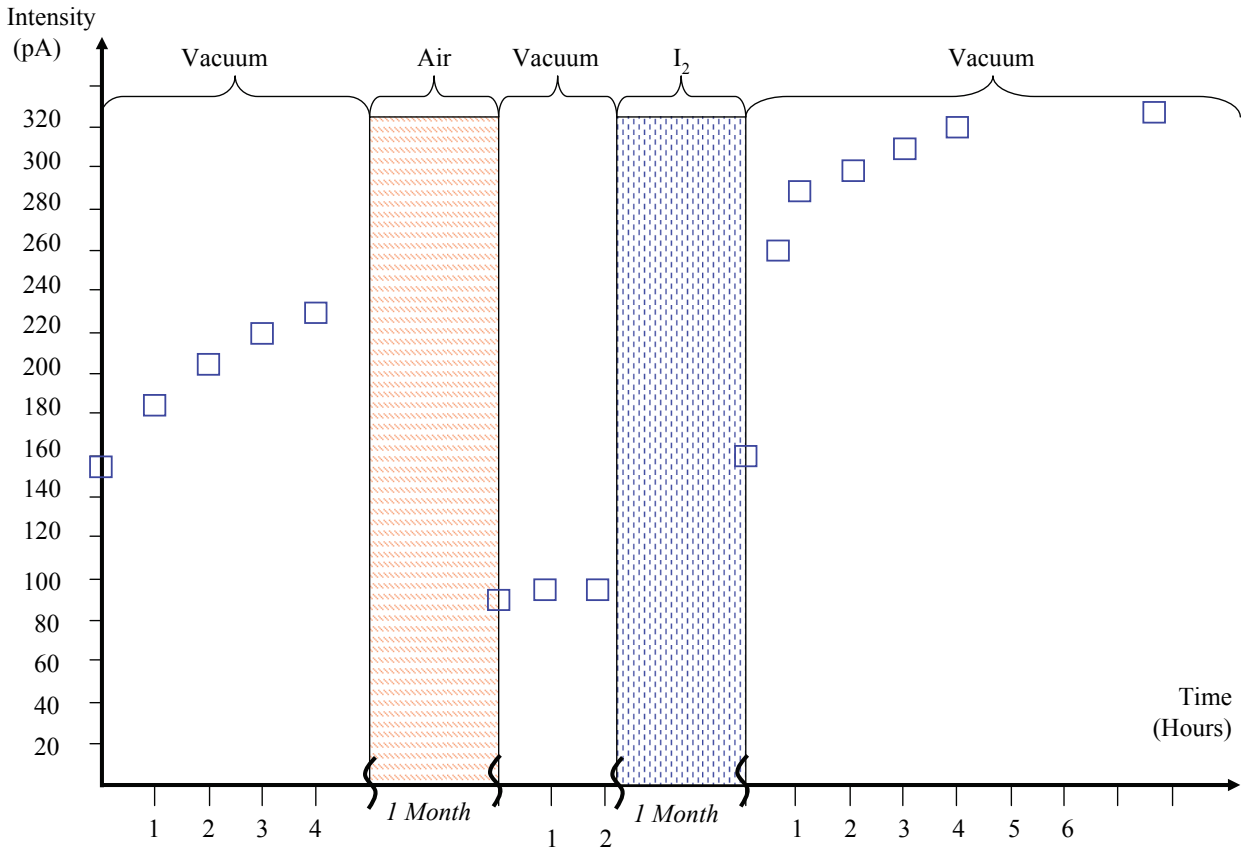

Figure 7.13 : *Summary of the evolution of the quantum efficiency of the sample of* $CsI_3(C)$. *after* first introduction in vacuum, one month stay in air, *and* Re-exposure to I_2.

After the CsI sample was exposed to I_2, there is an increase of efficiency when it is left in air. The sample then becomes sensitive to pollution, and an exposure to air results in a drop of efficiency. A re-exposure to I_2 enables to recover the lost efficiency, and is even beneficial for the maximum intensity obtained is then higher than after direct introduction of the sample.
A further cycle of exposure to I_2 and stay in vacuum gave the same results.

CsI crystal from St Gobain.

As already explained, the performances of the CsI crystal by St Gobain could not be measured, because of space charging. Only after it was exposed to I_2 it became conductive enough to enable measurements.
After a long exposure to I_2, as highlighted by the microstructure and color changes, a part of the sample turned into CsI_3.

Time (in hours)	Intensity measured (pA)
Introduction	120 ± 6
2	130 ± 6.5
10	151 ± 7.5
∞	did not increase further

Table 7.6 : *Evolution in vacuum of the intensity for the $CsI(Tl)$ sample by St Gobain, after exposure to I_2.*

The performances and behavior after exposure to vacuum and I_2 of this sample are similar to those of the "$CsI(C)$" and pressed pellet samples (table 7.6).

Then, after only one week in air, the intensity recorded was only $68 \pm 3.4\ pA$.
After it was exposed to I_2 for a few days, the intensity rose to approximately the same value of $154 \pm 7.7\ pA$ again.

So this sample follows the same trend as the previous one except that a second exposure to I_2 does not enable a bettering of the efficiency, but only a recovery of this efficiency after pollution of the sample by air.

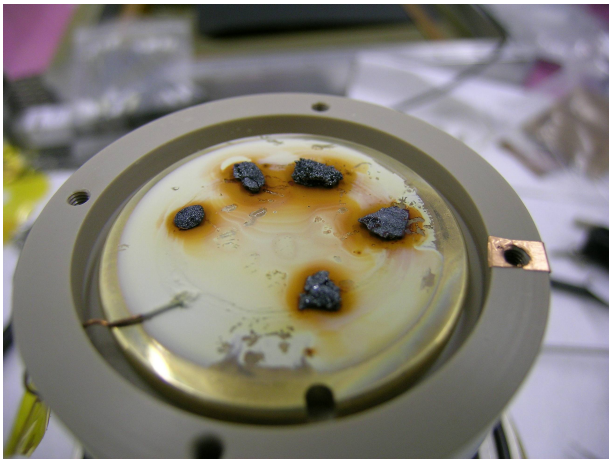

Figure 7.14 : *Exposure of the Luxel Sample to I_2 in open air.*

The CsI photocathode from Luxel.

A tentative was made to use the CsI photocathode from Luxel to make a CsI_3 one as with the crystal by St Gobain. Unfortunately, it turned out that the Aluminized mylar substrate used to grow the photocathode is very reactive to I_2. It was not the CsI of the photocathode, which reacted with I_2, but the aluminum of the substrate itself.
So the only way to obtain a CsI_3 photocathode from this sample was to put in open air, a solid iodine grain on the CsI deposited layer (Figure 7.14). The grains were deposited around the measured area,

Time (in hours)	Intensity measured (pA)
Introduction	390 ± 19
1	412 ± 20
2	580 ± 29
4	812 ± 40
∞	did not increase further

Table 7.7 : *Evolution in vacuum of the quantum efficiency of the porous CsI sample after exposure to I_2*

Time (in hours)	Intensity measured (pA)
Introduction	120 ± 6.0
0.5	141 ± 7.0
2	177 ± 8.8
4	200 ± 10
∞	did not increase further

Table 7.8 : *Evolution of the current of the CsI_3 pressed pellet in vacuum*

on place invisible to the X-rays (far from the $7 * 7\ mm^2$ enlightened area). Table 7.7 gives the results of the measurements of the photocurrent.

It is evident that such a method cannot guaranty a good homogeneity of the CsI_3 surface. So the result of those measurement must be taken with caution.

When the sample was removed from the chamber, it was completely white. So, if the value at the time of introduction is likely to be a measurement of the quantum efficiency of CsI_3, then, the sample progressively changed back into CsI.

This measurement was performed right after measuring the quantum efficiency of CsI, so the last value is a measurement of clean (less than a few minutes in air in total) but transformed -see structural analysis- CsI.

CsI_3 pressed pellets

The evolution of the quantum efficiency of the samples made of compacted CsI_3 follows the same trend as those obtained from CsI exposed to I_2. At the introduction, the samples typically return an intensity of $120 \pm 6\ pA$, and this values rises in a few hours to typical values of $200 \pm 10\ pA$ (table 7.8).

In the meantime, as explained earlier, the surface changes color, and the microstructure evolves as depicted earlier.

A tentative of study of the stability on the long-term was performed by leaving one of the samples of compacted CsI_3 in vacuum. But after one week, two pumps had broken, so the experiment was stopped (it is likely that the I_2 release was at the origin of this failure).

Still, the transformation of this sample had probably gone deeper than with the other samples, and

Intensity measured (pA)	
few hours	1 week
188 ± 9.4	31 ± 1.5

Table 7.9 : *The photocurrent at the reintroduction of the CsI_3 pressed pellets according to the time passed in vacuum, and after one month in air.*

Time in hours	Intensity measured (pA)	
Time in vacuum before left in air	few hours	1 week
Introduction	130 ± 6.5	31 ± 1.5
1	177 ± 8.8	32 ± 1.6
2	257 ± 12	35 ± 1.7
4	274 ± 13	37 ± 1.8
∞	did not increase further	did not increase further

Table 7.10 : *Recovery of the photocurrent in vacuum, for two CsI_3 pressed pellets, which stayed a few hours or one week in vacuum, and then one months in air and two days in presence of I_2.*

the color of surface had change to a brighter color than the one of the samples, which stayed only one or two complete days in vacuum.
After this, the two samples (the one pumped 1 week, and the one pumped only for the primary measurements: few hours) were left for one month in a plastic box in the clean room, and were tested again.
It turned out that the quantum efficiency of both samples evolved very differently.
At their reintroduction in the chamber, the intensities were rather different (table 7.9):

- The sample, which had stayed only a few hours in vacuum had an intensity of $188 \pm 9.4\ pA$.
- The sample, which had stayed one week in vacuum had an intensity of only $31 \pm 1.5\ pA$.

No real evolution was then recorded. So the samples were put in presence of I_2 vapors. After two days, the sample, which had been left only a *few hours* in vacuum was dark again, while the color of the sample which had been left in vacuum for one week did not change color. The quantum efficiencies of the two samples were tested again (table 7.10).
The sample which had stayed only a few hours recovered like the other samples its quantum efficiency, while the one which had stayed a long time in vacuum, kept a very low quantum efficiency. No further stay in I_2 of the sample left *1 week in vacuum* could change its color, and its quantum efficiency did not change neither (same value of $\sim 35 \pm 1.75 pA$).

Later, a tentative to remove mechanically the bright layer was successful: it detached easily when pressed by tweezers.
The uncovered layer was then tested, and showed similar properties to those of the freshly made

sample.

Summary

The typical values obtained with the different samples can be found in the table 7.11.
It appears that, despite the variations in the precise values, the general trend is the same for the different samples.
Some general conclusions can be already given when looking at the different values:

- Contrary to CsI, CsI_3 seems to be insensitive to air.
- The quantum efficiency of CsI_3 is lower than clean CsI (from the Luxel sample, probably a factor 7), but better than *exposed to air* CsI.
- When exposed to I_2 and then put in vacuum at least twice, the quantum efficiency is increased. This does not further increase after two cycles yet.
- A too long stay of CsI_3 in vacuum makes the sensitivity to air rise, and I_2 treatment does not enable to recover the best efficiency.

Also, both ways to obtain CsI_3 samples (from CsI and CsI_3) seem to be equivalent as they offer similar values at the time of introduction.

7.3.3 Analysis of the results obtained with CsI_3

The behavior of the CsI_3 as a photocathode can be explained by a transformation of the outer layer, following the reaction

$$CsI_3 \rightleftharpoons CsI + I_2 \qquad (1)$$

The CsI_3 samples, when put in vacuum transform according to the reaction (1) in the left to right direction, so a layer of fresh CsI is formed at the surface of the sample. This is visible by the change of color from dark red (CsI_3) to yellow-white (CsI).
The different test with pure CsI and CsI_3 show that CsI is a better emitter, so there is an increase of quantum efficiency when this reaction occurs, until all the CsI_3 of the active layer of the photocathode transformed in CsI.

The reaction does not stop as the I_2 released in the chamber is pumped, so the equilibrium vapor pressure is never reached. Eventually, a thick layer of CsI is formed on top of the sample, which corresponds to the one removed mechanically from the CsI_3 pressed pellet after it stayed one week in vacuum.
When left in a plastic box, there is no evolution of the microstructure, or of the emission characteristics, at least in the time scale of a few months. This indicates that when the equilibrium vapor pressure of I_2 is reached, there is no evolution of CsI_3.

When I_2 is released, there is a change of the surface microstructure as shown by the SEM pictures. This evolution is in favor of a greater quantum efficiency of the CsI left: the microstructure becomes

Samples	Test of CsI		Test of CsI_3		
	Before exposure to air	*After exposure to Air*	*After exposure to I2*	*After exposure to air*	*After (re)exposure to I2*
`CsI(C)`	144 ± 7.2	91 ± 4.5	$160 \pm 8 \rightarrow 230 \pm 11$	92 ± 4.6	340 ± 17
`CsI Crystal From Saint Gobain`	*Charging*		$120 \pm 6 \rightarrow 151 \pm 7.5$	68 ± 3.4	154 ± 7.7
`CsI from Luxel`	$1140 \pm 57 \rightarrow 760 \pm 38$	113 ± 5.6	$390 * \pm 19 \rightarrow 812 \pm 40$	370 ± 18	XXX
CsI_3	*XXX***		$130 \pm 6.5 \rightarrow 200 \pm 10$	short stay in vacuum	118 ± 5.9	270 ± 13
				long stay in vacuum	31 ± 1.5	37 ± 1.8

*: this value must be taken with caution.

**: No sense.

Table 7.11 : *CsI_3 measurements summary.*

porous, which betters the quantum efficiency of CsI as already known.

If the samples of CsI_3 are left in air after a long stay under vacuum, the thick layer of CsI gets polluted and the quantum efficiency of the photocathode drops rapidly, like it does for pure CsI samples. After a short stay in vacuum, CsI_3 seem to be less sensible to air pollution.

It seems that the state of degradation of the CsI layer (after a stay in air, so after exposure to moisture) has an impact on the possibility to re-transform in CsI_3.

In conclusion:

- If the CsI_3 did not stay too long in vacuum, it can be "recovered" (the formed CsI layer can retransform in CsI_3) even after a long stay in air.
- If the CsI_3 stayed a long time in vacuum, the recover can occur only after a short exposure to air.

This indicates that exposure to I_2 does not enable to regenerate a thick layer of degraded CsI (or that the reaction is much slower).

7.3.4 Conclusion on the use of CsI_3 as a photocathode

The study performed on CsI_3 show that it is itself an interesting photocathode, providing a good quantum efficiency, and a good robustness to pollution and moisture. It has the disadvantage that it is unstable in vacuum, so it is mandatory to let the gas in the detector reach the equilibrium vapor pressure to enable its use as a photocathode.
The most promising approach is its use as a precursor to CsI. Indeed, CsI_3 is not an emitter as good as CsI in terms of quantum efficiency. But its instability under vacuum and its insensitivity to air degradation makes it a very attractive choice to create porous CsI photocathode.
Indeed, as the material is very easy to manipulate in air, it is very easy to place the photocathode in gas-filled detectors. Then, simply pumping the chamber enables to obtain a porous CsI photocathode, which is the best photocathode available (eventually several cycles of pumping and exposure to I_2 can be necessary to obtain the best structure / quantum efficiency).
Later maintenance operations are also easier to perform if the photocathode is first exposed to I_2, it then transforms in CsI_3, which makes it much more robust to air damages. This method does not enable to recover the efficiency of a CsI which was severely polluted though.

This study shows that CsI_3 can potentially be a good way to fabricate porous CsI photocathodes.

Bibliography

[1] R.M.Bozorth et al., "Unknown title," *The Journal of American Chemical Society*, vol. 47, p. 1561, 1925. *This reference could not be obtained.*

[2] H.A.Tasman et al., "Re-investigation of the crystal structure of csi_3," *Acta Cryst.*, vol. 8, 59, pp. 59–60, 1955.

[3] J.Runsink et al., "Refinement of the crystal structure of $(c_6h_5)_4asi_3$ and csi_3 at 20^oc and at -160^oc," *Acta Cryst.*, vol. B28, pp. 1331–1335, 1972.

[4] T.R.Briggs et al., "The polyiodides of cesium, cesium iodide, iodine, and water at 25^oc," *The Journal of Physical Chemistry*, vol. 34, pp. 1951 – 1960, 1930.

[5] L.E.Topol et al, "Thermodynamic studies in the polyiodides systems $rbi-rbi_3$, $nh_4i-nh_4i_3$, $csi-csi_3$, and $csi_3 - csi_4$.," *Inorganic Chemistry*, vol. 7, pp. 451–454, 1968.

[6] V.Dandendorf et al., "Progress in ultrafast csi-photocathode gaseous imaging photomultipliers," *Nucl. Inst. and Meth. A*, vol. A308, pp. 519–532, 1991.

[7] E.Shefer et al., "Photoelectron transport in csi and csbr coating films of alkali antimonide and csi photocathodes," *J.Appl.Phys.*, vol. 92(8), pp. 4758–4771, 1993.

[8] A.Breskin et al., "New ideas in csi-based photon detectors: Wire multiplication and protection of the photocathode," *IEEE Trans.Nucl.Sci*, vol. 42(4), pp. 298–305, 1995.

[9] B.L.Henke et al., "The characterization of x-ray photocathodes in the 0.1-10kev photon energy range," *J.Appl.Phys.*, vol. 52(3), pp. 1509–1520, 1981.

[10] J.E.Lees et al., "Thermally annealed soft x-ray photocathodes," *Nucl. Inst. and Meth. A*, vol. 381, pp. 453–461, 1996.

Chapter 8

Conclusion

The aim of this work was to develop new photocathodes with improved quantum efficiency and robustness to allow their use as a first stage X-ray electron converter in gas-filled detectors.

This implied both theoretical studies and practical experiments to identify the most promising techniques to develop such device.

This work allowed the development of a simulation tool using a Monte Carlo method for prospecting new materials and structures. It turned out that the tool could not simulate properly the photocathodes' physics, leading to unreliable results. Deep investigations highlighted that it was the method and not the specific program, which is adequate for such simulations. The Monte Carlo method can be used to develop material already well known and better understand them, by developing specific codes for this material. Unfortunately, this approach is of no help to investigate prospective materials, which properties are not known. This limit finds its root in the strong variation of the electrons dynamic in the bulk and at the surface of the material with its precise structure and chemical state. So any Monte Carlo Study of a photocathode material implies a deep study of the materials properties, which is just longer than a direct experimental study.
Still the development of this tool helped in understanding the key parameters which govern one photocathode quantum efficiency.

In order to enable reliable tests of the quantum efficiency of the photocathodes, an experimental setup was developed and built. This setup showed excellent characteristics, as it was able to measure very weak photocurrents, while being very flexible. Currents of less than 1 fA were successfully measured. The setup then served as a basis for all study of the quantum efficiency of prospective photocathodes.

The last part of the work consisted in developing methods to better the quantum efficiency of photocathodes. Various approaches were investigated, and eventually experimentally tested. In particular, the study of the impact of microstructures on the material efficiency was performed, and the in-

vestigation of a scintillator-low energy photocathode system was performed. The most promising approach, and which was more extensively investigated is the use of CsI_3 as a precursor to CsI, which is currently the best known photocathode.
The use of CsI_3 as a photocathode is advantageous in several ways:

- Contrary to CsI, CsI_3 is not hygroscopic, and is rather resistant to pollution. Thus, it can be easily manipulated in air.
- When put in vacuum, it releases I_2, and transforms in CsI with a porous structure. Porous CsI is known for being the best photocathode in terms of quantum efficiency. So CsI_3 is a way to obtain structured photocathodes, without using complex evaporation systems, which enable the growth of porous CsI photocathode. A simple deposition of CsI_3 or even of unstructured CsI later exposed to I_2 vapors is enough to obtain a structured CsI photocathode.
- The reaction $CsI_3 \rightleftharpoons CsI + I_2$ is reversible. So one can protect CsI from air pollution by exposing it to an atmosphere saturated with iodine. This is a very attracting method for it simplifies dramatically the maintenance operations.

So the use of CsI_3 as a photocathode is technologically promising. It can lead to the fabrication of gas-filled detectors, which can answer the growing need of fast, large areas counting detectors in photon science...
Further study will need to validate experimentally this approach to create and protect CsI photocathodes.

Appendix A

Detector characteristics

A.1 Position resolution in the case of gas-filled detectors

The spatial resolution gives information on the accuracy of the position returned by the detector. The position resolution is the result of four main contributions [1]:

$$\sigma_{det} = (\sigma^2_{noise} + \sigma^2_{diff} + \sigma^2_{er} + \sigma^2_{aval})^{1/2}.$$

where

- σ_{noise} is the r.m.s contribution from the electronic noise. I depends on the type of readout.
- σ_{diff} is the contribution due to electrons diffusion.
- σ_{er} is the contribution from Auger electrons and photoelectrons.
- σ_{aval} is the contribution from avalanche centroid fluctuation. It is due to statistical variations and varies greatly with gas gain. It is often the main contributor and depends on both pressure and gas mixture.

More details on each contributions can be found in [1] and in chapter 4 of [2].

A.2 Energy Resolution

The Energy resolution is usually defined as the full width half maximum of the spectral response of the detector to a given energy.
Indeed, with an excellent precision($\sim$ 1%), the response has a gaussian shape. More precisely, The resolution R is given by: $R = \sqrt{(electronic\ noise)^2 + (Fano)^2}$:

→ *Electronic noise* gives the contribution of the electronic to the error of measurement. This term is itself the result of several contributions.

→ *Fano* is the contribution due to the **Fano Statistics**: the generation of electrons and holes charges is the result of a statistical process. The energy of the incoming particle/photon is

shared between *lattice excitation* ($\sim 2/3$) and the *generation of charge carriers* ($\sim 1/3$). The resultant spread in energy is $FWHM_{Fano} = 2.35\sqrt{F\varepsilon E}$ with ε being the charge pair creation energy (ex. 3.63eV/e-h for Si), F the Fano factor ($F \approx 0.12$ for Si, F is not a constant), and E the energy.

A.3 Space Charging in gas-filled detectors

The space charging effect is important because it can be physical limitation to counting rate characteristics. Two methods have been given by Sipilia et al. in 1980 and later by Mathieson et al. in 1992 [3, 4].
It concerns the reduction of the electric field between the anode and cathode due to ions in the volume. This presence is unavoidable for the amplification process necessarily creates such ions (ionization avalanche). The two models calculate the effective field reduction at the anode surface.

Bibliography

[1] G.C.Smith, "Gas-based detectors for synchrotron radiation," *Journal of Synchrotron Radiation*, vol. 13, pp. 172–179, March 2006.

[2] G.F.Knoll, *Radiation Detection and Measurement*. Willey, 2000.

[3] H.Sipila et al., "Mathematical treatment of space charge effects in proportional counters," *Nucl. Inst. and Meth.*, vol. 176, pp. 381–387, 1980.

[4] E.Mathieson et al., "Gain reduction due to space charge in a multiwire proportional chamber irradiated by a uniform beam of rectangular section," *Nucl. Inst. and Meth. A*, vol. 316, pp. 246–251, 1992.

Appendix B

Monte Carlo Application Examples

B.1 Simple Examples of statistical sampling methods

In this section, some of the most classical example of statistical sampling methods are given. Those methods can be considered as particular application of the Monte Carlo Method[1].

B.1.1 Calculus of an integral

As a first approach to the Monte Carlo method, an example of calculation of an integral is given: Let assume the function ϕ is to be integrated between a and b:

$$\int_a^b \Phi(t)dt = \sum_{i=0}^{N-1} \Phi(x_i)\frac{b-a}{N} + O(\frac{1}{N}) \qquad with \quad x_i = a + \frac{b-a}{N-1}i.$$

This is the classical formula of the trapezoidal rule.
Instead of a uniform sampling, imagine an evaluation where the positions $\{x_i\}$ are random numbers *uniformly distributed* in the interval $[a, b]$; this yields a Monte Carlo integration:

$$\int_a^b \Phi(t)dt = \sum_{i=1}^{N} \Phi(x_i)\frac{b-a}{N} + O(\frac{1}{\sqrt{N}}) \qquad with \quad a \leq x_i \leq b.$$

In this particular example, the methods appears to be less efficient than the trapezoidal rule for its absolute error is in $1/\sqrt{N}$ *instead of* $1/N$. Though the Monte Carlo approach has a strong advantage over it: it is independent of the number of dimensions. So, contrary to the uniform sampling, which has an error scaling as $N^{-1/d}$, the Monte Carlo Method will stay with an error scaling as $N^{-1/2}$. This is a direct consequence of the *central limit theorem*.

[1]The name *statistical sampling method* is used instead of Monte Carlo Method, for those methods were developed before the name *Monte Carlo Method* was given and presented as a general method.

B.1.2 An historical example: Buffon's needles

One of the first statistical approach to solve a mathematical problem is due to the mathematician **Comte de Buffon**.

Figure B.1 : *Georges Louis Leclerc* Comte de Buffon

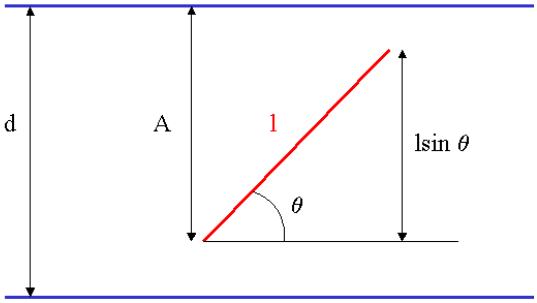

Figure B.2 : *The needle problem by Buffon*

He invented a method to calculate an approximation of π. Here is the problem he solved, which leads to the approximation method of π: *if a needle of length* l *is dropped several times on a horizontal surface ruled of parallel lines separated of a distance* d¿l*, what is the probability* $\wp$ *that the needle cross one line?*

That outcome will happen only if $0 \leqslant A \leqslant d \quad and \quad 0 \leqslant \theta < \pi$.

If we assume that the vector (A, θ) is randomly distributed on the region $[0, d[\times[0, \pi[$, then the probability density function is $\frac{1}{d\pi}$, and the probability that the needle cross the line is:

$$\wp = \int_0^{\pi}\int_0^{l\sin\theta} \frac{1}{d\pi} dA d\theta$$

So the probability is $\wp = \dfrac{2l}{d\pi} = \dfrac{E(M)}{n}$ if M is the random variable for the number of times the needle cross the line, and n the number of drops.

It appears that $\dfrac{n}{E(M)}\dfrac{2l}{d}$ is a statistical estimator for π. So to determine π, one can evaluate E(M), which is easily done, just dropping needles.

Développement de photocathode de meilleures efficacités quantiques pour détecteurs à gaz

Résumé en français.

Introduction

Ce travail de thèse vise à explorer différentes voies d'amélioration de l'efficacité des photocathodes. Plus généralement, il prend place dans le développement de détecteurs à gaz de rayons X de grandes surfaces, susceptibles de répondre aux besoins croissants en matière de vitesse et de taille des détecteurs utilisés dans les domaines du médical et de la recherche mobilisant le rayonnement synchrotron.

Les photocathodes pour détecteurs à amplification par gaz

Détecteurs à 2 dimensions

Les détecteurs à 2 dimensions (ou à 1 dimension) sont par opposition aux détecteurs ponctuels capables de fournir une information spatiale sur la particule détectée.
Ce type de détecteur présente l'énorme avantage qu'il dispense de systèmes mécaniques pour couvrir l'ensemble de l'espace (dans le cas de l'espace réel comme réciproque). Ainsi il est possible d'effectuer beaucoup plus rapidement les expériences d'imagerie. Certaines expériences nécessitent même l'utilisation de détecteur 2D, soit pour des raisons de temps d'exécution autrement trop longs (cas de la tomographie 3D par exemple) soit même pour des raisons de dégradation de l'échantillon qui ne peut supporter le faisceau qu'un temps très court (notamment dans les domaines de la biologie ou dans le cas des analyses médicales !).

Les détecteurs à amplification par gaz

Les détecteurs à amplification par gaz (aussi appelés ≪ *détecteurs gazeux* ≫), sont parmi les plus vieux systèmes de détection de rayonnement ionisant. Ils sont en particulier les premiers à avoir offert

une détection électronique du passage d'un rayonnement ou d'une particule ionisante.
L'exemple le plus célèbre de ce type de détecteur est le *Tube Geiger* introduit par **Geiger** et **Mueller** en 1928 après que Geiger et Rutherford aient découvert le principe de la multiplication électronique dans un gaz.
Ces détecteurs sont basés sur une multiplication interne des électrons ionisés à la suite d'un dépôt d'énergie par la particule/le rayonnement traversant le gaz. Cette multiplication des électrons est rendue possible par la présence d'un champ électrique au sein de la chambre à gaz, qui accélère les charges présentes. Si *l'énergie cinétique* gagnée par ces charges entre deux collisions avec une molécule du gaz est supérieure à *l'énergie d'ionisation d'une particule de gaz* (typiquement 35eV), alors la particule devient susceptible de ioniser une particule de gaz, et est donc à la source d'une cascade de ionisation. L'augmentation exponentielle du nombre de charges permet alors une détection aisée par simple collection des charges sur des électrodes.
Les détecteurs à gaz constituent maintenant une technologie mature. Ils ont comme avantage principal de permettre la fabrication de détecteurs de grande dimension et rapides à un coût acceptable, tout en permettant un fonctionnement en comptage (par opposition aux détecteurs fonctionnants avec des écrans fluorescents, qui impliquent un mode d'opération en intégration, et donc un bruit plus important).
Ils présentent aussi des inconvénients, notamment un phénomène de parallax, qui dégrade fortement la résolution dans le cas des incidences obliques, et une efficacité quantique limitée notamment aux énergies supérieures à 10keV. En effet, l'efficacité d'absorption du gaz augmente avec la pression, alors que l'efficacité d'amplification est optimum pour les faibles pressions.
Une approche pour contrebalancer ces deux inconvénients, consiste en l'utilisation de photocathodes solides comme convertisseurs photon → électrons, permettant ainsi une séparation (et donc une optimisation séparée) des deux fonctions d'absorption et d'amplification.

Les photocathodes dédiés à une utilisation dans des détecteurs à gaz

Les photocathodes permettent une conversion de la lumière incidente en électrons par le biais de l'effet photoélectrique.
Les photocathodes ont principalement été utilisées au sein de photomultiplicateurs, dans lesquels elles sont couplées à une série de dynodes, capables d'amplifier fortement le signal électrique.
Le mécanisme qui mène à l'éjection de l'électron à l'extérieur de la photocathode est en fait complexe : l'électron(s) émis à la suite de l'absorption par effet photoélectrique du photon incident subit une série d'interactions avec les autres électrons présents dans le matériau et perd rapidement cette énergie. Au cours de ce trajet, il ionise lui-même d'autres atomes et crée ainsi une série d'électrons chauds secondaires au sein du matériau. Eventuellement, un ou plusieurs de ces électrons peuvent atteindre la surface et quitter la photocathode.
Cependant, pour quitter le matériau, l'électron doit passer une barrière de potentiel appelée *affinité électronique* dans le cas des semi-conducteurs, ou *travail de sortie* dans le cas des métaux. Du fait de leur thermalisation rapide après éjection de l'atome, peu d'électrons peuvent effectivement passer cette barrière et les rendements d'émission sont en général faibles.

Les photocathodes présentant les meilleurs rendements présentent la particularité de présenter une *affinité électronique négative*. Ainsi, les électrons chauds présents dans le matériau sont facilement éjectés et les rendements sont élevés. Cependant, ces matériaux présentent aussi une grande sensibilité à toute forme de pollution de leur surface, qui leur fait perdre cette affinité électronique négative.
En conclusion, idéalement une photocathode pour détecteurs à gaz présente les caractéristiques suivantes :

Une affinité électronique négative : afin de laisser sortir un maximum d'électrons chauds créés à la suite de l'absorption du photon incident.

Un grand pouvoir d'arrêt : afin de garantir que les photons seront absorbés près de la surface d'éjection des électrons. Le pouvoir d'arrêt est en général plus élevé avec des éléments de numéro atomique Z élevé.

Une faible réactivité chimique : afin d'éviter une trop grande sensibilité de la photocathode à la pollution par le gaz utilisé pour l'amplification du signal (en particulier, les ions générés lors de l'avalanche électronique sont une grande source de pollution).

Modalités de l'étude de photocathodes à efficacité quantique supérieure

L'étude entreprise lors du travail de thèse comporte Trois étapes principales :

1. Une étude théorique des photocathodes. En particulier un code de simulation par Monte Carlo a été développé pour simuler l'efficacité des photocathodes.
2. L'étude et la fabrication d'un dispositif expérimental permettant de tester concrètement des photocathodes.
3. L'étude de différentes méthodes pour améliorer l'efficacité des photocathodes, et l'étude de nouveaux matériaux potentiellement bons photo-émetteurs.

Chacune de ces étapes est décrite brièvement ci-dessous.

Le développement d'un code de simulation par méthode Monte Carlo

introduction à la méthode Monte Carlo

A la suite de sa première utilisation au cours du *Projet Manhattan* à Los Alamos au lendemain de la seconde guerre mondiale pour le développement de la bombe nucléaire américaine, la méthode Monte Carlo pour la simulation du transport de particules dans la matière est devenue un outil standard de la physique des particules.
Cette méthode permet de rendre compte de l'aspect aléatoire de l'interaction des particules avec la matière. Elle consiste à simuler le trajet des particules en calculant la probabilité d'interaction d'une particule au moyen d'un générateur de nombres aléatoires, et des densités de probabilités d'interactions pour chacun des mécanismes d'interaction connus. Ces densités de probabilités sont évaluées au moyen des tables de *sections efficaces*, qui sont des grandeurs expérimentales.

le code développé

Le développement d'un code de simulation par Monte Carlo est un projet très ambitieux en soi, aussi une librairie standard de simulation par Monte Carlo a-t-elle été utilisée pour écrire le code.
Le choix a été porté sur **Geant4**, une librairie développée par un consortium de laboratoires et pilotée par le CERN. L'ensemble du code ainsi qu'une documentation détaillée est disponible sur le site du CERN, ce qui a fortement participé à la popularité du code, outre ses performances de simulations reconnues.
En particulier, c'est la présence de plusieurs bibliothèques dédiées aux basses énergies qui a justifié l'adoption de Geant4 comme base du code.

Les simulations devaient permettre de prédire le gain en efficacité de certaines microstructures, et de prédire les efficacités quantiques de certains matériaux encore non étudiés.
Malheureusement, il s'est avéré que le code était beaucoup trop imprécis pour mener à bien ce type de calcul. Les efficacités prévues par le code se sont avérées complètement fausses dans un certain nombre de cas déjà connus.
Une étude plus approfondie a montré que la simulation de photocathodes est actuellement impossible avec ce type de simulations. Deux facteurs principaux expliquent cela :

Les tables de sections efficaces utilisées par les codes Monte Carlo sont trop imprécises. En effet, l'obtention de valeurs de sections efficaces à basse énergie est beaucoup plus difficile qu'à haute énergie, du fait du nombre d'interactions que subissent les particules à ces énergies. De ce fait, les tables de sections efficaces à basse énergie sont basées sur des modèles semi-empiriques, et sont entachées de nombreuses incertitudes.

L'approche interaction particule/atome qui est utilisée est globalement trop grossière : elle ne permet pas de rendre compte efficacement de l'état chimique du matériau et de sa surface. En particulier, l'état de surface, qui s'avère être une donnée cruciale n'est pas modélisable par une approche purement atomistique.

Le code n'a donc pas pu être utilisé pour effectuer des simulations de photocathodes.

Etude et construction d'un dispositif expérimental

Afin de pouvoir tester expérimentalement les photocathodes envisagées, un dispositif adapté a été créé.
Il consiste essentiellement en une chambre à vide munie de connecteurs et d'une fenêtre adaptée, et d'un ampèremètre très précis : la chambre possède une fine fenêtre de beryllium permettant de laisser passer une large proportion du flux de rayons X. Des connecteurs triaxs permettent de connecter directement sur la chambre le pré-amplificateur associé à l'ampèremètre. Au sein de la chambre, l'ensemble des pièces supportant la photocathode au plus près de la fenêtre est réalisé en PEEK, matériau présentant à la fois une grande dureté et une résistance électrique élevée. Une grille de collection est montée environ 5mm au-dessus de la photocathode testée. Enfin, un connecteur CF standard permet la connection à une pompe.

L'ampèremètre utilisé est un Keithley 6430. Cet appareil est capable de mesurer des courants inférieurs au fA, grâce à la présence d'un pré-ampli extérieur, qui permet d'approcher autant que possible les connecteurs de la source de courant.
Le dispositif de mesure a été testé avec succès avec une source radioactive à des courants de l'ordre de 0,5fA. Le courant de fuite étant inférieur à 10% de la valeur mesurée.
Cependant, le dispositif a été essentiellement utilisé avec un tube conventionnel de rayons X, cathode de cuivre. L'ensemble des opérations de montages du dispositif et des échantillons s'est déroulé en salle blanche.

Les photocathodes étudiées et leur efficacité

Principalement deux approches ont été adoptées pour améliorer l'efficacité des photocathodes existantes :
– L'étude de certaines microstructures et de leurs effets
– L'étude de nouveaux matériaux

Des microstructures pour améliorer les matériaux déjà connus

L'effet de microstructures sur l'efficacité des émissions a été étudié.
Deux types d'effets ont été recherchés :
– Un effet purement géométrique afin de profiter de l'augmentation du rendement d'émission dans le cas d'incidence oblique.
– Un effet d'émission de champ a été recherché par l'étude de micro-pointes de silicium.

Emission de champ

Dans le cas de structures très pointues, telles que des pointes de silicium, il se produit une concentration du champ électrique aux alentours de la pointe. L'idée était donc de profiter de cette concentration du champ électrique normalement utilisé pour faire migrer les électrons photo émis vers la grille de collection, pour étudier un éventuel phénomène d'augmentation du rendement d'émission par effet de champ.
Malheureusement, aucun courant n'a pu être détecté par ce biais. C'est probablement le faible pouvoir stoppant du silicium qui peut expliquer la très faible efficacité quantique du silicium dans ce cas. En effet, si les électrons sont créés trop loin de la surface de la photocathode, une très faible proportion d'entre eux parvient à la surface, ce qui se traduit par un rendement global très faible.

Effet de l'angle

Dans le cas d'une incidence oblique des rayons X sur la surface du matériau, il se produit une augmentation du rendement de la photocathode. En effet, une plus large proportion (facteur $\frac{1}{\cos\alpha}$ si α est l'angle d'incidence vis-à-vis de la normale à la surface) des photons est absorbée au sein de la *zone active* de la photocathode (immédiatement à proximité de la surface). Il s'en suit donc une augmentation du nombre d'électrons qui peuvent s'échapper.

L'effet de structures, facile à obtenir sur de larges surfaces (il s'agissait en fait de papier de verre classique ou de type Trizact), a révélé que l'on obtient facilement un doublement de l'efficacité quantique avec de simples structures pyramidales régulièrement placées à la surface de la photocathode.

Le CsI_3 comme nouveau matériau de photocathode

Le matériau le plus efficace actuellement connu est le CsI. En effet, ce sel de deux composés de numéro atomique Z élevé présente un pouvoir stoppeur important, doublé d'une affinité électronique négative.
De ce fait, le CsI peut revendiquer des efficacités de plusieurs pour-cents à des énergies de quelques keV.
Malheureusement, comme tous les matériaux à affinité négative, il est aussi fortement sensible à la pollution due à son environnement, et, à moins de le laisser sous ultra-vide (ce qui est réalisable au sein des photomultiplicateurs scellés) son utilisation ne peut être envisagée au sein d'un détecteur à gaz (et ce malgré de très nombreuses études dans ce sens).
En substitution à ce matériau, le CsI_3 : un de ses dérivés, peut constituer une alternative intéressante.
Le CsI_3 est un matériau de couleur marron-orangé, instable sous vide (il se décompose selon la réaction $CsI_3 \rightarrow CsI + I_2$), présentant une densité de $4,51 g\dot{c}m^{-3}$. C'est un cristal dont la structure appartient au groupe Pmcn.
Le matériau est commercialisé par des entreprises telles que *Sigma-Aldrich* ou peut être obtenu en mettant un échantillon de CsI au sein d'un atmosphère saturée d'iode.

Les tests du CsI_3 ont montré une efficacité intrinsèque intéressante, qui de plus augmente après quelques heures placé sous vide (pression de l'ordre de 10^{-4} $mBar$).
Une étude plus poussée de ce matériau a permis d'établir un scénario permettant d'expliquer cette amélioration.
Lorsque la photocathode est laissée sous vide, le CsI_3 se décompose en CsI. Ceci explique l'amélioration de l'efficacité alors constatée, en effet le CsI est actuellement le meilleur matériau connu pour la constitution de photocathodes. Il présente cependant le défaut d'être particulièrement sensible à la pollution par le milieu, et en particulier, il est très hygroscopique.
A l'inverse le CsI_3 semble être particulièrement peu sensible à la pollution. Il peut de plus être régénéré après un passage sous vide (et donc la transformation de sa surface en CsI) par mise dans une enceinte contenant de l'iode solide, et donc où la pression partielle de I_2 est importante.
L'étude a aussi montré une modification de la structure de la surface qui prend un caractère poreux lors de la transformation $CsI_3 \rightarrow CsI + I_2$. Ainsi, lorsque le processus de mise en contact avec I_2 puis mise sous enceinte sous vide est répété, l'efficacité s'en trouve améliorée.
L'utilisation de CsI_3 comme précurseur du CsI est donc intéressante en soi, car elle permet une structuration du CsI. On perd cependant la plus grande insensibilité du CsI_3 en regard à celle du CsI. Ainsi, même si le CsI pur est plus efficace que le CsI_3 (facteur 8 environ), une fois pollué, le CsI est beaucoup moins efficace que le CsI_3.
Cette approche peut s'avérer très utile pour permettre l'utilisation du CsI comme photocathode dans

le cas des détecteurs à gaz. En effet il est possible de fabriquer les détecteurs munis de la photocathode sous forme de CsI_3 ce qui permet sa manipulation sous air. Ensuite, le détecteur étant hermétique, la transformation du CsI_3 en CsI permet l'obtention d'une photocathode présentant un caractère poreux, et donc d'une grande efficacité. Ceci apporte aussi une solution au problème de la maintenance qui nécessite souvent l'ouverture du détecteur. On peut en effet protéger la photocathode de CsI en l'exposant préalablement à de l'iode (I_2) ce qui la rend résistante à l'humidité. Ainsi il n'est plus nécessaire d'ouvrir le détecteur en enceinte protégée de l'humidité.

Acknowledgements / Remerciements

The first thank of course goes to my supervisor **Menyhert Menhard Kocsis**.

Not much to say, apart that I would not have done much without his help and support. He did not help only for the work, but he also showed great courage to defend me at a moment I had a very bad time.

Thanks a lot Menhard !

I would like to thank then people in chronological order :
Mes parents, ma famille pour leur soutient avant et pendant ce travail.

Mes grands parents car ils ont eu une importance décisive dans mes choix d'étude, et l'orientation que j'ai donnée à mon travail.

Mlle. Lenoble ma professeur de physique en classe de $1^{ère}$ qui a su rendre une matière alors bien fatiguante beaucoup plus attractive ! Vous voyez Mlle. Lenoble, j'ai fini par vous écouter et aller chercher tout seul les réponses aux questions auxquelles la physique n'a pas encore répondu...

Julie ! Et oui elle a certainement dû m'aider même lorsque je ne m'en rendais pas compte...

My colleagues from the ESRF :
The whole ISG group.
In particular *Christophe, Francis, Thierry, Cedric* who provided me with a great and constant support and taught me so much.
Also thanks a lot to *Joel, Jose-Maria, Emmanuel, Laurent, Marc, Paul-Antoine, Pablo, Herve, Ricardo, Jean-Claude, John, Ernesto, Cyril, Roland, Jean-Jacques, Denis...* And last, as a former guy

from ISG, *Heinz* who certainly had a peculiar place in this work...

Narayanan for being my tutor during this PhD. Thesis.

The Scisoft Group In particular Claudio and Romeu for sharing their knowledge concerning the Monte Carlo method and programming.

The whole id15 beamline For their support each time they could give me a hand.

And also : *Irina* for the SEM images, *Harald* for the help in preparing the samples in the chemistry lab, *Gemma* for the access to the die/press, *Elizabeth* for her help in preparing *job interviews*, *Philippe* for providing me with a Pump, *Fabienne* for her daily help, and her bread ! *Delphine* for her help with the administration from the University, *Werner* for his help with the mechanical pieces, *Stephanie* and *Patrick* for the help with the safety aspects...

.. Guillaume, Andy, Virgile, Anne, Alex, Sylvain, Manuel, Chantal, Julio, Jorge, Davide, Valentina, Simo, Moritz, Paul-Antoine, Paul, Adeline, Oier, Gemma, Florian, Yvonne, Frank, Delphine, Pascal, Benoit, Sebastian, Sebastian (bis), Ioana, Olivia, Irmi, Jean-Michel, Wolfgang, Claudio, Romeu, Rainer, Olivier, Mohamed, Bertrand, Christian, Julia, Peter, Till, Andreas, Stefen, Alex, Roberta, Caroline, Elizabeth, Benedicte, Jose, Riccardo, Kieran, Nicolas... and those I forget, but who still have a place in my heart !
for all the good moments I had at the ESRF.

Mes tuteurs de l'Université

Vincent Comparat et **Johann Collot** qui ont assuré le suivi académique et ont été de patientes et passionnantes sources de conseils pour ce travail de thèse.

☺